EVALUATION OF SONICALLY ENHANCED AGMD FOR INDUSTRIAL SCALE WATER TREATMENT

A thesis submitted by

Osamah Allawi Naji

For the award of

Doctor of Philosophy

2019

ABSTRACT

As the global supply of freshly available water becomes a scarce commodity, low energy and cost-effective schemes to reuse and rectify contaminated water sources are becoming essential. This research investigates air-gap membrane distillation (AGMD), a novel low energy technology aimed at reclamation of contaminated water sources. While previous studies have delved into the control mechanisms of AGMD, they have only been used at extremely small scales, and cannot be readily expanded to an industrial level. In this study, key parameters which affect permeate-flux production such as feedwater temperature, concentration and flow rates were compared with two membrane types on an AGMD system which was around 14 - 18 times larger than the typical systems previously studied.

A novel remediation method has been developed to tackle membrane fouling which is the most commonly encountered problem in membrane technologies. Without cleaning, membrane fouling decreased permeate-flux by approximately 25% after 70 hrs of running with feedwater of 4000 - 12 000 μS/cm. In stark contrast, the external application of ultrasonic energy with a low power range of 40 - 120 W/m^2, resulted in a consistently high permeate-flux production (200 - 300 % compared to non-sonicated AGMD) with no signs of fouling evident after a 70 hrs of operation. With this low level of ultrasonic power, the occurrence of cavitational effects is highly unlikely. Hence, the observed permeate-flux improvement was attributed mainly to cleaning effects, along with mass and heat transfer enhancements. This was confirmed by microscopic examination of the membrane surface, which showed no signs of fouling or damage afterwards.

CERTIFICATION OF THESIS

This Thesis is entirely the work of Osamah Allawi Naji except where otherwise acknowledged. The work is original and has not previously been submitted for any other award, except where acknowledged.

Principle Supervisor: Dr. Leslie Bowtell

Associate Supervisor: Dr. Vasanthadevi Aravinthan

Associate Supervisor: Professor Noreddine Ghaffour

Student and supervisors' signatures of endorsement are held at the University.

ACKNOWLEDGMENTS

I would like to express my deepest gratitude to my supervisors, Dr. Les Bowtell and Dr. Vasanthadevi Aravinthan at University of Southern Queensland for their exceptional guidance, caring, encouragement and patience, and for providing me with an excellent atmosphere for doing research. I would also like to thank Dr. Raed Mahmood for his help and support.

I would like to express the deepest appreciation to my associate supervisor: Professor Noreddine Ghaffour at KAUST, who the attitude and the substance of a genius: he continually and convincingly conveyed a spirit of adventure in regarded to research. Without his guidance and persistent help this dissertation would not have been possible.

I would like to express my gratefulness to Dr. Alla Alpatova for her help in shaping my PhD project in the early stages and contributing her valuable time and knowledge.

I would also like to thank my father, mother, sisters, and brothers. They have always supported me and encouraged me with their best wishes.

Most importantly, a huge thank-you to my wife princess Dr. Hawraa AL-Turaihi and her family for their full support and almighty God for his grace in me.

I also thank my wonderful children, Shahad, and Ali, for always making me smile.

We would like to acknowledge the technical support of the Scarab Co. staff and provision of membranes from Donaldson filtration.

I would like to acknowledge the support by ministry of higher education and scientific research (Iraq) during my research.

LIST OF PUBLICATIONS

Naji, O., Bowtell, L., Al-juboori, R.A., Aravinthan, V. and Ghaffour, N., 2018. Effect of air gap membrane distillation parameters on the removal of fluoride from synthetic water.

O. Naji, L. Bowtell, R. Al-juboori, A. Alpatova, N. Ghaffour, 2019. Mitigation of Air-Gap Membrane Distillation (AGMD) fouling and flux enhancement using ultrasonic technique, Ultrasonics Sonochemistry. ***(Under Review).***

O. Naji, L. Bowtell, R. Al-juboori, A. Alpatova, N. Ghaffour. High Salinity Water (RO Reject Water and Natural Groundwater) Treated Using Pilot Scale AGMD, Science of the Total Environment. ***(Under Review).***

O. Naji, L. Bowtell, R. Al-juboori, A. Alpatova, N. Ghaffour. High Salinity Water (RO Reject Water and Natural Groundwater) Treated Using Large Scale AGMD, 4th International Conference on Desalination using Membrane Technology. ***(Under Review).***

Contents

LIST OF FIGURES

LIST OF TABLES

1

CHAPTER 1: INTRODUCTION

1.1 Background

Water is an essential natural resource, which in the past, has been considered to be abundant and cost-free. Surface water supplies suitable for fresh water usage have steadily declined due to increases in population, industry and agriculture stressors. Globally more populations are becoming increasingly dependent on groundwater resources for domestic and agricultural purposes. This is especially true in inland areas where seawater desalination is not a viable option. Many people in developed countries are enjoying good quality water through the use of centralised municipal water supply systems. However, in under-developed and developing countries safe drinking water is often a scarce commodity. Every year, millions of people die as a result of drinking polluted water. Contaminants in drinking water are one of the most significant issues globally, and millions of people are suffering from its hazardous effects. Various technologies such as reverse osmosis (RO), microfiltration (MF), ultrafiltration (UF), forward osmosis (FO) and nanofiltration (NF) are effective in removing water contaminants but remain beyond the financial reach of the majority of third world countries. Hence, there is a need to develop water treatment technologies suitable for countries which cannot afford expensive technological solutions.

Membrane distillation (MD) is one of the many processes which rely on a membrane-based separation technique. This promising technology was first introduced in the 1960s (Weyl, 1967, Findley, 1967). However, MD is still not commercialised for use in general industrial water treatment systems. The development of membrane engineering techniques began in the early 1980s (Andersson et al., 1985, Mehta, 1982), and although MD has been studied for more than 50 years, it is still in the developmental stages.

The driving force of MD is different from that used in other conventional membrane technologies such as RO, FO, NF, UF and MF. The driving force of the conventional membrane technologies is a pressure or concentration gradient, while the driving force of MD is the vapour pressure difference across the membrane. MD is dependent on the temperature difference across the membrane. The MD membrane needs to be hydrophobic and microporous in nature because the MD process is based on water vapour transport and the membrane should not be affected by wetting while allowing vapour transport. A hydrophobic microporous membrane is an effective barrier for the liquid phase, allowing the gaseous water-vapour passage while preventing the flow of the water in liquid water form (Fig 1.1).

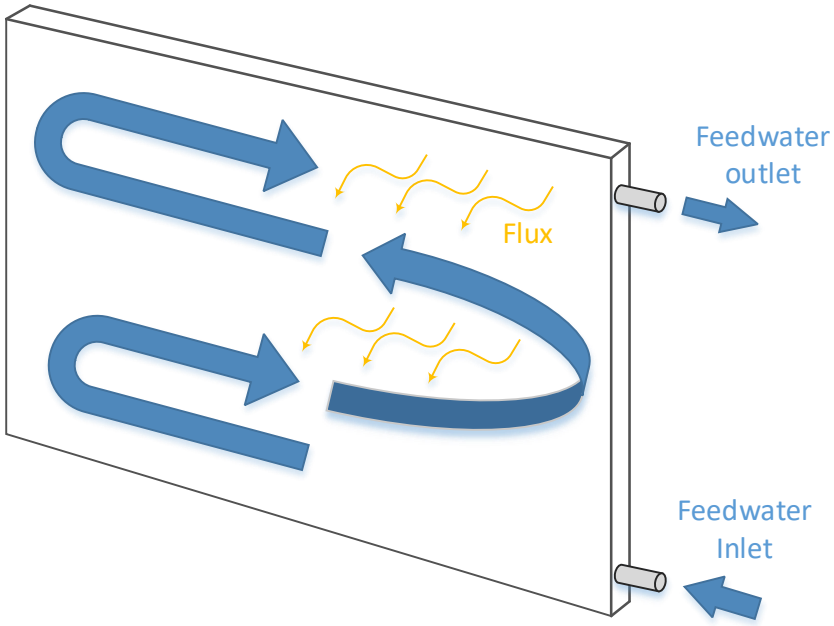

Figure 1.1: A diagram showing water vapour vs feedwater

Various materials are used to make MD membranes such as polytetrafluoroethylene (PTFE), polypropylene (PP) and polyvinylidene difluoride (PVDF) (Lawson and Lloyd, 1997). Essential characteristics of the MD process require the membrane to be porous, allowing only water vapour to be transported through the pores of the membrane. It is also important that the membrane does not change the vapour equilibrium of the different components in the process liquids as, for each component, the driving force of the MD operation is a partial pressure gradient in the vapour phase. For MD to be effective, the membrane should not be wetted by process liquids (Fig 1.2). At least one side of the membrane should be in direct contact with the process liquid, and it is essential that no capillary condensation occurs inside the pores of the membrane.

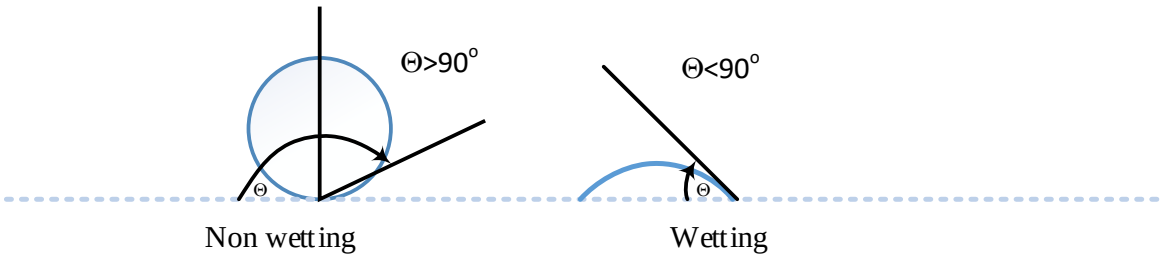

Figure 1.2: Non-wetting and wetting liquids

The inherent contaminant rejection of MD is higher than that of conventional technologies, and this is essentially a result of the comparatively small pore size of the MD membrane. The pore size range of MD membranes is typically 0.2–1.0 μm (Gryta and Barancewicz, 2010). MD flux production allows a high rejection of contaminants because of the selective mass transfer of water vapour across the MD membrane. As MD requires low system operational pressures and only low grade thermal energy sources, operation is very economical when compared to other thermal processes (Camacho et al., 2013). Another economic advantage in MD's favour is its inherently low maintenance requirement, as the membrane is not subjected to the same mechanical stressors as conventional high-pressure techniques (Susanto, 2011) and has no requirement for chemicals or pre-treatment (Gálvez et al., 2009).

The cost of MD differs from location to location, depending on the available energy sources and feedwater characteristics. The official cost of MD is still not clear because it is yet to be widely used on a commercial scale, with installations (to date) at a small scale. The estimated cost for a small scale MD with heat recovery is in the range of $1.17- $4.04 per cubic metre (Al-Obaidani et al., 2008).

Fluoride is a commonly occurring highly reactive natural metallic element often found in groundwater. The removal of excess fluoride is necessary to protect both public health and the environment. Fluoride can find its way into water sources through various pathways stemming from the food industry, pharmaceuticals, cosmetics, semiconductors, ceramics, electroplating, fertilizer, coal-fired power plants, as well as from anthropogenic sources (Kemer et al., 2009), (Drouiche et al., 2008). Small amounts of fluoride are useful for the mineralization of bones and teeth (Ramdani et al., 2010) hence, it is commonly added to dental hygiene products such as toothpaste and mouthwash, as well as being added to many western countries'

municipal water supplies. However, excess fluoride can result in dental and skeletal fluorosis and may also cause cancer, neurological, muscular, urinary tract and gastrointestinal problems along with lesions of the thyroid (Mohapatra et al., 2009), (Drouiche et al., 2009). The World Health Organization (WHO), sets out a maximum permissible safe limit for fluoride levels in drinking water of 1.5 mg/L (Organization, 2006).

Fouling is a widely encountered problem with all types of membrane technologies used in water treatment. It is often the result of two main mechanisms in membrane systems: pore blockage and surface crystalline formations. The extent and prevalence of fouling as an issue depends on many factors including type and concentration of the chemical compounds found in the feedwater along with operational conditions such as temperature and flow rate. Crystalline salt deposits on the membrane surface commonly cause the partial or complete blockage of membrane pores. High salt concentrations in the feedwater solution coupled with relatively low flow rates can lead to fouling build up around the membrane pores, which can be sufficient to prevent or impair the transport of permeate-flux (Warsinger et al., 2015). Separating the membrane surface from the feedwater solution results in a reduction of permeate-flux through the membrane pores due to increased thermal and hydraulic impedances from the fouling layer on the membrane surface. Fig.1.3 shows the visible fouling that can block the membrane and prevent the permeate-flux from passing through the pores. The extent of this fouling effect depends on a number of factors related to the general characteristics of the fouling layer along with system characteristics such as effective membrane area, flow rate and temperature (Tijing et al., 2015), and (Curcio et al., 2010b).

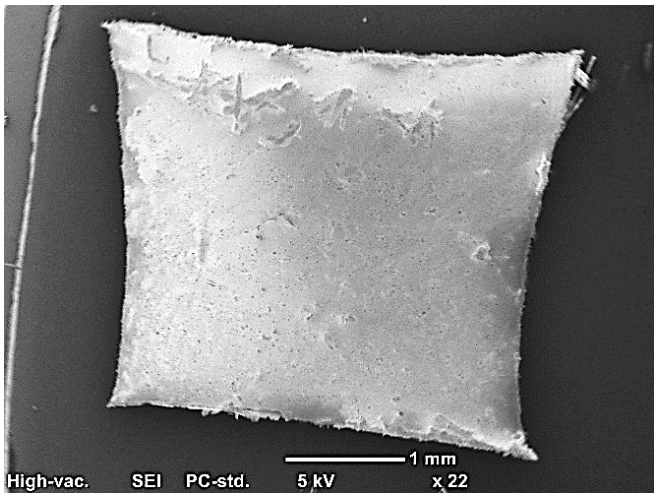

Figure 1.3: Partially Fouled membrane.

Cleaning and removal of contaminants by ultrasonic techniques have been practiced in industry for many decades. The application of ultrasound is widespread in electronics and component level cleaning as well as in a wide variety of industrial mixing homogenisation, cleaning and degassing processes. Ultrasound technology by definition uses energy in the frequency spectrum (> 20 kHz) which exceeds the human hearing limit (Mason and Peters, 2002). Ultrasound is a chemical-free energy that can be used in different applications such as water treatment (Al-Juboori et al., 2012). The type of ultrasonic treatments can be categorized as micro-streamers, micro-jets, acoustic streamed shock waves and vibrations (Lamminen et al., 2004b). Several different approaches have been reported by different researchers for reducing the fouling layer from the membrane surface by applying ultrasound. However, the exact mechanisms behind how the ultrasound cleans the membrane surface are still unclear (Lamminen et al., 2004b). In this study, ultrasound was used to reduce or remove the caked fouling layer from the membrane surface as well as to increasing vapour flux.

1.2 Scope of the Study

This research evaluates two treatment approaches: AGMD only and combined ultrasound with AGMD for two membrane types, PTFE and PVDF membranes with the same pore size of 0.3 μm. Feedwater solutions ranging from synthetic to natural groundwater and high salinity RO reject water were used to experimentally evaluate fluoride removal, as well as high concentration natural water to assess the combined performance of AGMD and ultrasound. This study was conducted with a focus on industrial scalability, and the research was performed as follows:

1. Evaluate the feasibility of the MD process for use in pilot-scale treatment of fluoride contaminated water sources, with a focus on the effects of feedwater concentration, temperature, flow rate and membrane effective area on permeate-flux produced
2. Study the effects of high salinity feedwater (reverse osmosis reject stream brine) on the performance of the pilot-scale AGMD module
3. Investigate the feasibility of ultrasound application on a pilot-scale AGMD module to achieve high permeate-flux and reduce fouling layer adhesion on the membrane surface.

1.3 Membrane Separation Processes

1.3.1 Reverse osmosis (RO)

Reverse osmosis (RO) is a well-established conventional desalination and water purification technology that uses a semipermeable membrane to remove a range of different particles (chemical compounds, bacteria, viruses, etc.) from drinking water sources (Fig.1.4). RO technology has become a common technology in the industrialised world to produce drinking water, dewater sewage and is also used in food processing, e.g. dewatering milk and whey before powder production. In water applications, it is used for treating varied sources such as surface water, seawater and groundwater with mixed success and efficiency. This technology has many advantages such as high contaminant removal and low temperature influence. While it has the disadvantage of being relatively expensive, sensitive to pH and ionic strength and, most notably, a high energy consumer.

Other problems associated with RO technologies are the requirement for pre-treatment and high membrane fouling levels resulting from the small pore size. Pre-treatment combinations incorporating some or all of UF, MF and chemical additions are required: all of which increase the cost of treatment. As this technology essentially depends on pressure to transport water molecules through the membrane, it requires high pressure (usually 0.2-1.7 MPa or 2–17 bar) for fresh and brackish water, and 4-82 MPa (or 40–82 bar) for seawater. These high pressure demands translate into high energy costs of water treatment (Shih, 2005). By applying high pressure, the membranes also become susceptible to fouling which clogs their pores (Jiao et al., 2004) and reduces the flux produced.

The membranes that are used in RO technologies need to be changed regularly because of the high pressures applied as well as other mechanical and chemical stressors due to backwashing and fouling. As a result of this high-pressure utilisation membranes typically need to be changed after around 1.5 years of service, rather than the three year life expected in nanofiltration (NF) (Abejón et al., 2015). The range of membrane pore sizes used in this type of technology are generally < 0.001 μm (Le My, 2015).

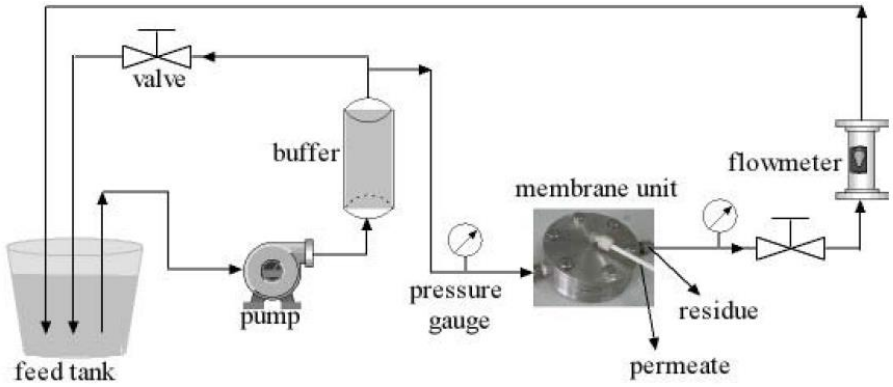

Figure 1.4: Reverse osmosis System (Li et al., 2010)

1.3.2 Nanofiltration (NF)

Nanofiltration (NF) is a mainstream technology used to treat drinking water and for another purposes. It used to remove particles bigger than 0.001 - 0.01 μm range from water sources (Fig 1.5). NF works in a similar manner to RO technology with water transferred from the low-pressure side, to a high pressure side via a membrane. By comparison, NF is normally more economic than RO because it has lower operational pressure requirements, hence lower inherent energy needs (Pérez-Sicairos et al., 2009), (Pontié et al., 2008). The working pressure of NF technologies is typically in the range of 6.9 - 41.4 bar (Le My, 2015). In these systems, the osmotic pressure is exceeded, breaking the bonds between the water and ions. However, energy costs are still high because this technology requires relatively high pressures compared to the general pumping requirements of large volumes of water from reservoirs.

NF is an effective treatment despite the relatively high pressures and energy costs. The contaminant rejection ability of NF is dependent on surface charges and pore size of the membrane used. These considerations can be addressed by manufacturing special membranes with doped compounds, to improve their separation characteristics. The pore sizes of the membrane typically used in this technology are in the range of 0.001 - 0.01 μm (Le My, 2015). Membrane properties have a significant impact on NF technology rejection rates (Pérez-Sicairos et al., 2009). Typically, NF is used as a pre-treatment for RO systems, to efficiently remove the larger particles from the water to be treated.

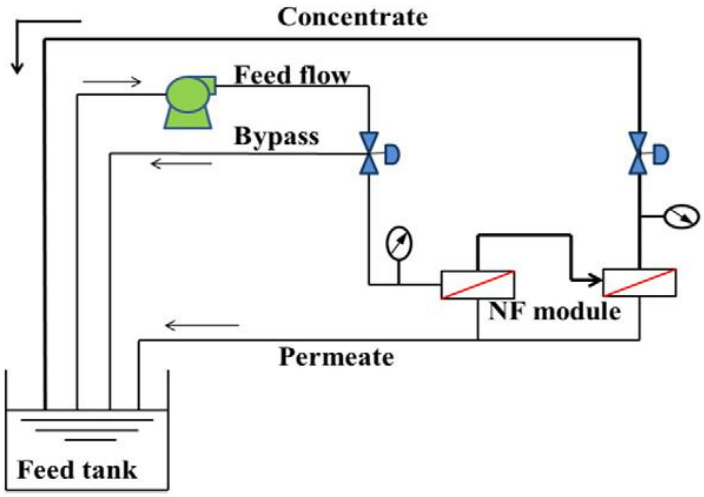

Figure 1.5: Nano filtration system (Xu et al., 2015)

1.3.3 Microfiltration (stand alone or as pre-treatment)

Microfiltration (MF) is a type of filtration that can be used to remove large particles from water. The rejection rate is dependent on the pore size of the membrane, so the rejection achieved with this technology is generally effective for larger contaminant particle sizes in the range of 0.1 - 1.0 μm. The typical pore size of MF membranes is in the range of 0.1 - 1.0 μm (Le My, 2015). The working pressure of MF technology systems is typically 1 - 8.6 bar (Le My, 2015). MF technology can only remove particles that are larger in size, such as dissolved organics, bacteria, viruses and sand, but other smaller sized particles and colloids can readily pass through the MF membrane pores.

1.3.4 Ultrafiltration (stand alone or as pre-treatment for RO)

Ultrafiltration (UF) is also a type of membrane filtration dependent on pressure or concentration gradients in order to remove particles from water (Fig 1.6). UF is similar to MF, but the relative pore size range is smaller than those used in MF systems. Even though the pore size is smaller than the MF membrane, it still cannot remove some common materials that are smaller in size than the pores of the UF membrane. The pore sizes of UF membrane are in the range of 0.005 - 0.2 μm (Sato et al., 2002). The working pressure of ultrafiltration technology systems are typically 4.8 - 13.8 bars (Le My, 2015). This technology is commonly used as pre-treatment for RO systems or for regional and remote townships without the infrastructure and energy supply requirements of RO.

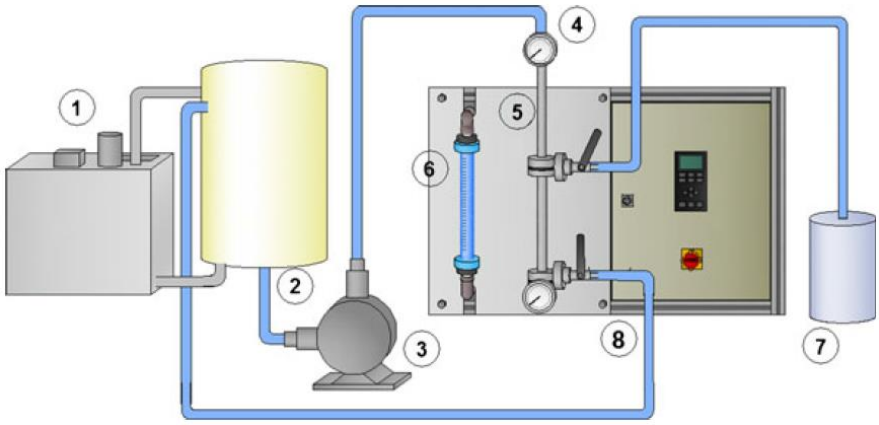

Figure 1.6: Ultrafiltration and microfiltration system (dos Santos Bazanella et al., 2012).

1.3.5 Electrodialysis (ED)

Electrodialysis ED technology essentially depends on an electrochemical separation process in which charged membranes are used to separate ionic species from a mixed aqueous solution of different components. It is driven by a DC electrical potential difference. In the case of ED, the respective process forces, the voltage potential and solution concentration differences, lead to the transport of solute and water through the ion exchange membranes. In contrast with pressure-driven membrane technologies, the driving force of ED does not depend solely on pressure and is affected by the salinity of the feedwater and potential difference. It is typically used most effectively for low concentration or brackish water treatment and process efficiency is significantly lower in the case of more highly contaminated feedwaters. During ED, the feedwater stream becomes more dilute and a corresponding brine stream becomes more concentrated (Gong et al., 2005). Ion-exchange membranes move ions from one solution to another with little passage of water through the membrane. The selectivity of an ion-exchange membrane is due to the Donnan equilibrium and is not due to physical blocking or electrostatic exclusion of specific charged species.

1.4 Emerging membrane processes

1.4.1 Forward osmosis (FO)

Forward osmosis, or FO, is the polar opposite to the RO process. The FO process uses the natural osmotic pressure difference between solutions of different concentrations to transfer water through a semipermeable membrane, from the higher solute concentration side to the lower solute concentration side. By contrast

to RO and other membrane technologies, FO does not require pressure application. FO is much more energy efficient than RO (Gray et al., 2006). However, the main limitation of the FO process is that a high flow rate required and resulting permeate-flux production is very low compared with other pressure-driven membrane technologies.

1.4.2 Membrane distillation (MD)

Membrane distillation MD is the only thermally driven membrane separation technology in which separation is enabled due to phase change. The distillation mechanism of MD is dependent on the temperature difference between either side of the membrane. There are typically five different MD configurations: direct contact membrane distillation (DCMD), vacuum membrane distillation (VMD), sweeping gas membrane distillation (SGMD), material gap MD (MGMD) and air-gap membrane distillation (AGMD). MD has key system parameters such as feedwater temperature (40 - 90^{o}C), coolant temperature (10 - 25^{o}C), feedwater flow and coolant flow rates. MD technology is primarily dependent on the temperature difference between the feedwater and the cooling streams, hence, it does not require high energy to break the bonds between water and ions like RO. As there are many naturally occurring instances of feedwater being hotter than ambient by 20-50^{o}C, especially in the case of groundwater, processes such as MD can leverage this natural driving force to remove contaminants. As MD technologies use very low pressures, resulting membrane lifetime is extended significantly when compared with traditional technologies such as RO. In general, MD has many advantages over other membrane processes such as a high rejection ratio of around 98%, low operating pressure, use of low-grade and potentially naturally derived heating and cooling sources, minimal membrane damage, no requirement for costly pre-treatment, low sensitivity to pH and salts, and easy installation and general maintenance. The MD process will be presented in detail in the next section.

1.5 The key objectives of this study are as follows:

- Investigate the feasibility of the MD process for treating fluoride contaminated waters on a pilot-scale with a focus on the effect of the feedwater matrix, temperature, flow rate and membrane effective area on flux produced
- Using the knowledge gained in Step 1 to investigate the effect of high salinity water (RO brine) on the performance of pilot-scale AGMD
- Investigate the feasibility of ultrasound application to a pilot-scale AGMD module to improve permeate-flux production and reduce fouling of the membrane surface.

2

CHAPTER 2: LITERATURE REVIEW

2.1 Introduction to membrane distillation

MD is a thermally driven membrane separation technology in which separation is due to the phase change. A hydrophobic microporous membrane presents a barrier for the liquid phase, allowing evaporation of volatile molecules, i.e. a vapour phase (e.g., water vapour) pass through the dry membrane's pores and so being separated from the feedwater solution. The driving force of the process is provided by a partial vapour pressure difference, as a result of the imposed temperature difference.

In MD, the feedwater solution is in direct contact with one side of the membrane and the hydrophobic nature of the membrane prevents the water from passing through the membrane due to the high surface tension between the membrane surface and feedwater. Water vapour, however, is freely transferred to the permeate side. Separation in the MD process depends on water evaporation and its transportation through the membrane pores (Tomaszewska, 2000). The vapour pressure difference across the membrane works as a driving force for vapour transportation from the feedwater side to the permeate side. The quality of water produced by the MD process is similar to that of thermally driven processes (e.g. multi-stage flush). However, the vapour flux production rate in the MD process is typically much lower than that produced in thermally driven processes.

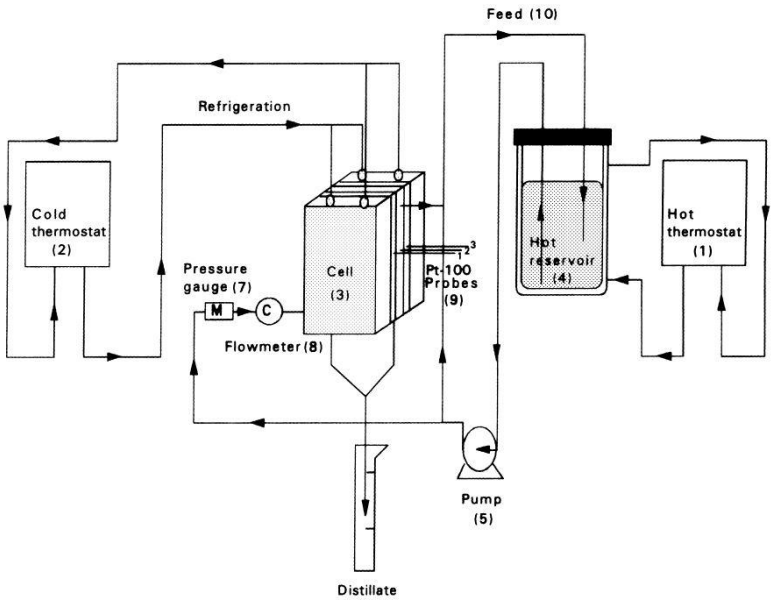

Figure 2.7: Schematic representation of an AGMD system (Izquierdo-Gil et al., 1999).

MD is an economic technology (Pirnie, 1999). Using MD technology to obtain fresh water does not require high temperatures on the feedwater side. It can usually work at a temperature difference of 40°C (Velizarov et al., 2004), (Figoli et al., 2010), (Richards et al., 2011). Another advantage of MD technology is that it requires little maintenance, because it only depends on the temperature difference between the feedwater and permeate sides. Mechanical demands are also low (Figoli et al., 2010), (Richards et al., 2011). MD system construction is possible from assemblies of smaller equipment modules (Figoli et al., 2010). MD has a high rate of contaminant removal from feedwater, typically 98% or better, regardless of the feedwater type.

2.2 Advantages of MD

MD has several advantages over traditional membrane-based water treatment technologies, including improved cost efficiency, lower chemical demand, the ability to use waste heat or solar power sources and sufficient vapour fluxes achieved at moderate feedwater temperatures (Camacho et al., 2013). In addition, feedwater pre-treatment and transmembrane pressure are not required, compared to other membrane-based desalination technologies, neither does MD require feedwater pre-treatment (Camacho et al., 2013). This, in turn, results in more sustainable membrane operations, less membrane damage and reduced energy demand (Susanto, 2011), (Gálvez et al., 2009). The low enthalpy heat used in MD is of a much lower grade energy (less exergy) than the electricity used to create the mechanical pressure

in RO. Using MD in cold countries will not need to consume energy for the coolant side as the water will already be cold. On the other hand, using MD in hot countries, such as those in The Middle East, would consume low energy for heating the feedwater because the water temperature there is quite high. Finally, generally MD requires energy input for one side only.

2.3 Configurations of MD membranes

There are two general types of membrane configurations:

Hollow fibre membranes fundamentally designed from PP, PVDF and PVDF-PTFE composite materials (Teoh and Chung, 2009), (Song et al., 2007).

Figure 2.8: Hollow fibre membrane (Zhang, 2011)

Hollow fibre membranes have large surface areas (Gryta et al., 2001), but the main disadvantage of the hollow fibre membrane is its typically low permeate-flux (generally 1 - 4 $L.m^{-2}h^{-1}$ at 40 - 60°C) (Bonyadi and Chung, 2007), (Bonyadi and Chung, 2009). On the other hand, high permeate-flux of the hollow fibre membranes with various advantages suitable for membrane distillation use have been developed recently, such as double-layer hydrophilic-hydrophobic fibres with a very thin but effective hydrophobic PVDF layer (50μm), and hollow fibre membranes with a sponge-like structure and thin walls (Zhang et al., 2010), (Teoh and Chung, 2009).

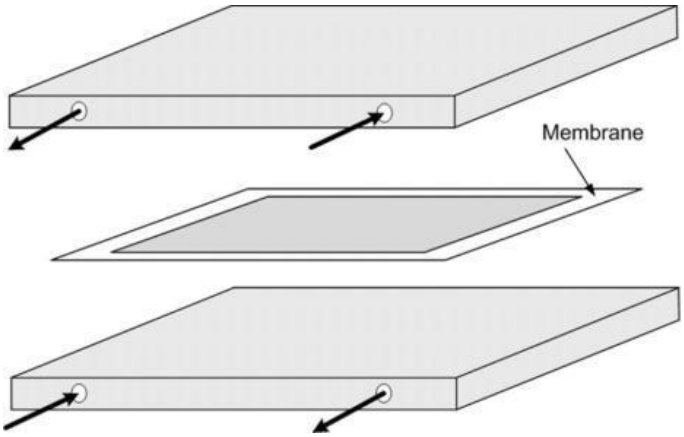

Figure 2.9: Flat sheet membrane (Zhang, 2011)

Flat sheet membranes are typically cast from PP, PTFE, and PVDF polymers. The vapour flux through from flat sheet membranes is about 50-70 $kg{\cdot}m^{-2}{\cdot}h^{-1}$ at feedwater temperatures in a range of 80 - 90°C (Teoh and Chung, 2009), (Bonyadi et al., 2009). Usually, the polymeric membrane shown in Fig. 2.9 is composed of a porous support layer and thin active layer. This structure is able to provide enough mechanical strength for the membrane, so the active layer is designed to be as thin as possible to decrease the mass transfer resistance.

2.4 Configurations of membrane distillation system

Four typical configurations that have been used in membrane distillation such as DCMD, SGMD, VMD and AGMD.

2.4.1 DCMD

The DCMD is the simplest and most frequently applied MD process. In the MD, the temperature at the feedwater side must be higher than at the coolant side to produce the temperature difference (i.e. driven force) between each side of the membrane (Meindersma et al., 2006). In this configuration, both membrane surfaces are in contact with the feedwater and coolant sides (Meindersma et al., 2006), which means the conductive heat transfer is higher due to direct contact (Fig 2.10). The transmembrane water vapour flux through the membrane can be increased proportionately by increasing the temperature at the feedwater side. However, the driving force of DCMD is low due to the high conductive heat transfer through the membrane compared with AGMD.

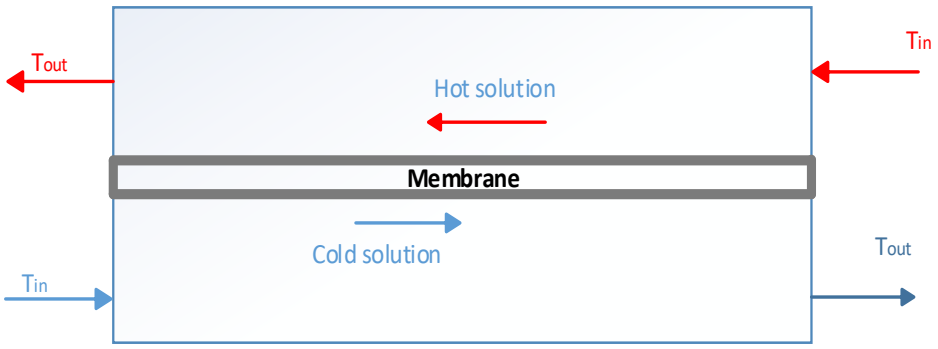

Figure 2.10: Direct contact membrane distillation (DCMD).

2.4.2 SGMD

The mechanism of the SGMD process is shown in Fig 2.11. In this process, a sweep gas is flown on the permeate side to carry the vapour away from the membrane surface. In this case the vapour is condensed outside the module (Meindersma et al., 2006). However, the use of a sweep gas as a driving force is a problem because the additional gas component causes negative effects on the condenser capacity (requiring increased capacity) (Meindersma et al., 2006). The application of small flows of sweep gas can lead to an increase in sweep gas temperature, resulting in a lowering of the partial pressure difference between each side of the membrane. This, in turn, reduces the overall efficiency of the process (Meindersma et al., 2006).

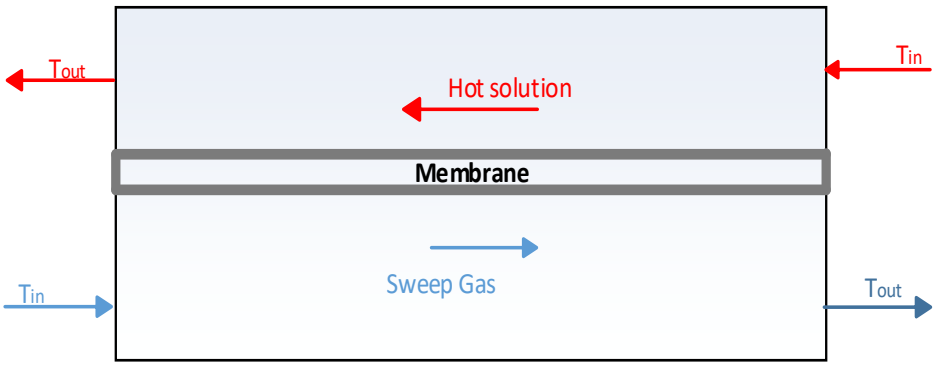

Figure 2.11: Sweeping gas membrane distillation (SGMD).

2.4.3 VMD

The principle of the VMD configuration is similar to that of SGMD. In this configuration (Fig 2.12), the vacuum pump can be added to permeate membrane side to create vacuum pressure. This strategy leads to an increase in the pressure difference between the sides of the membrane, and vapour flux through the pore size of the membrane. In the VMD process, a hydrophobic porous membrane allows the

immobilisation of the liquid–vapour interphase at the pores of the membrane. The liquid feedwater has direct contact with the membrane surface, and evaporation of the components of the feedwater occur at the pores' entrance.

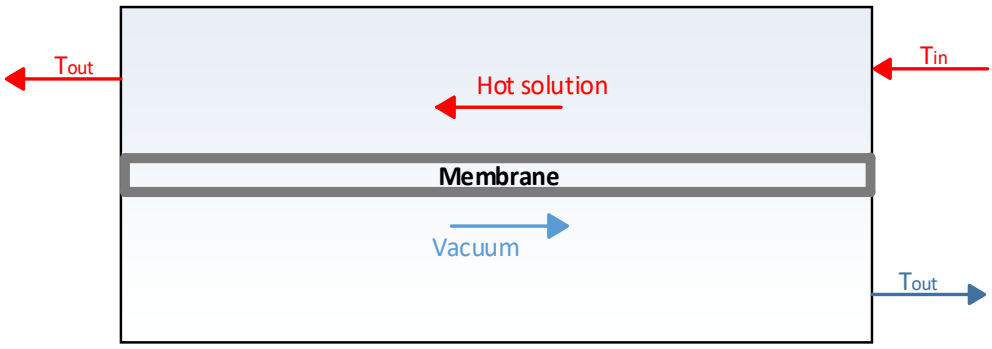

Figure 2.12: Vacuum membrane distillation (VMD).

2.4.4 AGMD

A schematic of the AGMD module is shown in Fig 2.13. In the AGMD configuration, while the feedwater solution is in contact with the membrane selective, the air-gap separates the membrane's other side and the coolant solution. The air-gap improves insulation between membrane and the cooling fluid and hence reduces energy demand (Meindersma et al., 2006), (Chernyshov et al., 2005). There are many advantages to using AGMD:

1. Low temperature polarization effects.

2. Possible internal heat recovery.

3. Lower heat loss (and therefore less heat demand) compared with other MD configurations.

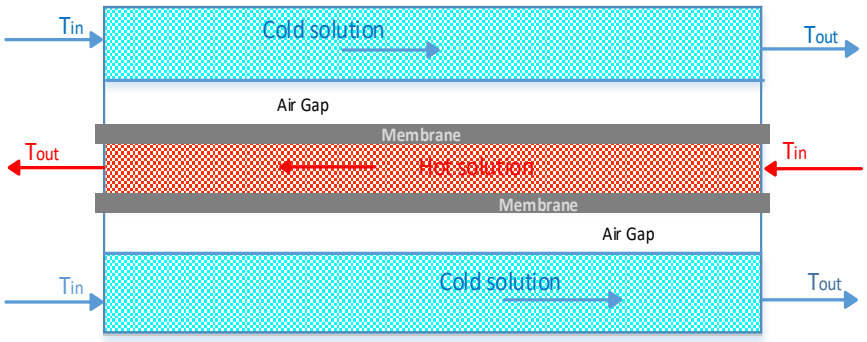

Figure 2.13: Air-gap membrane distillation (AGMD).

There are also newly proposed MD configurations offered by different authors, such as water gap MD (WGMD) and material gap MD (MGMD). In principle, these MD configurations are similar to AGMD, but the gap is filled with materials such as water, sand or sponge (Fig 2.14). The target of these new MD configurations is to increase the permeate-flux. The permeate flux was increased by about 200 - 800% when the gap was filled with sand and deionized water (Khalifa, 2015).

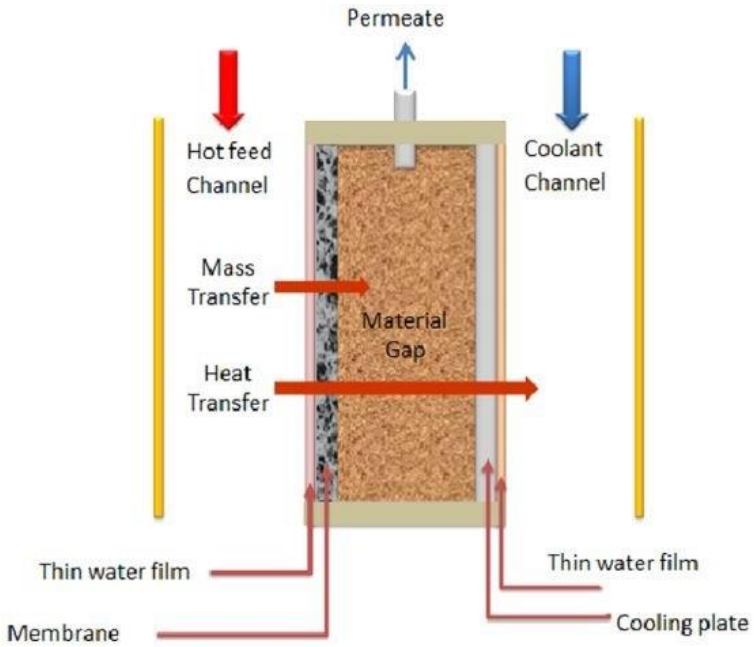

Figure 2.14: MGMD configuration (Francis et al., 2013).

2.5 Membrane materials and characteristics

In MD systems, membranes are selected based on the heat transfer from the hot side to the cold side rather than on the mass transport of compounds. Therefore, transfer of compounds across the membrane into the gas phase is driven by vapour pressure differences, and the membrane (microporous polymeric or inorganic) acts as a physical barrier between the coolant and feedwater sides. Microfiltration membranes made from hydrophobic polymers such as polypropylene (PP), polytetrafluoroethylene (PTFE) and polyvinylidene fluoride (PVDF) are used in the MD process (KULLAB, 2011). A good porous membrane should offer low resistance to mass transfer, high liquid entry pressure of water to keep the membrane pores dry, low thermal conductivity to prevent heat loss through the membrane matrix, good thermal stability and excellent chemical resistance to most of the feedwater solutions (Curcio et al., 2005), (Khayet et al., 2003).

2.6.1 Membrane materials

The permeate-flux produced by MD is based on water vapour transportation so hydrophobic membrane is the most suitable for membrane distillation because hydrophobic materials repel water from the membrane surface and prevent its passing through the pores while allowing the vapour to pass, which effectively makes a vapour–liquid interface at each pore entrance (Kullab (2011). Most of the membrane types used in MD were originally made for microfiltration purposes.

Different types of materials have been used for MD membranes such as polytetrafluoroethylene (PTFE), polypropylene (PP) and polyvinylidenedifluoride (PVDF) (Lawson and Lloyd, 1997). A few researchers have suggested new designs or surface modifications of MD membranes to make them more efficient (El-Bourawi et al., 2006), (Khayet et al., 2005), (Wu et al., 1992), (Peng et al., 2005). The surface energies of PTFE and PVDF materials are 9,1 and 30,3 kN/m, respectively. These materials are also characterized by low thermal conductivities in the range of 0.22 – 0.45 W/m·K. The purpose of a hydrophobic membrane is to prevent water from passing through the membrane pores and at the same time preventing wetting of the membrane surface, thus creating a vapour-liquid interface.

2.6.2 Membrane pore size

The pore size of the membrane has a large effect on MD performance in terms of permeate-flux, conductive heat transfer, fouling and rejection. In general, the range of the pore size of membranes used in MD is 0.2 – 1.0 μm (Gryta and Barancewicz, 2010). Feedwater pressures higher than LEP can result in membrane damage, the permanent loss of hydrophobicity is also considered as damage (Chernyshov et al., 2005). The smaller membrane pore sizes lead to low permeate-flux rates but prevents the membrane pore wetting (Kullab (2011).

2.6.3 Membrane porosity

Usually, the porosity of the membranes used in MD range between 60 - 85 % (Alklaibi and Lior, 2005c). The application of a membrane with high porosity results in higher permeate-flux, because the evaporation area of the membrane increases, and the conductive heat transfer is smaller compared to membranes with low porosity. This is applicable only when the feedwater temperature is low (Al-Obaidani et al., 2008).

2.6.4 Membrane thickness

The thickness of the membrane has an important effect on MD system permeate-flux, because it effects both heat and mass transfer (Schneider et al., 1988). The reported range of membrane thickness used in the MD process is 0.06 – 0.25 mm (Gryta and Barancewicz, 2010). In general, membranes with low thickness lead to high permeate-flux regardless of the MD configuration type. Membranes with higher thickness result in high heat efficiency. In AGMD, the effect of membrane thickness is of less concern owing to the relative effects of the air-gap (Khayet et al., 2005).

2.7 Effects of operating parameters

2.7.1 Effect of feedwater temperature

MD is a thermal separation process that utilizes a specific type of membrane for different applications (Eleiwi et al., 2016). Basically, feedwater temperature in all MD configurations is very important as these configurations depend on the water vapour. In this process, a porous membrane is installed inside the module to separate channels with the hot feedwater from the coolant water. The temperature difference between both sides of the membrane generates the driven force in the membrane distillation system. The water vapour pressure inside the feedwater side increases as a result of increasing the temperature in the feedwater side (Liu and Wang, 2013). Usually, the feedwater temperature ranges between 40 - 90°C in all MD configurations. In MD the vapour flux increases as a result of the increasing feedwater temperature (El-Bourawi et al., 2006). The feedwater temperatures that applied in this work were 50, 60 and 70°C. Fig. 3.18 shows how the permeate-flux increased when the feedwater temperature increased. Although it was technically possible to further increase feedwater temperature, they set 70°C as the upper temperature limit to avoid high energy consumption, high conductive heat transfer and increased temperature polarization which are associated with high feedwater temperatures (Alklaibi and Lior, 2005c), (El-Bourawi et al., 2006, Walton et al., 2004). Also, further increasing the feedwater temperature could negatively impact membrane properties (Gryta and Karakulski, 1999). The water vapour pressure in the feedwater side increases because of increasing the feedwater temperature based on the Antoine equation (Liu and Wang, 2013, Alklaibi and Lior, 2005d, Warsinger et al., 2015). Increasing the temperature gradient between the membrane surfaces will influence the diffusion coefficient positively, leading to a high vapour flux

(Gunko et al., 2006a, Qtaishat et al., 2008, Chen et al., 2009). Usually, the feedwater temperature ranges between 30 and 94^{o}C in most MD configurations (Curcio and Drioli, 2005a, Alkhudhiri et al., 2012b, Alklaibi and Lior, 2005d, Alsaadi et al., 2015, Chen et al., 2009, Fortunato et al., 2018, Alklaibi and Lior, 2007, Gryta and Barancewicz, 2010). In the MD process, the vapour flux increases due to increasing the feedwater temperature (El-Bourawi et al., 2006, Alklaibi and Lior, 2005c, Gunko et al., 2006a), whereas the vapour flux decreases when the heat transfer increase due to the decrease in the temperature of feedwater channel (El-Bourawi et al., 2006). The feedwater temperature has negative relationship with the size of the MD module. Scaling up the MD module leads to a reduction in the feedwater temperature as a result of increase the temperature difference across the membrane (Alsaadi et al., 2013).

2.7.2 Effect of coolant temperature

In general, coolant temperature has less effect on the vapour flux than feedwater temperature. The effect of the cold side temperature on the permeate flux is insignificant, regardless the feedwater temperature (Banat and Simandl, 1998b, Matheswaran et al., 2007). However, remarkable change in the permeate flux occurs when the coolant temperature decreases (Gunko et al., 2006a, Calabro et al., 1994). Furthermore, (Alklaibi and Lior, 2005c) found that the permeate flux can be doubled when compared to feedwater side at the same temperature difference. The MD process depends on the water vapour pressure, which is generated because of the feedwater temperature. The range of coolant temperatures in most MD configurations were between 5 to 30^{o}C (Alkhudhiri et al., 2012b, Alsaadi et al., 2015, Alsaadi et al., 2013, Bonyadi and Chung, 2009, Bonyadi and Chung, 2007, Bouguecha et al., 2003, Chen et al., 2009) while some researchers such as (Alklaibi and Lior, 2005d, Alklaibi and Lior, 2006, Alklaibi and Lior, 2007, Francis et al., 2014, Guillén-Burrieza et al., 2011) have applied coolant temperature over 30^{o}C. The coolant temperature is reduced further in the AGMD due to the presence of the air-gap and hence the conductive heat transfer coefficient in the AGMD is much lower (Alklaibi and Lior, 2006). Temperature difference across the MD membrane surface decrease with increase the coolant temperature (Alsaadi et al., 2013). Heat transfer could increase with increase in ΔT across the membrane. Control on heat transfer is required more energy to keep the temperature of both feedwater and

coolant side of the membrane in the required level. The coolant side requires energy to reduce the coolant temperature to the required level which means reduce the coolant temperature lead to increase in driving force across the membrane. With laboratory scale module, the coolant side required low energy due to small coolant plate, but the energy consumption keeps increasing with increasing the size of the coolant plate. This suggests that the heat transfer keeps rising while the permeate flux drops down due to increase in coolant temperature. The factor that can reduce the permeate flux because of coolant temperature is working with high coolant temperature because that lead to drop the driving force across the membrane. Controlling on coolant temperature is required to use membrane with high heat resistance to reduce the heat transfer and working with small ΔT between both sides of the membrane to reduce the heat transfer.

2.7.3 Effects of feedwater flow rate

The feedwater flow rate is one of the important MD parameters which effects permeate-flux as shown in Fig. 3.19. Increasing the feedwater flow rate results in increasing flux through the membrane pores. Increasing the feedwater flow rate leads to a reduction in the temperature and concentration differences between the feedwater bulk stream and membrane surface as a result of the increased conductive heat transfer coefficient in boundary layer (Hou et al., 2010). An experiment was performed to study the effect of different feedwater flow rates (50 - 200 L/h) on the permeate-flux. It was observed that the permeate-flux increased with the feedwater flow rate increase regardless of feedwater temperature for all types of MD. The temperature polarization was reduced as a result of increasing feedwater flow rate and increased driven force between both sides of the membrane (Yang et al., 2011). The increase in the feedwater flow causes an increase in the transmembrane flux and corresponding increase in permeate-flux. The relationship between the transmembrane flux and feedwater flow rate is linear until it reaches a certain limit (Alklaibi and Lior, 2005c). Increasing the feedwater flow rate reduces the resistance time which would, in turn, result in reduced conductive heat transfer while increasing the permeate-flux transfer through the membrane pores. The Reynold's number is also increased as a result of the increased flow rate (Pal and Manna, 2010). The feedwater flow affects membrane fouling which decreases at higher feedwater flow rates.

2.7.4 Effects of coolant flow rate

Coolant flow rate is one MD parameter that can affect conductive heat transfer. However, this effect is less pronounced than that of the feedwater flow rate in all MD configurations. The effect of the coolant flow rate is relatively low in AGMD systems, because of the air gap which reduces the conductive heat transfer between the sides of the membrane (Alklaibi and Lior, 2005c).

2.7.5 Effects of fluoride concentration

Feedwater concentration is an important factor which can affect permeate flux. Increases in the feedwater fluoride concentration result in decreased permeate flux through the membrane pores. Increases in feedwater fluoride concentration promote the formation of a fouling layer on the membrane surface, thereby decreasing the mass transport through the membrane pores. Use of feedwater with higher salt concentrations can eventually result in pore blocking (Warsinger et al., 2015). (Gryta, 2008) found that the permeate flux decreased as a result of increased feedwater salt concentrations during MD. In this study, experiments were performed to study the effect of different fluoride concentrations (6.6, 12.2 and 15.4 mg/L) on the permeate-flux. It was observed that the permeate-flux decreased when the fluoride concentration in the feedwater tank increased, regardless of the feedwater temperature. Clogging of the membrane pores due to high feedwater concentration of contaminants led to a decline in permeate-flux through the membrane (Gryta, 2008). Increased feedwater concentration led to decreased vapour pressure (Raoul's law) as a result of the accumulation of salts on the membrane surface. The formation of a fouling layer on a membrane surface increases thermal and hydraulic resistances and the extent of such an increase depends on the characteristics of the fouling layer (Tijing et al., 2015), (Curcio et al., 2010a).

2.8 Cost and Energy Efficiency

MD is a thermal process which depends on temperature difference, so most energy is consumed on the feedwater side. 50-70 °C is commonly applied at the feedwater side while the coolant side is typically 20-25°C, which is typically room temperature. The energy and cost of water produced are still considered as a challenge for MD when compared to other membrane processes such as RO (Al-Obaidani et al., 2008). (Al-Obaidani et al., 2008) studied the total cost of water production in DCMD and the result with heat recovery was $\$1.17/m^{-3}$, which was greater than the cost of water

production by conventional thermal processes such as multiple effect distillation (MED), i.e. around ($1.00/$m^{-3}$) for desalination plants with a capacity of 31,822 m^3/d. The energy consumption for different thermal desalination processes are: 51.7 kWh/m^3 for multistage flush distillation (MSF), 45 kWh/m^3 for multi effect distillation (MED) and 8 - 6.7 kWh/m^3 for RO (Avlonitis et al., 2003). Generally, reduction in the cost of water production in MD is mainly dependent on two factors, namely the type of feedwater source and the use of a lower grade but more cost effective alternative energy sources such as solar thermal or low grade geothermal.

2.9 Cleaning techniques

Different techniques have been used to decrease membrane fouling, including back flushing/backwashing and chemical cleaning (Gutman, 1987). However, these methods have many limitations. For example, frequent backflushing/backwashing can reduce the life time of the membrane. Chemical cleaning can be expensive and might damage the membrane as well as negatively affect its characteristics (Li et al., 2002b). Also, the system must typically be shut down for the membrane cleaning which also negatively impacts the cost efficiency of the process. Ultrasound can be successfully applied to remove fouling from the membrane surface. This technique has more advantages such as no chemicals are used and no shut downs are necessary (Chen et al., 2006).

2.9.1 Application of Ultrasound

Ultrasound is a longitudinal wave with frequency ranging between 16 kHz and 500 MHz (Thompson and Doraiswamy, 1999). Ultrasound waves are normally created by converting electrical or mechanical power into vibrational power using transducers. Three types of transducers are used for producing ultrasound waves based on three different physical principles: liquid-driven (liquid whistle), magnetostrictive and piezoelectric transducers (Povey and Mason, 1998). Ultrasound equipment is typically operated in two modes: continuous mode and pulsed mode. Ultrasound technology is affected by several factors such as system operating conditions, medium characteristics and design-related aspects (Thompson and Doraiswamy, 1999). The varied operating parameters of ultrasonic technology include power, frequency, treatment time and shape of the exciting waves. The medium characteristics that have an effect on ultrasound performance include medium viscosity, pressure, temperature and presence of solid or gas impurities.

2.9.2 Modelling of membrane Distillation

Several theoretical models have been developed to evaluate MD performance (Lawson and Lloyd, 1997). The target of those models was to estimate the temperature and concentration polarization coefficients, as well as to estimate the values of the permeate-flux based on membrane characteristics, module design and operation conditions (Mengual et al., 2004). This section briefly presents heat and mass transfer models.

2.9.3 Heat Transfer

Heat transfer is considered an important factor for all MD configurations, as MD relies on temperature differences, Fig. 2.15 shows the heat transfer mechanism across the AGMD module. Heat transfer is carried out in four steps: (1) heat flux from the feedwater solution to the liquid-vapour interface across the thermal boundary layer into the feedwater channel, (2) heat flux by conduction and latent heat of vaporization across the membrane, (3) heat transfer from the permeate side of the membrane to the condensation layer/film on condensation plate, and (4) heat transfer from the condensation film to the cooling liquid across the condensation plate and thermal boundary layer of the cooling liquid.

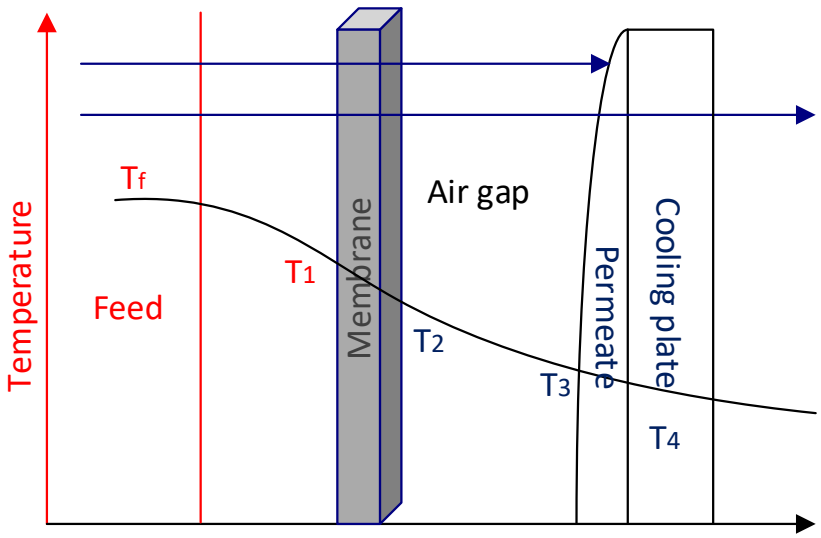

Figure 2.15: The schematic temperature profile in air-gap membrane distillation

2.9.4 Heat flux from the feedwater solution to the evaporation surface

The thermal boundary layer at the feedwater side of the membrane exerts resistance on the conductive heat transfer from the feedwater solution to the membrane surface which creates temperature difference. The effect of this layer is referred to as a temperature polarization effect. The temperature polarization coefficient (TPC) is used to quantify this phenomena:

$$TPC = \frac{T_{me} - T_{cf}}{T_h - T_c} \quad 2.1$$

Where T_{me} is temperature at the membrane surface, T_{cf} is temperature at condensation film, T_h is temperature at hot/feedwater bulk solution and T_c is the temperature at the cooling bulk liquid. The lower the *TPC* value, the higher the temperature polarization effect, and vice versa. The temperature polarization effect increases with the increase in feedwater temperature (Chernyshov et al., 2003). The thermal boundary layers depend on fluid properties, operational and hydrodynamic conditions (El-Bourawi et al., 2006).The heat flux Q from the feedwater bulk to the interface at the membrane side is described by (Bouguecha et al., 2003) and (Kubota et al., 1988):

$$Q = (h_{m+}\, n_w C_1)(T_{h-T_{me}}) \quad 2.2$$

Where h_m is the film heat transfer coefficient, n_w is the mass flux, C_l is the liquid specific heat capacity.

2.9.5 Heat flux by conduction and latent heat of vaporization

Heat transfer over the membrane is the total of the conductive heat transfer of the membrane material. The heat flux is described as:

$$Q = \frac{k_m}{d}(T_{me} - T_{mp}) + n_w \lambda\,; \quad 2.3$$

$$k_m = \varepsilon k_g + (1-\varepsilon) k_s \quad 2.4$$

Where k_m is effective thermal conductivity of the membrane (solid material and air in the pores), d is the membrane thickness, T_{mp} is temperature at the permeate/air-gap side of the membrane, λ is the latent heat of evaporation, ε is the membrane porosity, k_s is thermal conductivity of the solid material and k_a is the thermal conductivity of the air.

2.9.6 Heat transfer from permeate side to condensation plate

The total heat transfer can be described by:

$$Q_T = (\frac{k_g}{b} + n_w C_g)(T_{mp} - T_{cf}) + n_w \lambda \quad 2.5$$

Where C_g is the specific heat at a constant pressure in the gas phase of the water, n_w is the mass flux, λ is the latent heat of evaporation, k_g is the gas phase thermal conductivity and b is the air-gap width.

2.9.7 Heat transfer from the condensation film to the cooling liquid

From the condensation layer interface to the cold bulk liquid, the heat transfer rate can be described by:

$$Q = h_f (T_{cf} - T_{cp1}) - n_w C_l (T_{me} - T_{cf}) = \frac{k_p}{e}(T_{cp1} - T_{cp2}) = h_m (T_{cp2} - T_c) \quad 2.6$$

Where h_f is the heat transfer coefficient of condensation film, T_{cp1} and T_{cp2} are the temperatures of inner and outer side of the cooling plate, respectively; k_p and e are the thermal conductivity and thickness of condensation plate, respectively.

2.10 Mass Transfer

Mass transport of the volatile species occurs in three steps (El-Bourawi et al., 2006): (1) mass transport from the bulk feedwater solution to the membrane surface, (2) mass transport through the membrane pores, and (3) mass transport from the membrane surface to permeate bulk liquid. In the case of AGMD configuration, the mass transport is caused by diffusion due to the presence of the air-gap (Bouguecha et al., 2003).

2.10.1 Mass transport from feedwater solution to membrane surface

The high salinity feedwater solution has substantial contact with the membrane surface to give a strong chance for the mass to transfer through the membrane pores. Concentration of the solute at the membrane surface becomes higher than in the feedwater bulk due to mass transfer across the membrane. The increase in the solute concentration on the membrane surface creates a fouling layer which further reduces mass transfer through the membrane. The concentration polarization coefficient

(CPC) is used to quantify resistance within the fouling layer (El-Bourawi et al., 2006). It is defined as:

$$CPC = \frac{C_m}{C_b} \tag{2.7}$$

Where C_m is the concentration at the membrane side of the feedwater and C_b is the concentration at the bulk feedwater. The molar flux N_w of water through the concentration polarization layer is defined by (El-Bourawi et al., 2006):

$$N_w = CK_{wf} \ln\left(\frac{C_b}{C_m}\right) \tag{2.8}$$

Where C is the bulk total molar concentration, K_{wf} is the mass transfer coefficient of the volatile compounds through the concentration polarization layer.

2.10.2 Mass transport through the membrane

The mass transfer mechanism is controlled by three mechanisms: Knudsen diffusion, Poiseuille flow, and molecular diffusion or a combination of them, and the dusty-gas module is used as a general model describing the mass transport through the membrane (El-Bourawi et al., 2006). Mass flux is described by the following relation:

$$n_w = K\Delta P \tag{2.9}$$

Where K is membrane permeability and ΔP is the vapour pressure difference across the membrane.

$$n_w = M_w\left[\frac{K_{total}}{R}\left(P_{me} - P_{cf}\right)\right] \tag{2.10}$$

$$K_{total} = \frac{1}{\frac{1}{K_D} + \frac{1}{K_a}} \tag{2.11}$$

Where Mw is molecular weight of the water, P_{me} and P_{cf} are the partial pressure at T_{me} and $T_{cf,}$ respectively, R is the ideal gas constant, K_{total} is the total mass transfer coefficient, KD is the diffusive mass transfer coefficient through the membrane and K_a is the convective mass transfer coefficient through the air-gap.

2.11 Fouling effects in membrane distillation

Membrane fouling is a persistent problem affecting all types of membranes used in water treatment systems. Membrane fouling is predominantly caused by compounds present in feedwater, which can form a layer on the membrane surface or may block its pores. Usually, feedwaters with high salinity are more prone to membrane fouling (Warsinger et al., 2015). Membrane fouling effectively screens the membrane surface from the feedwater solution, which in turn reduces the permeate-flux through the pores, increasing thermal and hydraulic resistance. The degree of permeate-flux decline and corresponding increase in hydraulic resistance depends on the fouling layer characteristics (Tijing et al., 2015), (Curcio et al., 2010a). There are three basic categories of fouling in MD discussed in the following sections.

2.11.1 Inorganic salt scaling

Inorganic salt scaling can take place in MD as a result of alkaline, non-alkaline, and uncharged materials present in the feedwater solution (Al-Amoudi, 2010). These materials can impose a negative effect on permeate-flux due to scale precipitation and subsequent blocking of pores.

2.11.2 Scaling in membrane distillation

Scaling is a real problem in MD that occurs when the salt concentration in the feedwater solution is high. The increase in feedwater temperature and high vapour flux can cause scale precipitation, which blocks pores and reduces vapour flux. Scaling also causes membrane wetting, eventually leading to water passage through membrane structure (Warsinger et al., 2015), (Guillen-Burrieza et al., 2013).

2.11.3 Particulate and colloidal fouling in MD

Membrane fouling due to particulate and colloidal materials is another common problem in water treatment applications using membrane technologies. Particulate and colloidal fouling includes clay, silt, humic or melanoid type substances, debris and silica (Flemming et al., 1994). These materials are variable in size and are generally removed during pre-treatment processes. However, particulates and colloids with small particle sizes are not removed by existing pre-treatment technologies, and could be present in the membrane plant water supply. The most common particulate foulant is silica, which is usually found in water supplies in three forms: colloidal silica, particulate silica, and dissolved silica (or monosilicic acid) (Warsinger et al., 2015).

2.11.4 Biological fouling

Biological fouling or biofouling is one of the common fouling types occurring in MD. Biofouling includes bacteria and fungi deposition followed by biofilm formation and growth (Warsinger et al., 2015). The biofouling that occurs in MD is usually less severe than that observed in high pressure membrane processes such as NF, UF and RO (Gryta, 2002). In MD processes, biofouling leads to pore wetting, allowing the feedwater to pass through the membrane pores. In such cases, the quality of permeate is significantly decreased when wetting occurs (Warsinger et al., 2015).

2.12.1 MD fouling control and cleaning

Historically, multiple methods have been used to control fouling which occurs in MD processes. The current techniques for the control and mitigation of fouling comprise feedwater pre-treatment and membrane cleaning (Alkhudhiri et al., 2012a). Membrane fouling can also be reduced by designing new membrane modules with improved hydrodynamic conditions or changes in membranes' physicochemical parameters which would include repulsion of the foulant particles from the membrane surface (Gryta, 2008).

2.12.2 Pre-treatment

Pre-treatment of the feedwater before MD processes results in more stable membrane operation compared to MD processes without feedwater pre-treatment (Karakulski et al., 2006). Pre-treatment can lead to increased permeate-flux and salt rejection. Furthermore, MD operation after pre-treatment requires low pressure and energy. Without pre-treatment, membranes need to cleaned more frequently, which requires higher energy input and increases total operational costs.

2.12.3 Chemical techniques

Zeta potential is known as the potential at the surface of shear. Zeta potential is an important parameter in the evaluation of electrokinetic phenomena near membrane surfaces (Tijing et al., 2015). The value of zeta potential is determined by indirectly measuring the difference in potentials between the dispersion medium and the charged surface. The determination of zeta potential is used to estimate the surface charge of a membrane which dictates the possible interaction between the particles (foulants) and the membrane surface (Tijing et al., 2015). The mechanical integrity of a membrane is an important factor for its long-term performance. Tensile strength

is an important signal of how the membrane resists the stress associated with the MD operation before suffering permanent deformation or fracture. Tensile properties are known to be affected by fouling that can degrade or change the membrane structure when left untreated. Furthermore, extensive membrane cleaning negatively affects the mechanical lifetime of the cleaned membrane (Tijing et al., 2015).

2.13 Water sources

There are different sources of water such as seawater, brackish water, surface water and groundwater. In many cases, humans cannot drink directly from these sources unless the water is treated using various water treatment technologies to produce water which is of a high enough quality for drinking. The sources of water are as follows:

2.13.1 Sea water

The salinity of seawater is very high compared to the other mentioned water sources making seawater unsuitable for drinking unless it is desalinated. Concentration of dissolved salts in seawater is 300 times higher than in river water (Brown et al., 1995). Therefore, seawater treatment by high-pressure membrane technologies such as RO or thermal-based processes is energy-intensive and, as a result, costly.

2.13.2 Surface water

Surface water comprises water from streams, rivers, lake and wetlands. The treatment of surface water is generally more expensive compared to groundwater (Veley, 1992). Further, surface water sources are by several order of magnitude smaller than groundwater sources and their geographical distribution makes their availability limited. In addition, their fluctuating availability during the seasons does not provide a stable water supply.

2.13.3 Groundwater

Groundwater from shallow aquifers can provide a stable freshwater source not only to small scale single households but also to pilot-scale enterprises (which require large aquifers with good permeability). However, the deep aquifers are more costly to access due to drilling and maintenance of the wells. Compared to surface water, in many cases, groundwater does not require any pre-treatment.

However, in many areas groundwater is naturally contaminated, with trace metals due to rock/mineral dissolution into the groundwater.

These trace contaminants can also be of anthropogenic (industrial, agricultural) origin. Trace metal (loids) comprised of arsenic, uranium, cadmium, lead, antimony, etc., and halogens such as fluoride, can affect groundwater over large areas. The salinity of groundwater depends on location and is highly variable. The concentration of dissolved salts ranges from a few micrograms/L to a maximum of around 25,000 mg/L (Alkhudhiri et al., 2012a). However, in many cases groundwater quality is close to freshwater quality with only trace contaminants.

Table 2.1 Analysis of the RO reject stream water (RW) and natural groundwater (NW).

Characteristics	Concentration (mg/L) (RW)	Concentration (mg/L) (NW)
Ammonia-Nitrogen	<0.005	<0.005
$CaCO_3$	1,410	-
Chloride	2,900	900
Calcium	190	55
Magnesium	230	70
Sodium	2,070	550
Potassium	5.2	5.1
Nitrate	1.8	0.59
Nitrite	0.005	<0.005
Manganese (dissolved)	<0.001	-
Fluoride	0.51	0.09
Total nitrogen	0.58	0.67
Total organic carbon	<1.0	<1
Iron (dissolved)	<0.01	-
Barium	0.053	0.056
Solids (total)	1,900	1,900
Bicarbonate Alkalinity	-	324
Total Alkalinity	-	324
Total Sodium	730	550
Sulphate	140	150
Total Dissolved Solids	-	1,900
Silica (from Si)	-	34.3
Total Cations & Anions	-	1,932
Sum of Anions	4,270	1,250

The removal of these trace contaminants requires a low energy technology with simple design and low operational and maintenance needs, i.e. a low cost solution. This is especially important for the drinking water supply of small households or communities and/or for low-income regions in the developing world. Table 2.1 shows the water that has used in this study.

2.14 Liquid entry pressure (wetting pressure)

LEP is a significant membrane characteristic (Alkhudhiri et al., 2012a). LEP is the maximum limit of pressure that can be applied at the feedwater side of the membrane without membrane wetting occurring. Membrane wetting is a phenomenon which occurs when pressure is higher than the LEP is applied to the feedwater side of the membrane. Thus, causing water, rather than water vapour only, to be forced through the membrane pores. The characteristic of the membrane is very important in this stage because the LEP is different from one membrane to another. LEP depends on the pore size of the membrane and the feedwater solution (Alkhudhiri et al., 2012a):

$$\Delta P = P_f - P_p = \frac{-2B\gamma_l \cos\theta}{rmax} \qquad 2.12$$

Where P_f and Pp are hydraulic pressure on feedwater and permeate side, respectively, B is a geometric pore coefficient, γ_l is liquid surface tension, θ contact angle and r_{max} is the maximum pore size (Franken et al., 1987).

Increasing LEP aims to increase P_f so that more water vapour can pass through the membrane to the permeate side. A small value of the contact angle θ can increase the LEP, because the pressure that is applied during operation time can be focused on a small sized area of membrane. The pore size of the membrane has a significant effect on the LEP; i.e. increasing the pore size of the membrane leads to an LEP decrease. An increase in the geometric pore coefficient leads to an increase in LEP because the phase and size of pores affects the LEP. High liquid surface tension in the feedwater solution side also leads to a higher LEP (Alklaibi and Lior, 2005c).

3

CHAPTER 3: EFFECT OF AIR GAP MEMBRANE DISTILLATION PARAMETERS ON THE REMOVAL OF FLUORIDE FROM SYNTHETIC WATER

As freshly available water around the world becomes scarcer, schemes to reuse and rectify contaminated water sources are becoming a necessity. The implementation of conventional treatment processes increases stress on existing infrastructure resources, requiring significant quantities of energy and/or chemicals, including pre-treatment processes and ongoing maintenance. An unconventional alternative to these processes is air-gap membrane distillation (AGMD), an emerging technology delivering excellent rejection of contaminants over a broad range of operating conditions. While showing great promise, the size of membrane distillation systems in existing literature is not readily scaled to industrial levels. In this chapter, we present the results of our research in terms of permeate quality, rejection efficiency and scalability of a large laboratory scale AGMD system, with effective area of approximately 14 - 18 times larger than those presented in previous studies. This study found a large discrepancy in flux production when compared with small scale results, with experimental data analysed using normality and residual analysis tests. Statistical analysis of the AGMD process data provides insight into the key driving forces and interactions of feedwater temperature, concentration and flowrate on flux production. Results showed excellent rejection of contaminants (>98%) along with some fouling evident after approximately 25 hours of operation.

3.1 Introduction

Surface water supplies suitable for fresh water usage have steadily declined due to increases in population, industry and agriculture stressors. Globally more populations are becoming increasingly dependent on groundwater resources for domestic and agricultural purposes. This is especially true in inland areas, where seawater desalination is not a viable option. Groundwater is often available in suitable quantities, however the fluoride levels are unfortunately well above the safe drinking limits. According to the World Health Organization (WHO), the maximum permissible safe limit of fluoride in drinking water is 1.5 mg/L (Organization, 2004). Fluoride is a naturally occurring highly reactive metallic element found in groundwater. The removal of excess fluoride is necessary to protect both public health and the environment. Fluoride can find its' way into water sources through various pathways stemming from the food industry, pharmaceuticals, cosmetics, semiconductors, ceramics, electroplating, fertilizer, coal-fired power plants and from naturally occurring sources (Organization, 2004), (Ramdani et al., 2010). Small amounts of fluoride are useful for the mineralization of bones and teeth (Ramdani et al., 2010). Excess fluoride can result in dental and skeletal fluorosis and may also cause cancer, neurological, muscular, urinary tract and gastrointestinal problems along with lesions of the thyroid (Maheshwari, 2006), (Shih, 2005). Many researchers such as (Duong, et al., 2015, Kumar, et al., 2017, Eykens, et al., 2017, Kubota et al., 1988) have used larger scale systems, but none to our knowledge, have investigated them for fluoride removal. Moreover, different membrane configurations have been used by these researchers to study the performance of MD. Currently available technologies for the removal of fluoride are based on physical and chemical mechanisms. The techniques include: Coagulation with lime, alum, ferric hydroxide, ferric sulphate, sodium sulphate followed by flocculation; sedimentation and filtration; adsorption on activated carbon; ion exchange and reverse osmosis (Maheshwari, 2006), (Shih, 2005). These technologies have the following fluoride contaminant removal efficiencies: adsorption (80-90%), coagulation/ filtration followed by lime softening (18-33%); ion exchange (90-95%); and reverse osmosis (90-95%) (Maheshwari, 2006). Although the above-mentioned processes are efficient in treating a variety of affected waters, they require significant quantities of chemicals and energy to treat brackish waters contaminated with fluoride. These technologies are able to remove a high proportion of fluoride,

but they have some inherent limitations such as high energy consumption for processes such as reverse osmosis (Shih, 2005), high equipment capital cost and chemicals cost (Abejón et al., 2015). Other processes need pre-treatment to be effective, such as ion exchange (Piñón-Miramontes et al., 2003). By comparison, MD has several economic and environmental advantages by working at relatively low temperatures and pressures compared to traditional desalination processes like RO and similar treatments. This allows MD to have lower energy requirements and the inherent benefit of requiring fewer chemicals or pre-treatment processes (Gálvez et al., 2009). Another economic advantage of MD is the inherent low operating pressure and minimal maintenance requirements, as mechanical damage to MD membranes is significantly reduced compared to conventional techniques (Susanto, 2011).

MD is a non-conventional technology that may be a feasible alternative to remove contaminants from water such as fluoride. Limited research has been conducted on the feasibility of MD technology to remove fluoride from water. The few studies that have investigated fluoride removal from water have only been conducted on a very small scale (Boubakri et al., 2014), (Plattner et al., 2017). Fluoride removal on a pilot-scale has not been reported to our knowledge.

The MD process has four typical configurations: direct contact MD (DCMD); sweeping gas MD (SGMD); vacuum MD (VMD) and air-gap MD (AGMD). DCMD, SGMD and VMD have several disadvantages, namely high conductive heat transfer, running costs and higher energy consumption, respectively. AGMD is the configuration that has the lowest conductive heat transfer requirement as a result of having the air-gap between the membrane and condenser surfaces. AGMD also has better internal heat recovery, hence a lower energy requirement, making it our first choice for a pilot-scale plant (Xu et al., 2016).

The main objective of this chapter's research is to investigate the feasibility of the MD process for use in a pilot-scale treatment of fluoride contaminated water sources, with a focus on the effects of feedwater concentration, temperature, flow rate and membrane effective area on the vapour flux produced.

The influence of the membrane effective area on the productivity of flux was compared to previous studies to gauge the possibility of scaling up MD. Here, we present the results of the fluoride removal efficiencies using an AGMD process.

Thorough statistical analyses of the data was carried out to gain conclusive insights into the rate of flux produced for a range of concentrations, temperatures and flow rates of both feedwater and coolant.

3.2 Material and methods

3.2.1 Sample preparation

Synthetic water samples with a range of different contaminant concentrations were prepared using analytical grade sodium fluoride and subsequently used as the feedwater solutions. Three different masses of sodium fluoride were added to 30 L of distilled water to achieve fluoride concentrations of lower, equal to and higher than those concentrations found naturally in groundwater from South East Queensland, Australia, corresponding to 6.6 mg/L, 12.2 mg/L and 15.4 mg/L, respectively. After preparation, the respective sample solutions were added to the feedwater tank of the MD system to perform the experiments.

3.2.2 Experimental setup

A schematic representation of the air-gap MD (AGMD) setup is shown in Fig 3.16. The experimental setup contains two 33 L capacity, thermally insulated vessels, hot and cold, representing feedwater and coolant water respectively. Water flows from the feedwater and coolant tanks into the membrane cassette module through the 12 mm polyurethane hoses. These hoses are lagged with pipe insulation to reduce system heat losses. Two rotameters (variable area flow meter type 335, 4-20 mA output, 0-500 L/hr, supplied by Georg Fischer) measured the respective fluid flows from each of the two pumps (submersible model: 24 Volt DC-2.5 Amp, 4 L/min). Two additional centrifugal pumps are used to circulate both the hot feedwater and coolant water in a batch mode type operation. The main structure of the AGMD system was machined from aluminium and utilised 316 grade stainless steel fittings for connecting pipework. Seven industrial style temperature sensors (RTD Sensor - Pt100 type with pot seal) have been connected to the system (four in various locations on the feedwater side and three on the coolant side). Differential pressure transducers (Wika, type DP250, 0-250 mbar, 4-20mA o/p) have also been connected to the feedwater inlet and outlet sides in order to monitor membrane pressure conditions. In addition, two conductivity sensors (Microchem Conductivity Transmitter supplied by TPS) have been used in this study to measure the conductivity in the feedwater and permeate tanks (high range 0 - 1999 μS/cm and

low range 0 -19.99 µS/cm, respectively). An electronic balance with serial interface was used to record the AGMD permeate. All sensors were connected to a PLC controlled SCADA system for data logging and control purposes with local HMI.

To evaluate temperate effects, AGMD feedwater at temperatures of 50°C, 60°C and 70°C were tested while coolant temperature was kept at a constant 20°C. The range of feedwater temperatures has been selected as a result of AGMD investigations reported in literature. Moreover, working with feedwater temperatures higher than 70°C is risky for safety, but also at this range of temperatures MD cannot compete with the more mature MED process. Feedwater and coolant systems were continuously heated and cooled, to maintain consistent homogeneous solutions. In order to view flow rate effects, three different feedwater flow rates have been considered: 50 L/hr, 100 L/hr and 150 L/hr, whilst the coolant flow rate was kept constant at 200 L/hr. These values were selected to avoid membrane damage due to pressure effects, as well as having the added benefit of consuming less energy. The difference between the inlet and outlet feedwater temperature was no more than 2°C throughout the experiments.

The MD module consists of two thermal elements (feedwater and permeate) machined from aluminium, connected to a membrane module which was made of PTFE or similar material. While in practice for pilot-scale MD the heating and cooling sources would make use of waste or naturally occurring heat and cooling sources, we supplied these artificially in the laboratory to allow for a full range of adjustments. The feedwater compartment is connected to a heating system and was maintained at an elevated temperature, while the coolant compartment was connected to a refrigerated cooling system and maintained at a steady cooler temperature to maintain the temperature difference. The hydrophobic membrane was placed between the two compartments, able to make direct contact with the heated feedwater side while maintaining an air-gap between the membrane and coolant sides.

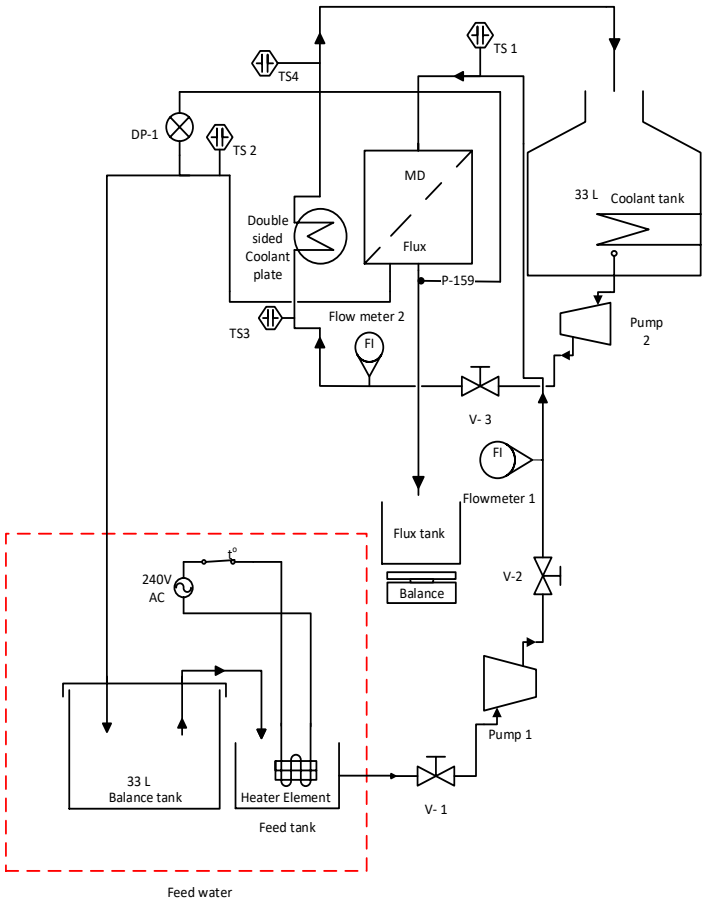

Item	Description
Pump 1	Submersible Model: LVMI3I 24 Volt DC-2.5 Amp flow rate 4 L/min
Pump 2	Submersible Model: LVMI3I 24 Volt DC-2.5 Amp flow rate 4 L/min
V1	Manual valve, control on the flow rate on/off heat side
V2	Manual valve, control on the flow rate, heat side
V3	Manual valve, control on the flow rate, coolant side
Flow meter 1,2	Variable area flow meter type 335 range 50-500 L/hr
TS	RTD Sensor -Pt100 with Pot Seal, Operating range: -75ºC to +350ºC, 3mm dia x 100mm long
DP-1	Wika, Differential pressure transmitter, Model: DP- 10 Range: 0-250 mbar
Chiller	Model: RC1, Volt: 240 V/50Hz,Range: 0-30ºC
Heater	Range 0- 90ºC
Ec-1	0 to 1 V DC or 0 to 5 V DC Outputs, k=1.0 Sensor....0 to 19.99 uS/cm
Ec-2	0 to 1 V DC or 0 to 5 V DC Outputs, k=0.1 Sensor....0 to 19.99 uS/cm
Ion Fl	0.02 to 19 000 mg/L F-, -0 to 60 °C (32 to 140 °F

Figure 3.15: Schematic representation of the Fluoride removal AGMD setup.

(a)

(b)

(c)

(d)

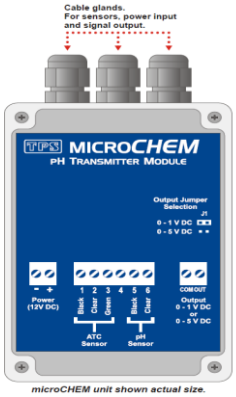

(e)

(f)

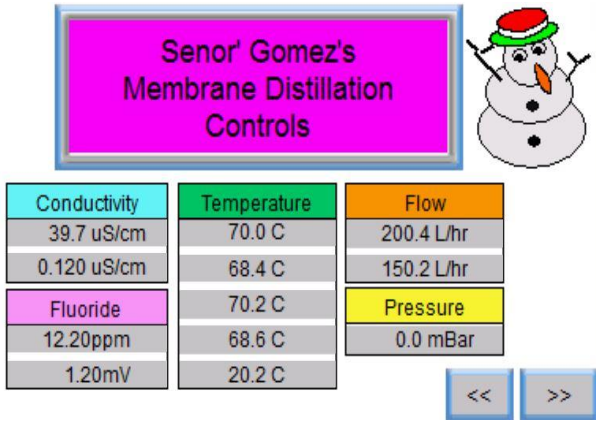

(g)

(h)

Figure 3.16: (a) AGMD system, (b & c) feedwater flow sensor, (d) ion selective electrode sensor, (e) conductivity transmitter, (f) mass balance. (g) system HMI screen, (h) Pt100 temperature sensor

3.3 Membrane characterisation

In this chapter's research, two commercially available membranes, PTFE laminated on typar 3161L spunbond polypropylene and PVDF membranes were supplied by Donaldson Filtration solutions. The specification of the membranes used are detailed in Table.3.2. The dimensions of the membrane cassette were as follows: 42 cm (length) × 1 cm (thickness) × 24 cm (width). Membranes were installed on both sides of the cassette with the total effective surface area of 0.2016 m^2. A membrane sheet was installed on either side of the cassette allowing feedwater to flow in the cavity formed between the two flat membrane sheets.

Table 3.2 Characteristics of PTFE and PVDF membranes from by Donaldson Filtration solutions.

Specification	PTFE membrane	PVDF membrane
Material	PTFE (Polytetrafluoroethylene)	PVDF (Polyvinylidene fluoride)
Support	Laminated on typar 3161L spunbond polypropylene	Without support layer
Pore size (µm)	0.3	0.3
Thickness (µm)	254	154
Porosity (%)	75	80
Effective area m^2	0.2016	0.2016
Contact angle (°)	114	85

3.4 Fluoride removal measurement

Fluoride removal effectiveness was measured by using an ion selective electrode (ISE121560, supplied by TPS) with fluoride ion measurement linear range of 0.02 mg/L to 19 000 mg/L and a response of -57 mV/decade with and error of +/-3 mV at 25°C. The fluoride ion sensor was installed in the inlet pipework of the permeate tank to allow online measurement.

3.4.1 Fluoride measurement error analyses

The fluoride probe was used to measure the fluoride concentration in the feedwater side of the system and to give an indication of the purity of the resultant permeate flux. As the concentrations used were quite low there was significant error in the fluoride measurements made with the Fluoride probe, especially when testing the permeate. In a typical case we were wanting to know if the rejection ratio was better than 98%. For a feedwater of 12.2mg/L the error in was +/-3mV for a -57mV output change between 2 and 20mg/L giving an error of +/-1mg/L, similarly for the reject water we are looking for concentrations of around 0.2mg/L so following the above approach for the 0.2 to 2 mg range we calculate an error of +/- 0.1mg/L at the lower range. As we needed better accuracy than this, we utilised the fact that EC can also be used to determine the rejection ratio, as we had a synthetic solution of fluoride and no other ion species present. The higher and lower ranges were both measured with a k = 0.1 type sensor (specifications are given in appendix A and B) and microchem unit in the 0 to 20μS range.

For the lowest range usage at 6.6mg/L in the feedwater the error is +/- 1mV for a 1V output of 20 μS/cm or 12.8 mg/L, giving an error of +/- 0.0128mg/L. For typical figures of 98% rejection this would mean a permeate concentration of 0.132mg/L to be measured within +/-10% in this range. Allowing for this measurement uncertainty, recorded values of the lowest concentration, and therefore the highest error of 0.064 mg/L +/- 0.0128 mg/L or (0.0512 to 0.0768 mg/L) or 98.8 - 99.2% were obtained, for simplicity shown as >98%.

3.5 Statistical analyses

Minitab software version 17 (Minitab Inc., PA, USA) was used in to measure the normality of experimental errors, interaction of operating parameters, and provide surface and contour plot interpretations of the results. The nominal operating parameters investigated are fluoride concentration, feedwater temperature and flow rate. A factorial design of 2^3 was applied in the experimental work. Three levels of each flow rate and temperatures of 50, 100 and 150 L/hr and 50, 60 and 70°C respectively were tested. The coolant flow rate and temperature were fixed at 200 L/hr and 20°C, respectively. Each experiment was repeated three times to ensure repeatability. The response of the permeate-flux for each scenario was also recorded.

It is important to note here that only brief statistical analyses were applied in this research to determine the significance of main and interactive effects on responses. This included studies of normality for the obtained data and producing surface plot figures for responses with the various combinations of factors' effects.

3.6 Effects of feedwater temperature

Figure 3.18 shows the effect of feedwater temperature ranging from 50°C to 70°C on the permeate-flux using PTFE and PVDF membranes. The feedwater temperature decreased by only 2°C between the inlet and outlet compartments of the AGMD system. As expected, an increase in feedwater temperature resulted in an increase in permeate-flux for both membranes tested. Feedwater inlet temperature plays an important role in the AGMD process due to its' impact on the temperature difference between either side of the membrane, i.e. causing increased trans-membrane vapour pressure leading to a corresponding net increase of vapour driving force.

The permeate flux achieved on PVDF membrane was slightly higher than that on PTFE membrane. However, these fluxes are 50% lower than what has been previously reported in small scale study (Warsinger et al., 2015). There are several proposed reasons behind the lower than expected flux obtained in our research. Firstly because of the larger effective area of the membrane used (42 cm x 24 cm for each of 2 sides in a cassette), around 18 times larger than the membrane used by (Eykens et al., 2017). There was more conductive heat transfer loss through the membrane surface creating a much lower transmembrane temperature difference and therefore lower flux. Moreover, the pore size of the membranes used in this study is 0.3 μm which is smaller than those used in previous studies (0.45 μm), this was also a logical reason for the lower flux output, as increasing the pore size results in an increase of the water flux across the membrane (Xu et al., 2016). The membranes used in this study also have a support layer which might be another reason for the lower than expected flux, the use of a support layer has been shown to decrease flux (Xu et al., 2016). Increasing the effective area of the membrane consumes higher energy due to the resulting conductive heat transfer. It should also be noted that in a pilot-scale system a higher feedwater flow is required to achieve the same flux level because of the longer residence time of the feedwater. The main reason behind the lower permeate-flux of the PTFE membrane compared to the PVDF membrane is that it has a higher thickness of 254 μm compared to 154 μm of the PVDF, as well

as having a lower porosity of 75% compared to the 80% porosity of the PVDF membrane. PTFE material was selected in this study as a model membrane due to its low cost and ready availability.

By comparison with smaller systems, the longer residence time creates a lower transmembrane vapour pressure and hence, lower flux per unit area was obtained (Francis et al., 2014). The relatively low permeate-flux of 0.5 kg/hr·m^2 was obtained using the pilot-scale modules (42 cm x 24 cm in a cassette design) compared to higher fluxes obtained using lab-scale modules. This poor performance is one of the major reasons for delaying the commercialization of the MD process.

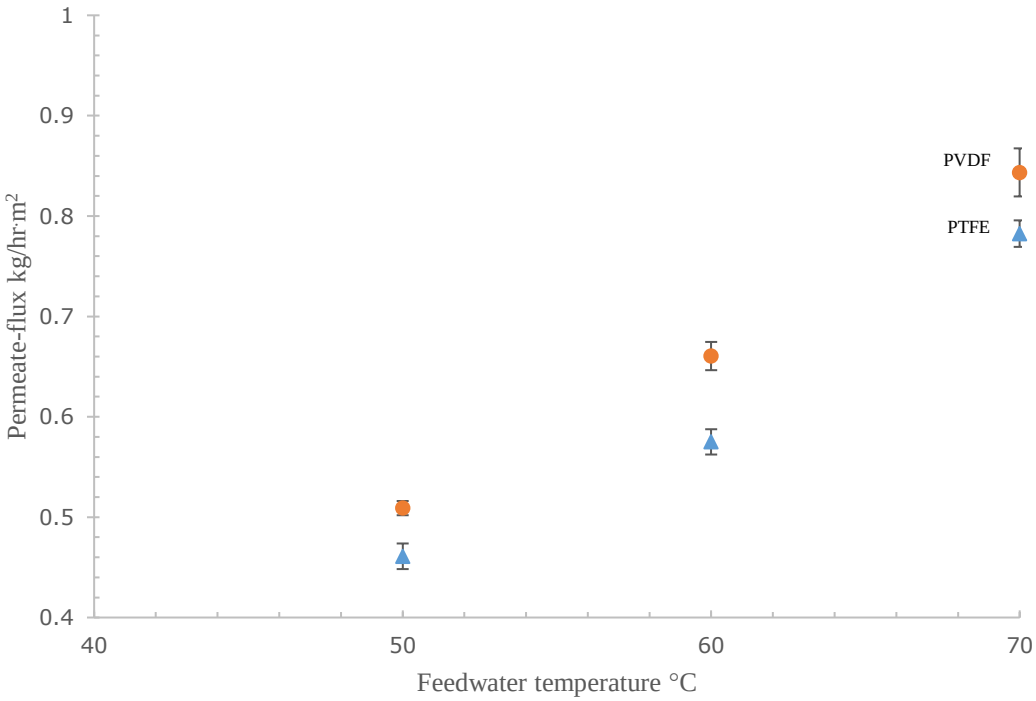

Figure 3.17: Effect of feedwater temperature on permeate flux, PTFE and PVDF membranes. F- = 6.6 mg/L, feedwater flow = 150 L/hr, inlet coolant temperature = 20 °C.

3.7 Effects of feedwater flow

Figure 3.19 shows the effects of the feedwater flow rate (50 L/hr, 100 L/hr and 150 L/hr) on the permeate-flux for PTFE and PVDF membranes. It appears that a significant increase of the feedwater flow rate from 50 L/hr to 150 L/hr results in only a 33% increase in the permeate-flux, a lesser effect than those presented in other studies which is the permeate flux increased from 0.8 kg/h.m^2 to 1.5 kg/h.m^2 when the feedwater flow increased from 50 to 150L/h. (Alsaadi et al., 2013).This is most likely due to the relatively large membrane surface area used in our experiments leading to higher residence time and relatively small ΔT, as discussed previously.

Another reason is that temperature polarization was reduced, because of increased feedwater flow rate and increased driven force between both sides of the membrane (Yang et al., 2011, Alsaadi et al., 2013, Alklaibi and Lior, 2005d, Yarlagadda et al., 2009). Temperature polarization effect reduce, and the thermal boundary thickness decreases as a result of increase the feedwater flow rate so the permeate flux increases (Alkhudhiri et al., 2012a, Martínez-Díez and Vazquez-Gonzalez, 1999a). Izquierdo-Gil (Izquierdo-Gil et al., 1999) reported that increasing the feedwater flow lead to decreased temperature and concentration polarization. The effect of flow rate on water vapour flux is strongly effected by membrane length (Alsaadi et al., 2013). The linear relationship between the transmembrane flux and feedwater flow rate occurred up to a certain limit using similar modules (Alklaibi and Lior, 2005b). Increasing the feedwater flow rate leads to a reduced temperature and concentration differences between the feedwater bulk stream and membrane surface (TP and CP). This is a result of the increasing conductive heat transfer coefficient in the boundary layer (Hou et al., 2010).

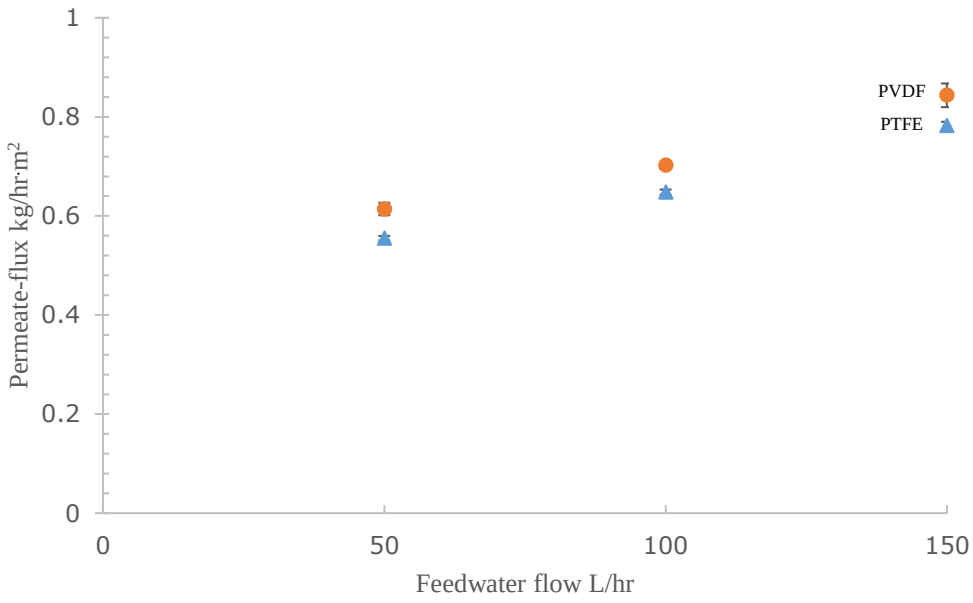

Figure 3.18: Feedwater flow-rate effects on permeate flux for PTFE and PVDF membranes.

3.8 Effects of fluoride concentration and rejection

Figure 3.20 shows the effect of fluoride concentration (6.6 mg/L, 12.2 mg/L and 15.4 mg/L) on fluoride rejection and permeate-flux production for PTFE and PVDF membranes. It is clearly shown that the descending gradient of the permeate-flux is more severe than the descending trend of the concentration for both PTFE and PVDF membranes. Several authors, e.g. (Gryta, 2008) found that the vapour flux decreased due to the increased salt concentration present in the feedwater. Increasing the fluoride concentration in the feedwater leads to an increased fouling layer on the membrane surface, which can cause a decrease in the mass transport through the membrane pores. This decrease is largely due to the high fluoride concentration in the feedwater solution leading to membrane pore blockage (Warsinger et al., 2015). Moreover, increases in the salinity of the feedwater lead to decreases in the vapour pressure, as discussed above.

Membranes with 0.3 µm pore size used in this study provided higher rejections of fluoride, but the fouling layer can form more quickly comparing to membranes with larger pore sizes and this is an additional reason for the low flux production rates. There are several factors that can affect the vapour flux at increased feedwater concentration of fluoride, such as concentration and temperature polarizations on the membrane surface (Banat and Simandl, 1994). Increasing the feedwater concentration also results in a corresponding decrease in vapour pressure on the membrane (Xu et al., 2016).

The increased fluoride concentration in the feedwater showed no effect on the rejection of fluoride for either membrane, with the rejection of fluoride being stable at around 98%, for both membranes over all of the different operating conditions. This finding is in agreement with results reported by (Hou et al., 2010) who investigated the removal of fluoride from groundwater using a DCMD process with a PVDF membrane. The advantage of using MD is the combined high flux production accompanied by high rejection of contaminants, because of the selective mass transfer of water vapour across the MD membrane. Other advantages of this process are the low electrical and thermal energy required during operation when compared to other thermal processes (Camacho et al., 2013). Another economic advantage in AGMD's favour is less damage of the membrane compared to conventional high pressure techniques (Susanto, 2011) and no requirement for chemical addition or pre-treatment (Gálvez et al., 2009).

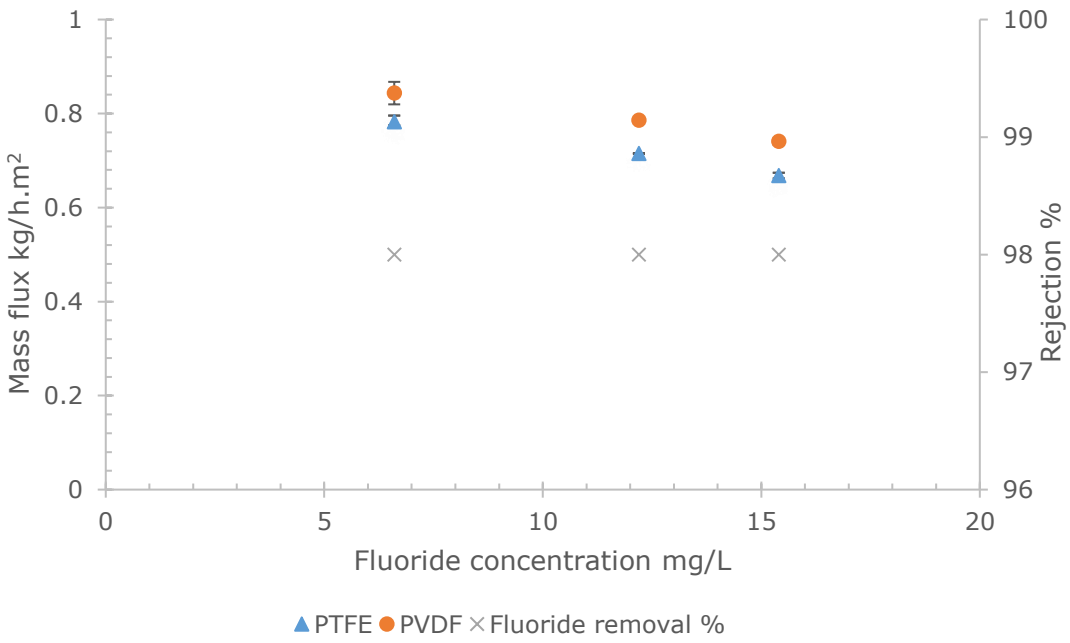

Figure 3.19: Effect of fluoride concentration on permeate flux and fluoride rejection for PTFE and PVDF membranes. Feedwater flow rate = 150 L/hr, inlet feedwater = 70°C, inlet coolant = 20°C.

3.9 Scalability of results

Figure 3.21 shows the effect of membrane effective area (0.2016 m^2) on the permeate-flux, compared to other studies using smaller effective areas of 0.005 m^2 (Alsaadi et al., 2015), 0.0108 m^2 (Eykens et al., 2017) and 0.0143 m^2 (Alkhudhiri et al., 2012). at a feedwater temperature of 60°C. In this study, the effective area of the membrane has been a focus, other factors are considered, but these are themselves influenced by the effective membrane area. For example, the effect of feedwater temperature, coolant temperature, feedwater flow rate and coolant flow are not independent of effective area. When the effective area becomes larger significant side effects com into play. Overall, these effects result in a lower permeate flux per m^2. The removal of fluoride in all previous studies, including in our own study is >98%. However, since all other studies have used AGMD module configurations, where produced water vapour is mixed with the coolant (dilution effect), we conducted our study using AGMD module (collection of pure water vapour) under similar operating conditions and membranes for a better accuracy. In addition, it is important to mention that despite the lower flux obtained in our study due to the larger membrane surface area and module configuration used (see discussion in previous sections) compared to the other studies, the fluoride removal rate was still consistently very high (Fig. 3.21).

The flux production rate decreases with a corresponding increase in the membrane effective area. Increasing the effective area leads to an increase in heat loss, which resulted in a decreased driving force, especially from the feedwater side of the AGMD module. Increasing the effective area from 0.005 m^2 to 0.0108 m^2 resulted in a permeate-flux decrease from 4 $kg/hr{\cdot}m^2$ to 2.5 $kg/hr{\cdot}m^2$. Increasing the effective area from 0.0108 m^2 to 0.0143 m^2 resulted in more decrease in permeate-flux which went from 2.5 $kg/hr{\cdot}m^2$ to 2 $kg/hr{\cdot}m^2$. In this study the effective area is 14 times larger than the area of membrane used by (Alkhudhiri et al., 2012) which results in more heat loss through the membrane surface and much lower trans-membrane temperature difference, hence producing less flux (Francis et al., 2014).

As previously discussed, there are several other reasons behind these lower flux production rates such as different types of membrane materials, pore sizes, porosities, and thicknesses. In this study, the PTFE membrane has a higher thermal conductivity, which results in a correspondingly lower flux production rate. Membrane materials with a high thermal conductivity show a lower thermal resistance, which means an increase in the conductive heat transfer through the membrane, leading to a decrease in the water vapour production (Alklaibi and Lior, 2007).

Increased membrane pore size also leads to increased water flux, however the thickness of the membrane has little effect on the permeate-flux production (Xu et al., 2016). All of these reasons have minor effects on the permeate flux production, while the largest effect can be attributed to the membrane effective area used in this study. According to our results, the difference in permeate-fluxes between both membranes is only 6%, with the PTFE membrane suffering slightly from the inclusion of a support layer. This again confirms that the lower permeate-flux obtained in this study is the result of the effective area of the membrane used, thereby highlighting the challenge in scaling up this process. The large variation of permeate flux results using different module sizes led us to perform normality tests, residual analyses and diagnostic statistics using the obtained experimental data to better understand our results.

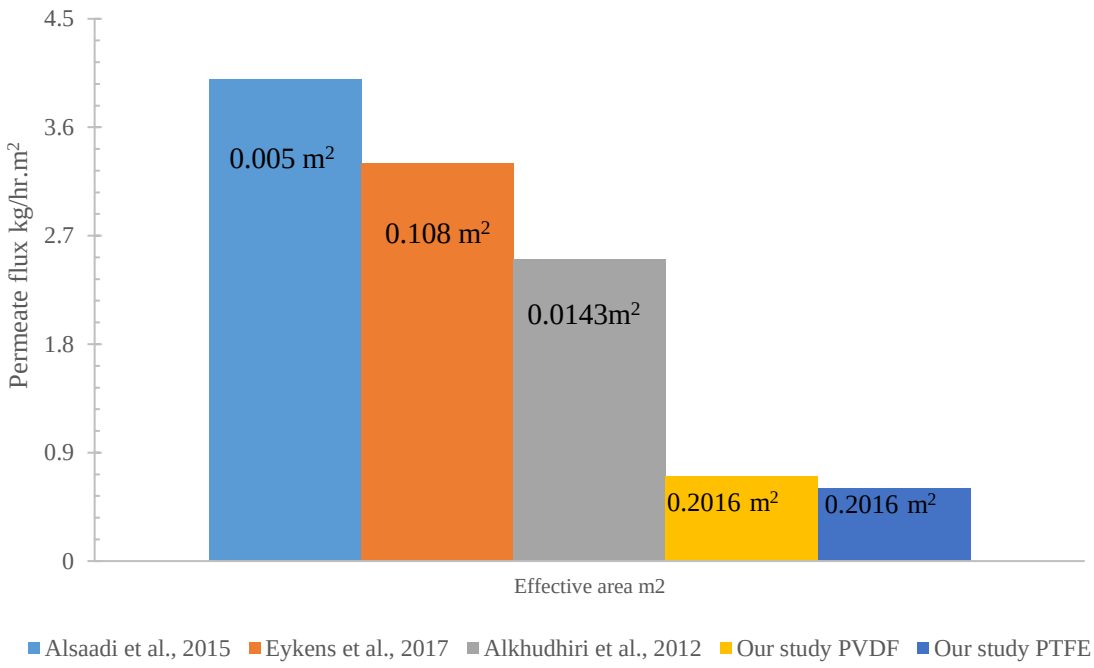

Figure 3.20: Effect of membrane effective area and other properties on permeate flux.

3.10 Normality tests and residual analysis of the experimental data

It is important to check the normality of the experimental errors for fluoride removal data with both PTFE and PVDF membranes through a number of diagnostic tests prior to commencing any statistical analyses on the experimental data to ensure the repeatability of the observations (Minis, 2010). If the errors are normally distributed, further statistical analysis can be conducted on the experimental data with no additional treatment required (Montgomery, 2017). Figure 3.22 shows the normal probability plot for both PTFE (A) and PVDF (B) membranes. It is clear from these figures that the errors are normally distributed, illustrated by the residual points being very close to the fitted regression line (Ruiz Espejo, 2006). The residuals frequency of occurrence being almost bell-shaped, in Fig 3.22 (c) and (d), provides additional evidence for the resulting normal distribution of experimental errors (Ranjan et al., 2009).

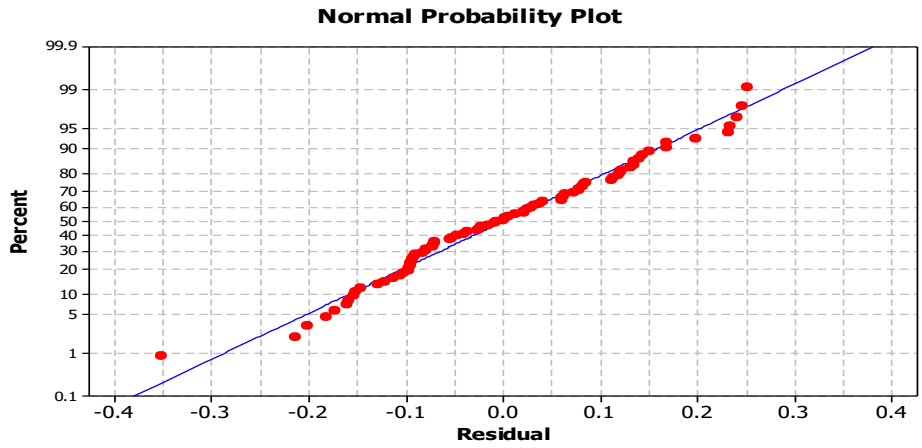
Normal Probability Plot
Percent
99.9
99
95
90
80
70
60
50
40
30
20
10
5
1
0.1
-0.4
-0.3
-0.2
-0.1
0.0
0.1
0.2
0.3
0.4
Residual

(a)

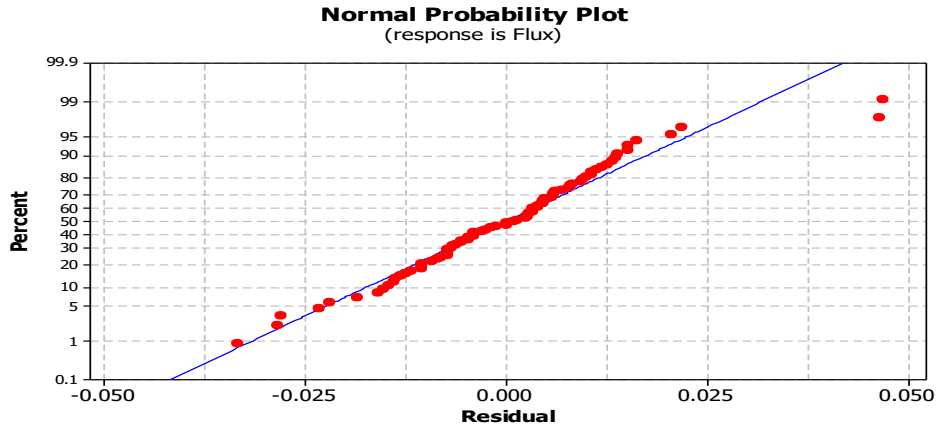
Normal Probability Plot
(response is Flux)
Percent
99.9
99
95
90
80
70
60
50
40
30
20
10
5
1
0.1
-0.050
-0.025
0.000
0.025
0.050
Residual

(b)

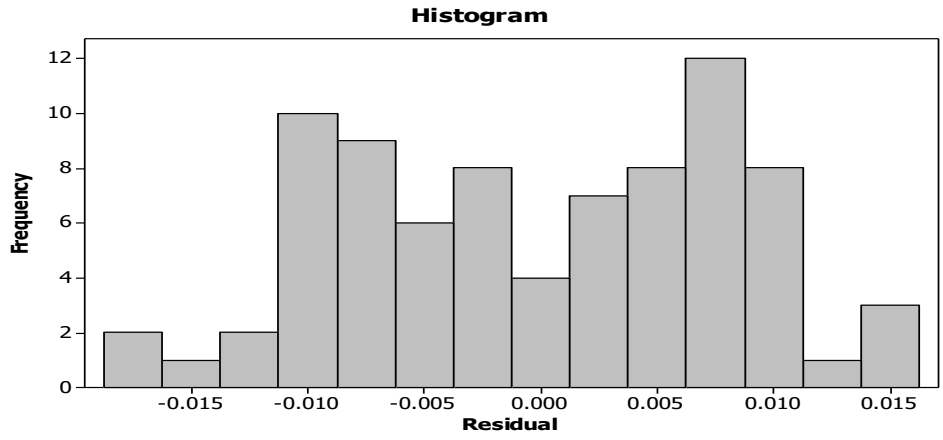
Histogram
Frequency
12
10
8
6
4
2
0
-0.015
-0.010
-0.005
0.000
0.005
0.010
0.015
Residual

(c)

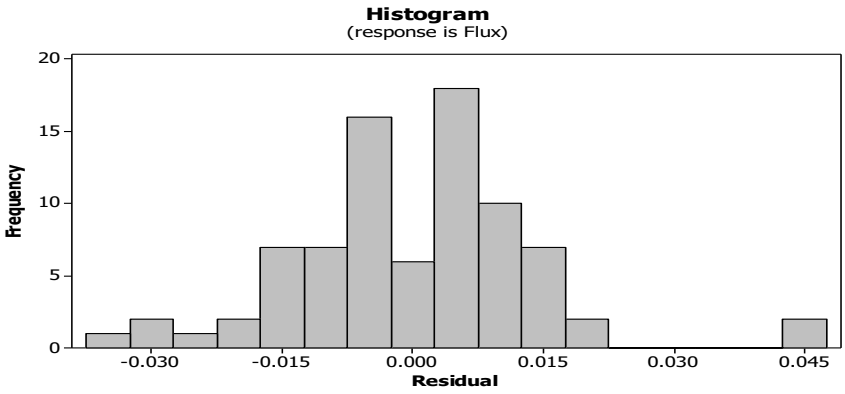

(d)

Figure 3.21: Normality test figures; (a) and (b) normal probability plot and (c) and (d) residual vs. frequency plot for PTFE and PVDF membranes, respectively.

It is also clear that the order in which the experiments were conducted had no effect on the distribution of errors as illustrated by the random variation of the residuals around zero in Fig 3.23 (a) and (b) (Trinh and Kang, 2010), (Al-Juboori et al., 2015a). Further diagnostic statistical tests were conducted on the residuals of fluoride removal using both PTFE and PVDF membranes data to explore time-related effects on error distribution and to verify the random distribution of the errors throughout the experiments. The external effects such as experimenter performance and conditions of the experimental environment had no noticeable effect on the experiments and measurements. The random distribution of the residuals vs. fitted values on both sides of zero suggests that the error was randomly distributed throughout the experiments (Venkatesan et al., 2015).

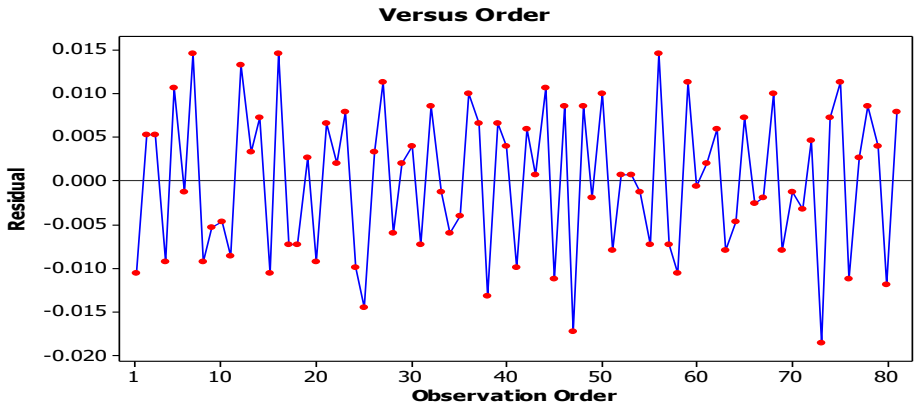

(a)

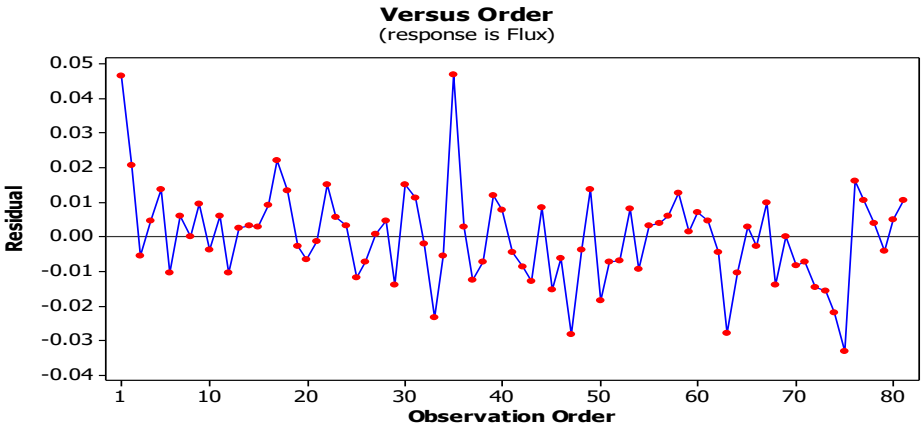

(b)

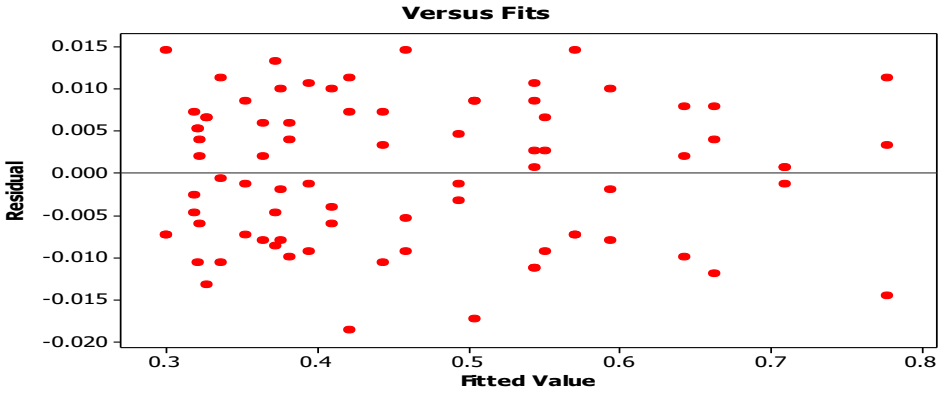

(c)

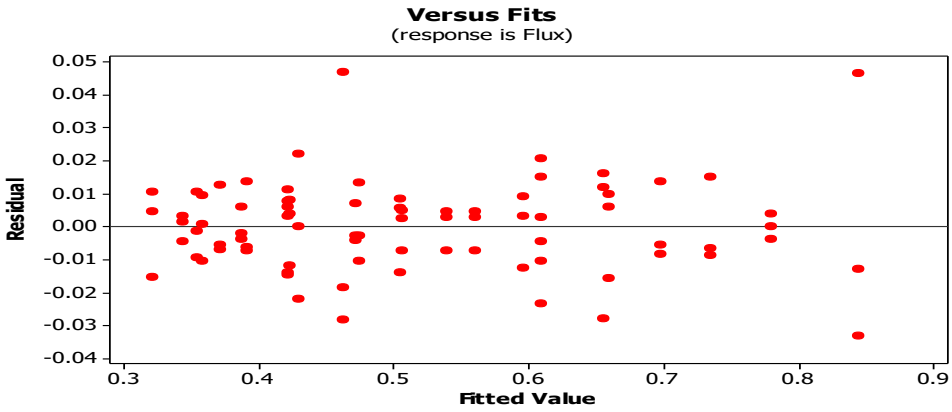

(d)

Figure 3.22: Residual distribution vs: (a) and (b) observation order, and (c) and (d) fitted values for PTFE and PVDF membranes, respectively.

3.11 Main effects and interactions of operating parameters

The significance of operating parameter effects and their interactions on permeate-flux using both PTFE and PVDF membranes are illustrated in the analysis of variance (ANOVA) in Table 3.3. The significance criterion (P-value) was set as 0.05. Any change in permeate-flux percentage of ≤0.05 is regarded as significant, otherwise the change is regarded as insignificant. It can be noted from Table 3.3 and table 3.4 that all operating parameters and their interactions had a significant effect on permeate-flux percentage except for flow × concentration and flow × concentration × temperature using PVDF which was found to be insignificant. All parameters and their 2-way interactions of feedwater temperature × feedwater flow and feedwater temperature × fluoride concentration had very significant effects (P-value = 0.005), and also the 2-way interaction of feedwater flow × fluoride concentration and the 3-way interaction of feedwater temperature × feedwater flow × fluoride concentration, were significant at P-values of 0.005.

Table 3.3 Analysis of Variance for flux, using adjusted SS for tests using PTFE membrane.

Source DF	**Seq SS**	**Adj SS**	**Adj MS**	**F**	**P**
T	2 0.827723	0.827723	0.413862	3995.93	0.000
F	2 0.085708	0.406799	0.203399	1963.87	0.000
C	2 0.085708	0.085708	0.042854	413.77	0.000
T*F	4 0.045240	0.045240	0.011310	109.20	0.000
T*C	4 0.009023	0.009023	0.002256	21.78	0.000
F*C	4 0.002736	0.002736	0.000684	6.61	0.000
T*F*C	8 0.005400	0.005400	0.000675	6.52	0.000
Error	54 0.005593	0.005593	0.000104		
Total	80 1.388222				

Table 3.4 Analysis of Variance for flux, using adjusted SS for tests using PVDF membrane.

Source DF	**Seq SS**	**Adj SS**	**Adj MS**	**F**	**P**
T	2 0.936674	0.936674	0.468337	1716.07	0.000
F	2 0.503095	0.503095	0.251548	921.72	0.000
C	2 0.119787	0.119787	0.059893	219.46	0.000
T*F	4 0.040242	0.040242	0.010061	36.86	0.000

T*C	4 0.005627	0.005627	0.001407	5.15	0.001
F*C	4 0.000918	0.000918	0.000230	0.84	0.505
T*F*C	8 0.004437	0.004437	0.000555	2.03	0.060
Error	54 0.014737	0.014737	0.000273		
Total	80 1.625518				

3.12 Surface plot interpretations

The surface contour plots were drawn by varying two factors and fixing the third. Surface plots provide a valuable tool not only for visual inspection of the response behaviour, but also for quick identification of the optimum parameters for the permeate-flux (Boubakri et al., 2014). The permeate-flux with various pairs of experimental parameters are illustrated in Figure.3.24. Generally, the figure shows that the flux pattern for both membranes is almost identical for various factors, such as the combination of concentration vs flux, where the PTFE membrane had almost a constant flux with different concentrations while the PVDF membrane showed a slight descending trend with increasing concentration. The similarity in the flux pattern shown in Fig 3.20 along with the results presented in Fig 3.20 suggests that the material type of the membranes used in this study has insignificant effect on its overall productivity. Figure 3.24 (a) illustrates the response of permeate flux to the change of feedwater temperature and feedwater flow while keeping the feedwater concentration constant. The permeate flux of PTFE and PVDF membranes clearly increased when feedwater flow and feedwater temperature were increased. Figure 3.24 (b) illustrates the response of permeate-flux to changes in feedwater temperature and fluoride concentration while keeping feedwater flow constant. The permeate-flux with PTFE and PVDF generally increased with increasing temperature. Figure 3.24 (c) illustrates the response of permeate-flux to the change of feedwater flow and fluoride concentration while keeping the feedwater temperature constant. For both membranes the permeate-flux increased when the feedwater flow increased and decreased accordingly when the fluoride concentration increased.

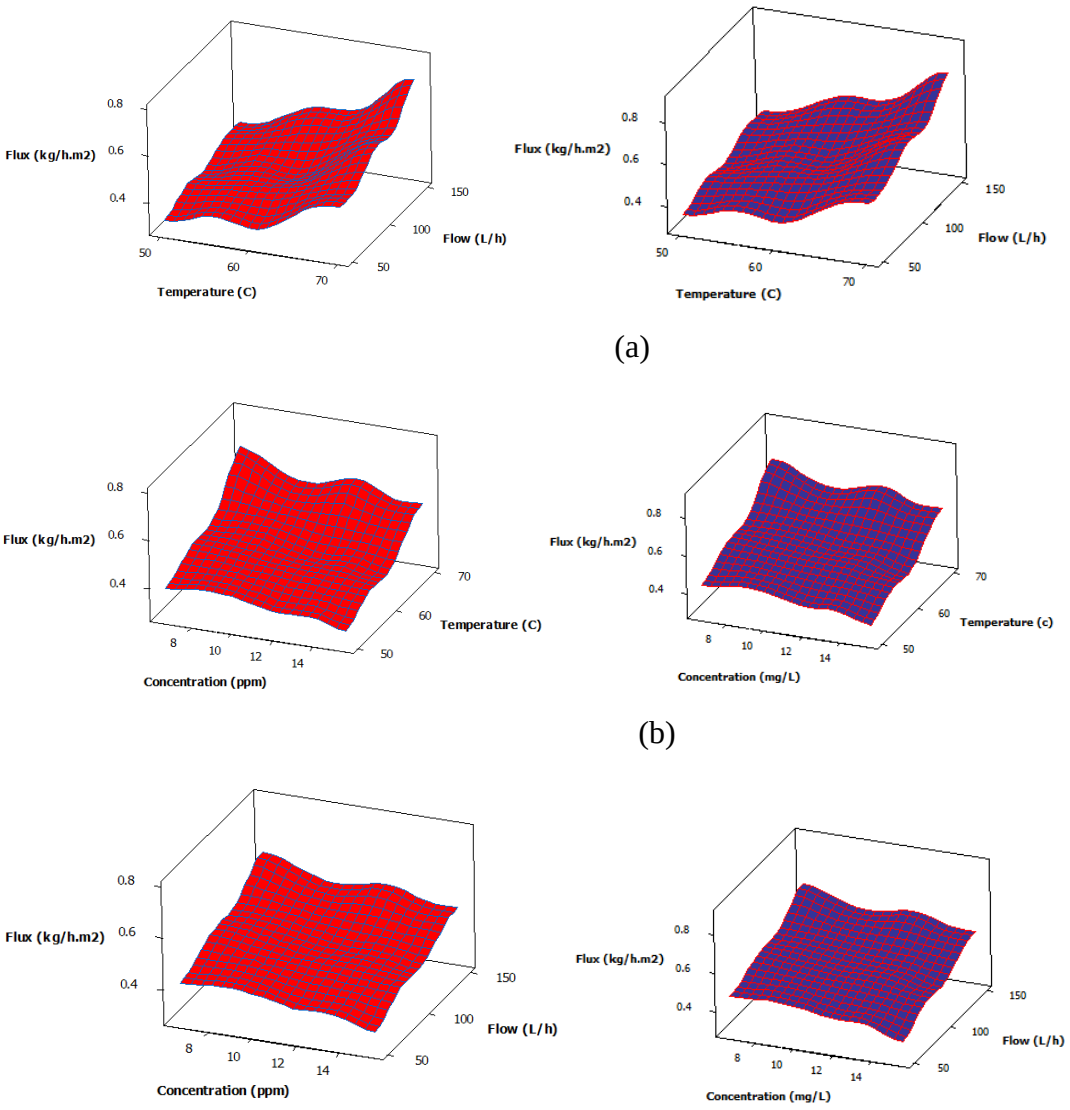

Figure 3.23: Surface and contour plots of permeate-flux (kg/hr.m2) at different feedwater temperatures, feedwater flow rates and fluoride concentrations: a) feedwater temperature and feedwater flow, (b) feedwater temperature and fluoride concentration and (c) feedwater flow and fluoride concentration for both PTFE (right) and PVDF (left) membrane.

3.13 Membrane surface characterization

The SEM pictures presented in Fig 3.25 show clear signs of fouling on the membrane surface as a result of 25 hours of fluoride removal. This fouling is likely the cause of the slight flux decay, shown in Fig 3.20. A high permeate-flux will inevitably create higher temperature polarization and concentration polarization (Alsaadi et al., 2014). The solute will then tend to precipitate on the feedwater side of membrane surface. In this synthetic feedwater solution, the percentage of solute is relatively low, thus the precipitation due to concentration polarization may be considered insignificant. Decreases in the flux during this 25 hrs period were very low, at around 25% as it is a short period. The reason behind this low reduction is because the feedwater concentration which have used were very low. The concentration of the feedwater flow was contained 6.6, 12.2 and 15.4 mg/L for all experiments.

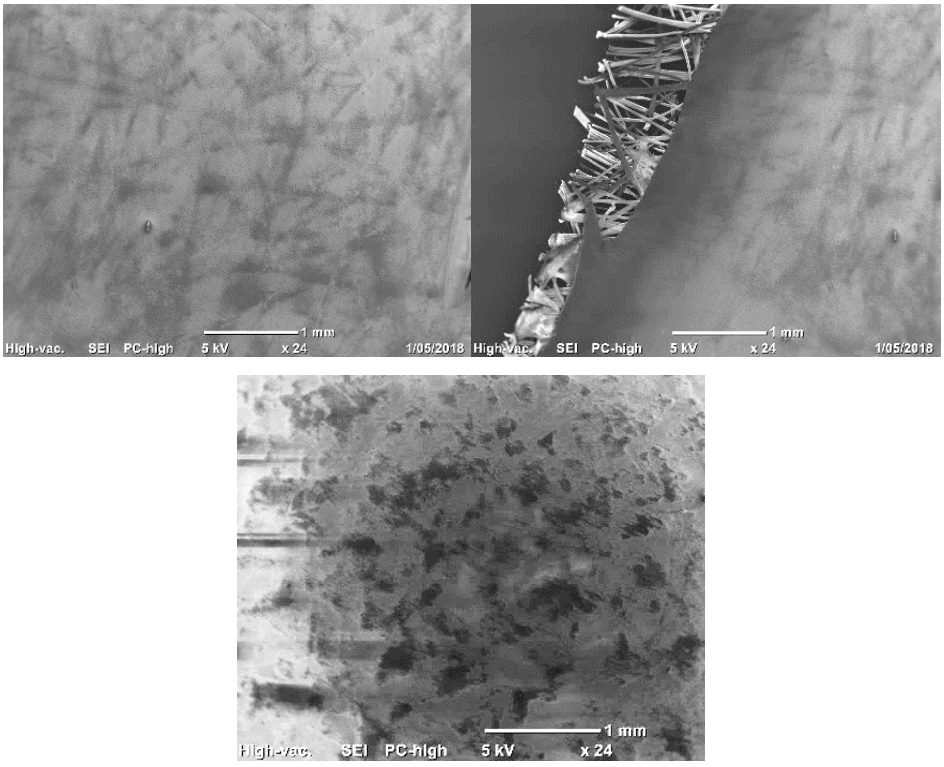

Figure 3.24: SEM images of the unused PTFE (Left), unused PTFE with support layer (middle) and used PTFE (right) membranes showing the fouling layer covering the membrane surface. (PVDF is not available).

3.14 Fluoride rejection estimation and measurement errors

The rejection ratio is defined as the component of contaminants blocked from transmission through the filtration process divided by the total present in the feedwater.

In order to quantify the process an ion selective fluoride probe was used to measure the feedwater concentration of the synthetic stock solution. This probe was a TPS brand uniprobe sensor with nominal linear range of 1.9 to 19000 ppm F. This probe was directly connected to the PLC analogue module in the SCADA system for display of feedwater concentration and recording purposes.

In addition to the fluoride probe the EC of both the feedwater and reject streams were measured by type k0.1 and k10 TPS brand EC sensors, fed into a Microchem transmitter unit and this analogue signal fed into the SCAD system.

3.15 Chapter summary

This study has determined and statistically validated the key factors influencing flux production in a large laboratory scale, air-gap membrane distillation unit. The analysis also confirms which effects are significant and this has provided greater insight into the mechanics of the process. It was noted that flux production did not scale linearly from previous work as a result of changes in operational parameters, which have been shown to have a strong effect on flux production. The permeate-flux of the two membranes made of different materials was different mainly due to their inherently different thicknesses, materials and porosities. Fouling of the membranes was observed after approximately 25 hours of production leading to a decrease in permeate-flux, but no pore wetting has been observed. Use of fluoride concentrations matching those naturally found in local water sources achieved fluoride removal 98% in all experiments. Theoretical modelling of the fouling process and remedial methods of membrane cleaning are under investigation and will be reported in following chapters.

4

CHAPTER 4: HIGH SALINITY WATER (RO REJECT WATER AND NATURAL GROUNDWATER) TREATED USING PILOT-SCALE AGMD

This chapter explores the testing of a pilot-scale air-gap membrane distillation (AGMD) desalination system using high salinity feedwater (natural groundwater and RO reject water). The performance of the AGMD was investigated under the different operating parameters of feedwater flows (50, 100 and 150 L/hr), coolant flow (200 L/hr), feedwater temperature (50, 60 and 70°C) and coolant temperature (20°C). Two different membrane types, PTFE and PVDF, were tested. Two conductivity sensors with ranges of 200 μS/cm – 20 000 μS/cm were used to measure the conductivity of both feedwater and permeate water. Results showed that increasing feedwater temperature for both membranes led to corresponding increases in permeate-flux, regardless of the feedwater concentration level. Increasing feedwater conductivity from 3,960 μS/cm to 12 500 μS/cm led to a slight decline in permeate-flux of both membranes. Increasing feedwater flow to 150L/hr led to significant increase in the permeate-flux with both membranes.

4.1 Introduction

Safe drinking water is one of the important basic needs of the word's people if they are to live healthy lives. The current water consumption rate rise is more than double that of the population rate of increase (Water, 2012). Safe drinking water should meet all the criteria set out in drinking water standards. RO reject water and natural groundwater have been used in this study; both being highly saline in nature. The brackish groundwater bores in Australia are also highly saline, with total dissolved solids (TDS) ranging from 15,000 to 30,000 mg/L (Herczeg et al., 2001), (Richards and Schäfer, 2003).

Many people in developed countries are enjoying good quality water through the use of centralised water supply systems. However, in undeveloped and developing countries the lack of safe drinking water can pose a great threat to communities. Every year, millions of people die because of contaminants present in drinking water. Contamination of drinking water currently is one of the burning issues in the world because millions of people are suffering from drinking hazardous water.

Various membrane filtration technologies, such as RO, are being employed for mitigation of contaminants in the developed world, but these technologies are quite expensive for the majority of people in under-developed countries. Thus, more attention should be paid to technologies suitable for clusters of people who cannot afford expensive technologies as they live below the poverty line or are situated in remote regions.

Membrane distillation (MD) is a non-isothermal membrane separation process which employs a microporous hydrophobic membrane with pore size ranging from 0.2 to 1.0 μm (Tarleton and Wakeman, 1990). The MD process has been known since 1963 and remains in testing stages, not yet fully implemented into industry. The main requirements of the MD process are that the membrane should not be wetted by the feedwater and only the water vapour and non-condensable gases should be present within its' membrane pores. The hydrophobic microporous membranes made of polytetrafluoroethylene (PTFE), polypropylene (PP), polyethylene (PE), and polyvinylidene fluoride (PVDF) are now commercially available.

Currently available technologies for high salinity water treatment are NF, and RO (Xu et al., 2016). These technologies require a high energy input to produce drinking water (Ghaffour et al., 2013). MD is, so far, one of the very few technologies which can produce drinking water with low energy demand because it works within a relatively low temperature range and is not pressure driven (Ghaffour et al., 2013). Other advantages of this technology are less damage to the membrane than conventional techniques (Susanto, 2011) and no requirement for the addition of chemicals and pre-treatment (Gálvez et al., 2009). In this study, a fouled layer was built on the membrane surface, but its effect was relatively low as a result of using a pilot-scale system.

The objective of this study is to investigate the effect of high salinity on the performance of a pilot-scale AGMD system. Some researchers have investigated the use of AGMD for water treatment, however, the effect of high salinity feedwater on the performance of pilot-scale AGMD module has not been reported to our knowledge. This study presents a performance evaluation of a pilot-scale AGMD system for the treatment of highly saline feedwater sources.

4.2 Materials and methods

4.2.1 Sample preparation

Two different types of water (natural groundwater and RO reject water) were used in this study. The water samples (each 30 L) were taken directly from the Dalby Water or Sewage Treatment Plant (PO Box 551, Dalby, Qld 4405 Australia) to the feedwater tank of the MD system. The physicho-chemical characteristics of the feedwaters are shown in Table.2.1. The water quality analysis has been done at the corresponding plants.

4.2.2 Experimental setup

A schematic representation of the AGMD setup is shown in Fig.4.27. The experimental setup contained two 33 L thermally insulated vessels, hot and cold, representing feedwater and coolant, respectively. Water flowed from the feedwater and coolant tanks into the membrane module through 12 mm polyurethane hoses. Two centrifugal pumps were used to individually circulate in both the hot feedwater and cold permeate in a batch mode operation. Seven industrial style temperature sensors (RTD Sensor - Pt100 type with pot seal) were connected to the system (four in various locations on the feedwater side and three on the coolant side). Two rotameters (variable area flow meter type 335, 4-20 mA output, 0-500 L/hr, supplied by Georg Fischer) measured the fluid flows from the two pumps (submersible model: 24 Volt DC-2.5 Amp, 4 L/min). In addition, two conductivity sensors (Microchem Conductivity Transmitter supplied by TPS) were used to measure the conductivity in the feedwater and permeate tanks (high range of 20 000µS/m and low range of 2000 µS/cm, respectively). An electronic mass balance with serial interface was used to record the weight of the AGMD permeate-flux. All sensors were connected to a SCADA system for data logging and control purposes with local HMI.

To evaluate temperate effects, AGMD feedwater at a temperature of 50°C, 60°C and 70°C were tested, while coolant temperature was kept constant at 20°C. Both sides, feedwater and coolant, used a sensitive pumps and flow rate meters. Feedwater and coolant systems were continuously heated and cooled, respectively to maintain homogeneous solutions. To test flow rate effects with and without ultrasound enhancement, a feedwater flow rate of 50, 100 and 150 L/hr were used, and the permeate flow rate was kept constant at 200 L/hr. the permeate flow rate was kept 200 L/hr because it has low effect on the permeate flux specially in AGMD. the effect of coolant flow rate is less pronounced than that of the feedwater flow rate. The effect of the coolant flow rate is relatively low because of the air gap in AGMD which reduces the conductive heat transfer between the sides of the membrane (Alklaibi and Lior, 2005c). The inlet and outlet temperature differences of both the feedwater and coolant sides were observed to be no more than 2°C throughout the duration of the experiments.

The MD module consisted of two thermal elements (feedwater and permeate) machined from aluminium, connected to a membrane module made of PTFE or a similar material. While in practice MD heating and cooling sources would make use of waste or naturally occurring heat and cooling sources, we supplied these artificially in the laboratory to allow for a full range of adjustments. The feedwater compartment was connected to a heating system and was maintained at an elevated temperature, while the permeate compartment was connected to a refrigerated cooling system and maintained at a steady cooler temperature to maintain the temperature difference. The air-gap (3 mm) between the other side of the membrane and the coolant side was assured by using a 1 mm stainless steel condensation plate. The hydrophobic membrane was placed between the two compartments and made direct contact with the heated feedwater side while maintaining an air-gap between the membrane and cooled permeate side.

To enhance the AGMD system and clean the membrane during operation time, two ultrasound transducers (model CU18A, Etrema Products, Inc.) were mounted externally on the AGMD module. Ultrasonic power was controlled by changing the supplied current and voltage as in the system described elsewhere (Al-Juboori et al., 2016), for which ultrasonic power levels in the range of 40-120 W/m^2 were applied. The ultrasonic waves could not effectively pass through the original soft plastic

spacers without significant attenuation, so the plastic spacers were replaced with laser cut 316 stainless steel metallic spacers directly connected to the ultrasonic transducers. The dimensions of the metallic spacers were 43 cm (length) x 1 cm (width) x 26 cm (height) which was the same dimension as the plastic spacer. The ultrasonic transducers were connected to the AGMD cell through two metallic rods which allowed the ultrasound waves to freely pass from the transducer into the metallic spacers.

4.3 AGMD process

The effect of AGMD time on process efficiency was tested for 70 hrs and the permeate flux was measured every 10 h (Fig.4.26). The experiments with no ultrasound treatment, continuous ultrasound and after ultrasound treatments were conducted with varying types of feedwater temperature and flow rate. The effect of ultrasound power on permeate flux was evaluated in a separate set of experiments. The experiments were repeated three times and the mean values presented with standard error bars. The effect of the feedwater temperature on process efficiency was tested at three different temperatures (50°C, 60°C and 70°C) and the coolant temperature was kept constant at 20°C. The inlet and outlet temperatures difference at feedwater side was maintained at no more than 2°C. Feedwater and coolant systems were continuously heated and cooled, respectively to maintain the required temperature. To test the effect of the feedwater flow rate, feedwater flow rates of 50 L/hr, 100 L/hr and 150 L/hr were applied, whilst the coolant flow rate was set at 200 L/hr.

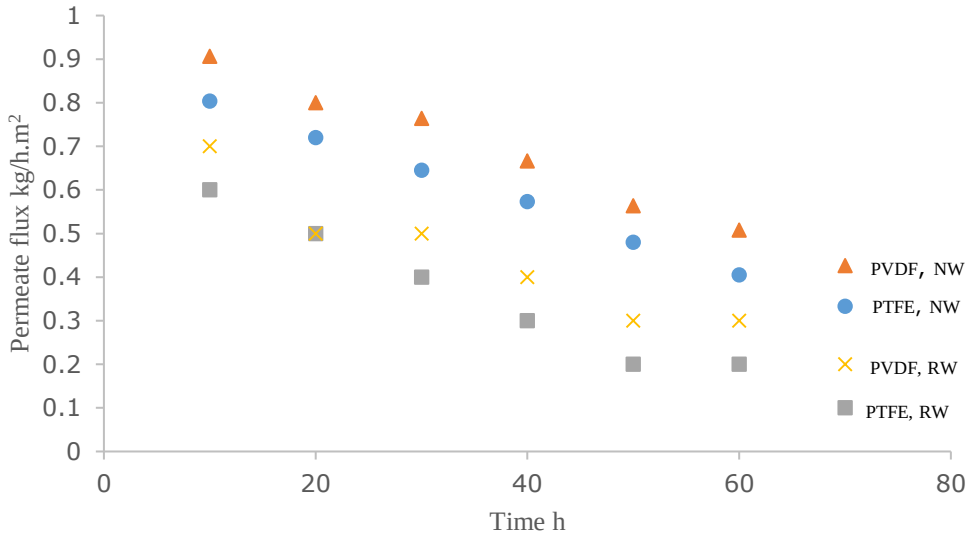

Figure 4.25: Primary results of both PTFE and PVDF membranes for (a) natural groundwater (NW) and (b) RO reject water (RW). Feedwater = 60 °C at 100 L/hr, coolant = 20 °C at 200 L/hr.

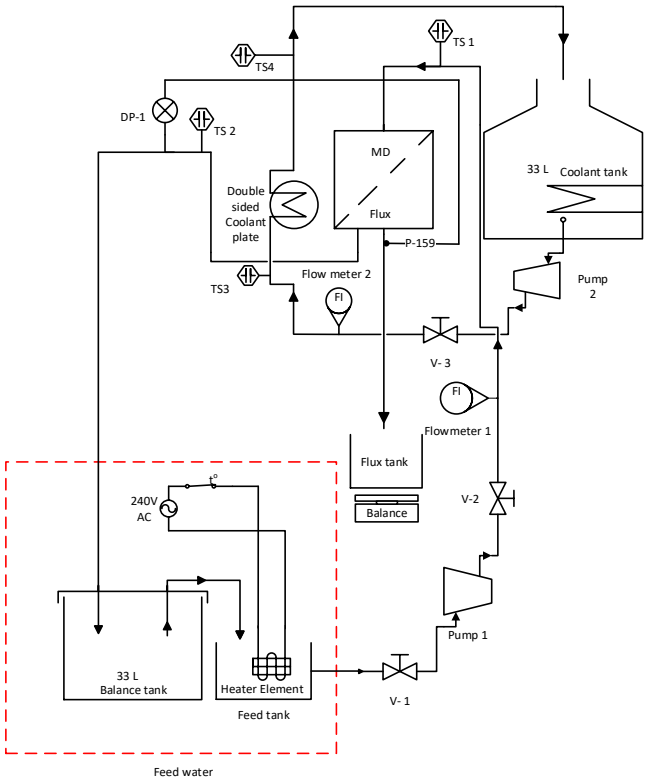

Item	Description
Pump 1	Submersible Model: LVMI3I 24 Volt DC-2.5 Amp flow rate 4 L/min
Pump 2	Submersible Model: LVMI3I 24 Volt DC-2.5 Amp flow rate 4 L/min
V1	Manual valve, control on the flow rate on/off heat side
V2	Manual valve, control on the flow rate, heat side
V3	Manual valve, control on the flow rate, coolant side
Flow meter 1,2	Variable area flow meter type 335 range 50-500 L/hr
TS	RTD Sensor -Pt100 with Pot Seal, Operating range: -75ºC to +350ºC, 3mm dia x 100mm long
DP-1	Wika, Differential pressure transmitter, Model: DP- 10 Range: 0-250 mbar
Chiller	Model: RC1, Volt: 240 V/50Hz,Range: 0-30°C
Heater	Range 0- 90°C
Ec-1	0 to 1 V DC or 0 to 5 V DC Outputs, k=1.0 Sensor....0 to 19.99 uS/cm
Ec-2	0 to 1 V DC or 0 to 5 V DC Outputs, k=0.1 Sensor....0 to 19.99 uS/cm
Ion Fl	0.02 to 19 000 mg/L F-, -0 to 60 °C (32 to 140 °F

Figure 4.26: Schematic representation of the AGMD setup.

4.4 Membrane characterization

In this study, two commercially available membranes, PTFE laminated on typar 3161L spunbond polypropylene and PVDF membranes were supplied by Donaldson Filtration solutions. The specifications of the membranes used are detailed in Table 3.2. The dimensions of the membrane cassette were as follows: 42 cm (length) × 1 cm (thickness) × 24 cm (width). Membranes were installed on both sides of the cassette with the total effective surface area of 0.2016 m^2. A membrane sheet was installed on either side of the cassette allowing feedwater to flow between the two flat membrane sheets.

4.5 Results and discussion

4.5.1 Feedwater temperature effects

The effects of feedwater temperature on permeate-flux was investigated and the results are shown in Fig 4.28. The Figure shows the effect of feedwater temperature (50°C, 60°C and 70°C) on permeate-flux production. Using PTFE and PVDF membranes, the ΔT was maintained at 2°C for all ranges of the feedwater temperatures used. The reason behind this reduction in the outlet feedwater temperature is a result of using a pilot-scale AGMD module. It is logical to expect a drop where there is a significant thermal mass involved, and this is something that has largely been unreported in small scale systems. Moreover, the feedwater flow is quite low when compared with the size of other systems due to the pressure constraints involved in a single flat membrane system. The results of this study show that increased permeate-flux for both membranes resulted from corresponding increases in the feedwater temperature. Permeate-flux slightly increased when the feedwater temperature was increased from 50°C to 60°C, and increased dramatically when the feedwater temperature was increased from 60°C to 70°C. This may be a result of the vapour pressure increase due to increased feedwater temperature (Guillén-Burrieza et al., 2011).

Another reason for permeate flux increases is that working at higher temperatures led to a decrease in the temperature polarization (Phattaranawik and Jiraratananon, 2001) such that the slight increase in vapour flux appeared at feedwater temperatures of 50°C and 60°C while the permeate-flux increased dramatically during the increase in the feedwater temperature from 60°C to 70°C. This difference is a result of the increase of ΔT between the feedwater and coolant sides.

The ΔT of both sides of the membrane surface is 30°C- 50°C which means it could well increase the permeate-flux of the membrane. The literature also indicates that the increase in temperature gradient between either side of the membrane should affect the diffusion coefficient positively (Chen et al., 2009), (Gunko et al., 2006). The vapour fluxes achieved on these membranes are approximately 60% lower than the flux achieved in a study by (Eykens et al., 2017). However, in our study the effective area is 0.2016 m^2, which is approximately 18 times bigger than that of (Eykens et al., 2017). Increasing the membrane length will result in increasing time required for conductive heat transfer across the membrane which will, in turn, reduce the feedwater temperature inside the module. It has also been reported that vapour flux decreases as a result of increased membrane length (Alsaadi et al., 2013). The ΔT measured at the feedwater inlet and outlet was 2°C which can provide a reason for a reduction in the permeate-flux, due primarily to the increased membrane length.

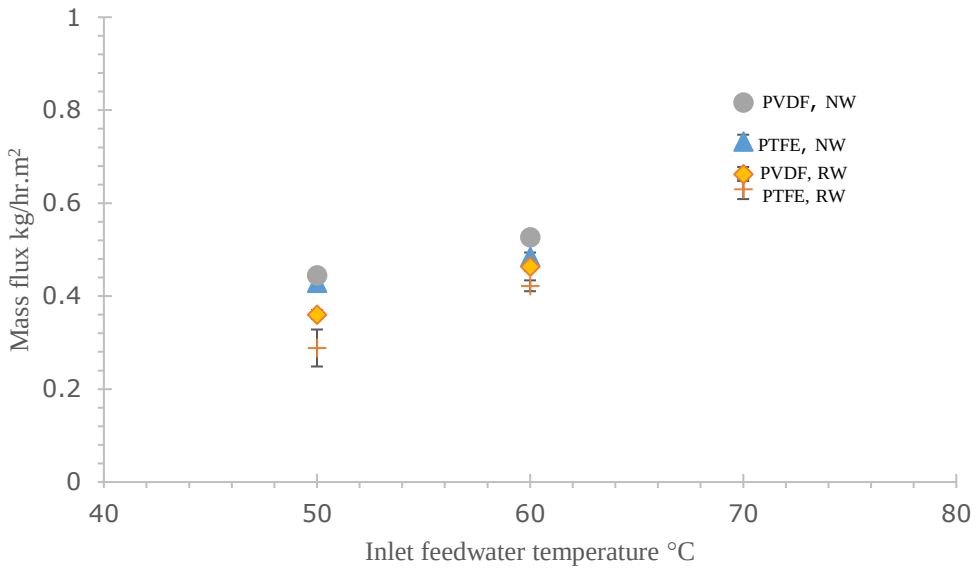

Figure 4.27: Effect of feedwater temperature on permeate flux using PTFE and PVDF membranes (natural groundwater and RO reject water). Feedwater: 150 L/hr at 3970 μS cm^{-1}, Coolant: 20°C at 200 L/hr.

4.6 Feedwater flow rate effects

The effect of feedwater flow was investigated, and the results are shown in Fig 4.29 below. Fig. 4.29 shows the effect of feedwater flow rate (50 L/hr, 100 L/hr and 150 L/hr) on the permeate-flux using PTFE and PVDF membranes. It is clear that the increase in the feedwater flow resulted in an increase in the permeate-flux. The relationship between the trans-membrane flux and feedwater flow is linear until a certain limit (Alklaibi and Lior, 2005a). The increase in the permeate-flux as a function of the feedwater flow is linear which means that feedwater flow has less effect on the permeate-flux than the feedwater temperature. The low feedwater flow (50 L/hr) lead to increases in the conductive heat transfer across the membrane surface which resulted in comparatively low permeate-flux across the membrane while increased feedwater flow rates led to slight increases in the permeate-flux. Increases in the feedwater flow reduced the feedwater residence time inside the module which thereby decreased the conductive heat transfer across the membrane surface (Alsaadi et al., 2013). The results of our study show that the achieved permeate-fluxes were approximately 60% lower than those reported by (Eykens et al., 2017). However, as described in previous chapters, it is worth noting that, in this study, the effective membrane area is around 18 times larger than that of (Eykens et al., 2017). A pilot-scale effective membrane area gives a greater opportunity to transfer heat across the membrane, which results in reduced temperature difference between the feedwater and the coolant. The membrane length has a strong effect on the feedwater flow (Alsaadi et al., 2013).

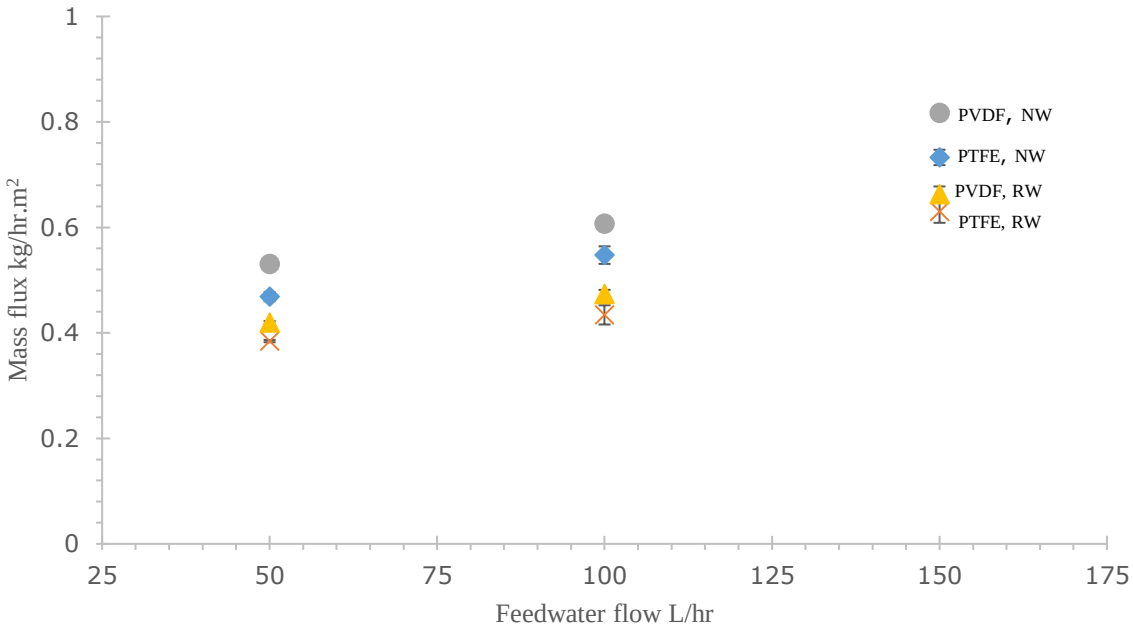

Figure 4.28: Effect of feedwater flow on permeate flux using PTFE (natural groundwater and RO reject water). Feedwater: 70°C at conductivity 3970 µS cm^{-1}, Coolant: 20°C at 200 L/hr.

4.7 Feedwater concentration effects and rejection

Figure 4.30 shows the effect of feedwater concentrations of 3970 µS/cm and 12 760 µS/cm on permeate flux for PTFE and PVDF membranes. MD can operate at very high salinities (Alsaadi et al., 2013). In this study, two different types of water have been used (natural groundwater and RO reject), so there are two different feedwater concentrations to compare. As shown in Fig.4.30, an increase in the feedwater concentration led to a slight reduction of permeate-flux for both membranes. The feedwater concentration was shown to have little effect on permeate-flux with the increase in feedwater salt concentration resulting in only a slight reduction in the permeate flux for both membrane types (Alsaadi et al., 2013). The increase in the feedwater salinity reduced vapour pressure on the feedwater side, consequently reducing permeate-flux (Alkhudhiri et al., 2012b). Our data showed that permeate-flux fell slightly regardless of the feedwater temperature and feedwater flow rate when the feedwater salt concentration increased. The permeate-flux is approximately 75% lower than the permeate flux of (Eykens et al., 2017). The reason behind this discrepancy is our high effective membrane area, while the effect of high feedwater salinity on the permeate-flux was very low even though the feedwater salt concentration was as high as 12 760 µS/cm. In this study the effective membrane

area is 0.2016 m^2 which is 18 times bigger than that of (Eykens et al., 2017). The membrane length rather than area is the main effect on operational parameters such as feedwater temperature and feedwater flow which tend to reduce permeate-flux.

The rejection of salts during AGMD with PTFE and PVDF membranes was investigated for both feedwater salt concentrations 3970 µS/cm and 12 760 µS/cm, with results shown in Fig 4.30. It appears that the increase in the feedwater salt concentration from 3970 µS/cm to 12 760 µS/cm had no noticeable effect on rejection by either of the PTFE or PVDF membranes. The rejection of salts for both membranes was >98%. In general, the range of the pore sizes of the membrane used for MD processes is 0.2 µm - 1.0 µm (Gryta and Barancewicz, 2010). These pores sizes are small enough to effectively prevent the passage of salt through the membrane pores.

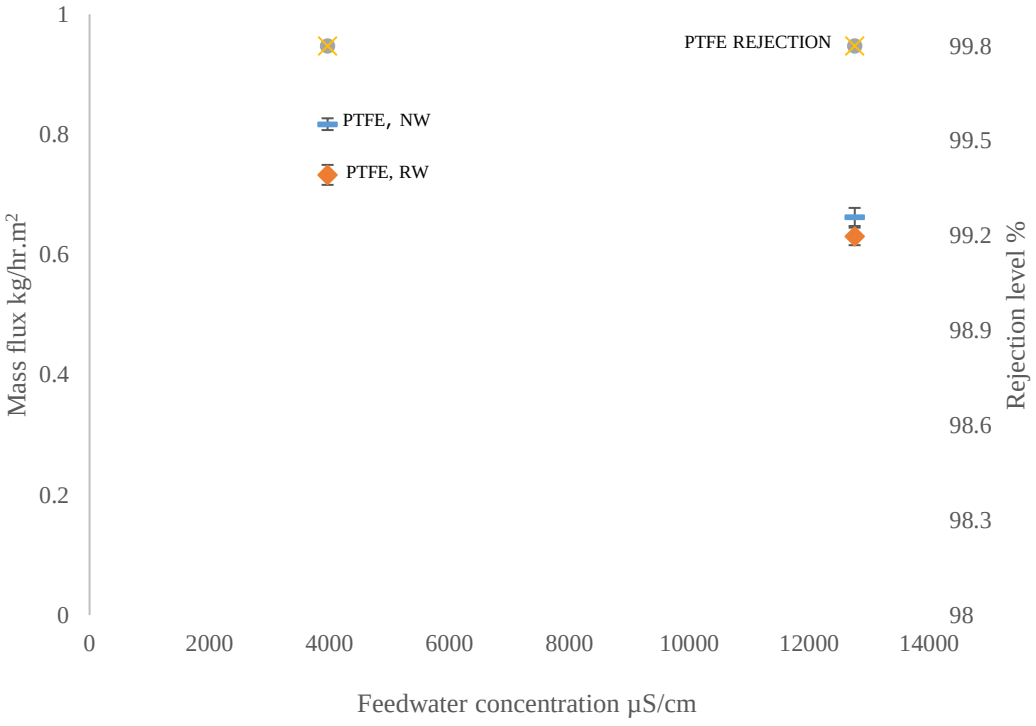

Figure 4.29: Effect of feedwater concentration (natural groundwater and reject water) on permeate-flux for PTFE membrane. Feedwater: 150 L/hr at 70°C, Coolant = 20°C.

4.8 Scanning Electron Microscope images

The SEM images are presented in Fig 4.31. and Fig.4.32 As seen in these figures clear signs of surface fouling appeared after 70 hours of high salinity feedwater, compared to the almost translucent surface of Fig. 4.31 where the image looks through the membrane surface and shows shadows of the underlying support layer. This fouling is likely the cause of the slight permeate-flux production decay, observed during the AGMD process period. A high permeate-flux will inevitably create higher temperature polarization and concentration polarization (Eykens et al., 2017). The solute will then tend to precipitate on the feedwater side of the membrane surface. In this high salinity feedwater solution environment, the percentage of solute is relatively low, thus the precipitation due to concentration polarization may be considered insignificant.

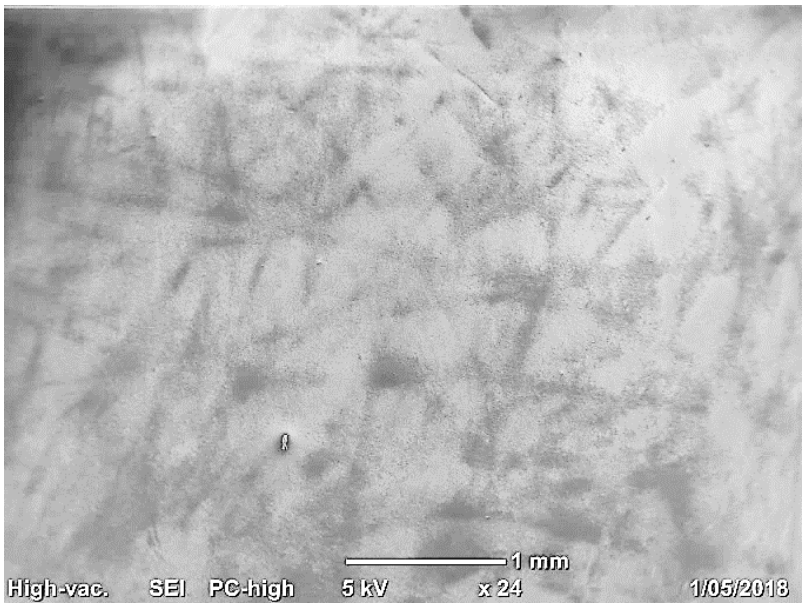

Figure 4.30: SEM image of unused PTFE membranes showing the support layer shadow underneath

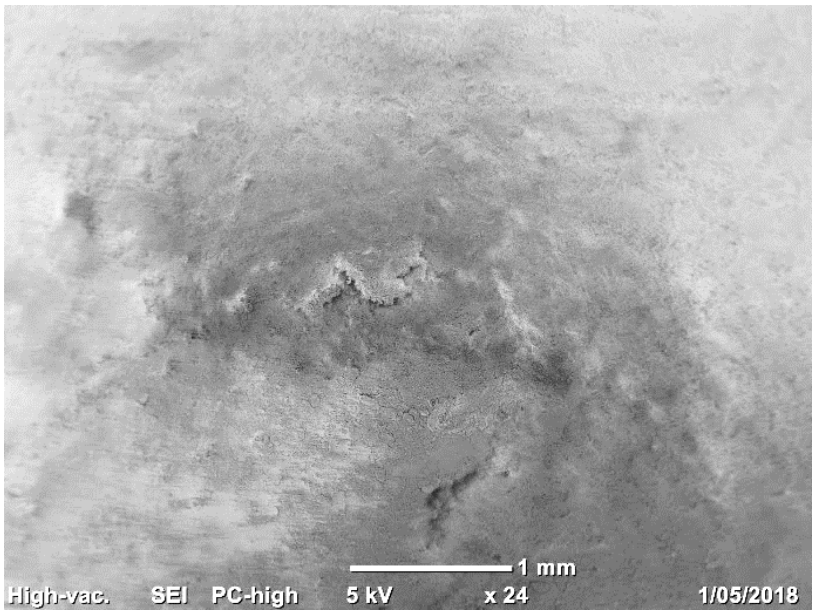

Figure 4.31: SEM image of used PTFE membrane, showing the surface fouling layer

4.9 Chapter summary

This study has investigated the performance of an AGMD with high salinity feedwater. The permeate-fluxes achieved with two membranes made of different polymers were different mainly due to their inherent membrane characteristics. The permeate-flux achieved on both membranes slightly increased when the feedwater temperature was increased from 50°C to 60°C followed by a slight increase when the feedwater temperature was further increased to 70°C. The feedwater flow rate range of 50-100 L/hr gave a slight increase in the permeate-flux, while the permeate-flux during the feedwater flow rate of 150 L/hr was slightly increased for both membranes. An increase in feedwater salt concentration from 3970 μS/cm to 12 760 μS/cm had little effect on the permeate-flux for both membranes. The salt rejections on both PTFE and PVDF membranes were higher than 98%. The SEM images showed that the membrane was fouled after 70 hrs of AGMD, but no indication of wetting or damage was observed.

5

CHAPTER 5: MITIGATION OF AIR-GAP MEMBRANE DISTILLATION (AGMD) FOULING AND FLUX ENHANCEMENT USING ULTRASONIC TECHNIQUE

Membrane distillation (MD) is a promising filtration technology for treating challenging feeds however, the low productivity of the membrane is a serious disadvantage. Membrane fouling exacerbates this problem further, therefore, researching membrane cleaning techniques is of the utmost importance for MD technology development. This study investigated the feasibility of ultrasound technology as an in-line cleaning technique for use in a pilot-scale (AGMD) module. The aim of ultrasound use was to reduce fouling on the membrane surface and to enhance permeate flux in the AGMD process. Two different types of MD membranes were employed to investigate whether ultrasound had a negative effect on the membrane surface. Further, two types of highly saline feedwaters, natural groundwater and reverse osmosis (RO) reject water, were used to evaluate ultrasound's ability to effectively reduce different fouling types during AGMD operation. To conduct this evaluation, the following parameters were investigated: feedwater temperature (50°C - 70°C), feedwater flow rate (50 L/hr - 150 L/hr) and ultrasonic power (40 -120 W/m^2). The PTFE and PVDF membranes with low power (40 W/m^2) and externally applied ultrasonic energy showed a consistently high permeate flux of 200% compared to non-sonicated AGMD. Moreover, no fouling was evident under the same operating conditions as compared to that of non-sonicated AGMD. The permeate flux improvement was mainly attributed to ultrasonic cleaning effects along with mass and conductive heat transfer enhancements. This was proven through SEM microscopy and ATR FT-IR examination of the membrane surface, which showed no sign of deposits or damage.

5.1 Introduction

Membrane distillation (MD) is being considered as a feasible alternative to conventional desalination technologies like multi-stage flush and multi-effect evaporation. MD has several economic and environmental advantages over the conventional desalination technologies including its ability to operate under atmospheric pressure and at relatively low feedwater temperatures (Camacho et al., 2013, Alsaadi et al., 2015). Other advantages which make the MD process economically feasible are fewer chances of membrane damage compared to pressure-driven processes (Susanto, 2011), no required feedwater pre-treatment and reduced use of chemicals (Xu et al., 2018).

Because of their versatility and effectiveness, the use of membrane processes in water treatment and desalination technologies has dramatically increased over the past decades. However, membrane fouling remains the main issue which significantly impedes the overall performance of membrane processes (Lamminen et al., 2004a). Depending on feedwater type, membrane fouling can be classified into three main types: colloidal, inorganic, and organic and biofouling (Flemming et al., 1994). As membrane filtration progresses, fouling materials are accumulated on the membrane surface or within membrane pores, decreasing its separation properties over extended periods of time (Lee et al., 2017). Thus, membrane scaling which is caused by salts accumulation and deposition on the surface of MD membranes due to feedwater evaporation, could compromise membranes' hydrophobicity and enhance pore wetting. The leakage of feedwater through the wetted pores to the permeate side of membrane will not only reduce vapour flux, but also promote salt passage across the membrane significantly deteriorating permeate quality (Noble and Stern, 1995), (Ho and Sirkar, 1992). Many researchers such as (Geng et al, 2014) have used pilot-scale AGMD to treat high salinity water. Another researcher, (He et al., 2014), used hollow fibre modules. Still more researchers (Kullab, and Martin, 2011; Hitsov et al., 2017; Eykens et al., 2017) used larger effective area modules, however, in their research their indirect application of the ultrasound did not improve the performance of AGMD nor did it reduce the fouling layer on the membrane surface.

A range of different cleaning techniques have been practiced to control membrane fouling. This include mechanical methods (Lamminen et al., 2004a) and/or chemical cleaning (Fortunato et al., 2017). Membrane lifetime could also be significantly reduced through a reduction in contact with aggressive chemicals during chemical cleaning (Li et al., 2002a). Moreover, the cleaning solutions, which are typically comprised of chemically aggressive compounds, possess a threat to the environment and must be treated before their discharge. With all of these cleaning techniques the system must also be shut down and, in some cases, the membranes must be removed, resulting in longer downtime or costly duplication of the filtration systems (Amy et al., 2017).

Ultrasound is considered to be a suitable alternative to existing cleaning methods and has been successfully applied to remove foulants from membranes (Kuehn et al., 1996) (Tarleton and Wakeman, 1990), (Chai et al., 1999). The advantages of this cleaning technique are no chemical usage (Chen et al., 2004), no system shutdown and no need for membrane removal from the system for *ex situ* cleaning so that possible membrane contact with the air is minimized. Ultrasound removes deposited particles from the membrane surface as a result of it shaking. As a result, permeate flux through the membrane is increased. Ultrasound can also increase a membrane's operation time without the opportunity for membrane fouling to occur.

Our previous study showed the successful application of pilot-scale low intensity ultrasound technology for the removal of organic contaminants and coliforms from surface waters (Al-Juboori et al., 2016). Based on these results, this study investigated the applicability of the non-cavitational ultrasonication at a power range of 40-120 W/m^2 for the in-line cleaning of a pilot-scale AGMD system to reduce membrane fouling from different types of MD membranes. Furthermore, we studied the effect of system conditions (feedwater flow rate and temperature) on the overall AGMD efficiency and permeate flux enhancement by using two types of feedwater with different feedwater matrices, RO reject water (conductivity = 12 760 µS/cm) and natural groundwater (conductivity = 3970 µS/cm).

5.2 Materials and methods

5.2.1 Sample preparation

RO reject water and natural groundwater samples (each 30 L) were taken directly from Dalby Sewage Water Treatment Plant (Dalby, Qld 4405) and were used as feedwater stock for the MD system. The physico-chemical characteristics of the RO reject water are shown in Table 2.1.

5.2.2 Experimental setup

A schematic representation of the AGMD setup is shown in Fig.5.33. The AGMD module is machined from aluminium and connected with stainless steel fittings. Two 30 L thermally insulated containers were used to hold feedwater and coolant solutions. Two centrifugal pumps (submersible model: 24 Volt DC-2.5 Amp, 4 L/min) were used to circulate feedwater and coolant through 12 mm polyurethane tubes. Seven industrial style temperature sensors (RTD Sensor - Pt100 type with pot seal) were connected to the system (four in various locations on the feedwater side and three on the coolant side). Two rotameters (variable area flow meter type 335, 4-20 mA output, 0-500 L/hr, supplied by Georgs Fischer) were employed for flow measurements. Two conductivity sensors and associated transmitters (K=0.1 and K=10, Microchem Conductivity Transmitter supplied by TPS) were used for measuring rejection effectiveness. An electronic mass balance with serial interface was used to record the weight of the AGMD permeate-flux. All sensors were connected to a SCADA system for data logging and control purposes with local HMI.

The temperature of the feedwater was maintained at 50°C, 60°C and 70°C and the coolant at 20°C using a (Precision Immersion Heater Circulator, Supplied by Ratek) for the feedwater side and (RC1 Immersion Cooler, Supplied by Ratek) for the coolant side. The flow rates of feedwater were 50, 100 and 150 L/hr and the coolant flowrate was set at a constant 200 L/hr. The temperature variation of feedwater and coolant were observed to be within a range of 2°C throughout the duration of the experiments. It is noteworthy that, in practice, heating and cooling sources are generated from low-grade waste or naturally occurring heat and cooling sources. In the laboratory environment, heating and cooling are generated electrically to allow for a full range of adjustments.

The air-gap in the module tested in this study was 3 mm between the sides of the membrane and the cooling plates and this was assisted by the use of a 1 mm stainless steel condensation plate. This plate provides additional support to the flat membrane under the side forces of pressure, so as to avoid tearing away of the membrane from the frame and causing subsequent leakage. This support is on the permeate side and not subject to the highly saline feedwater, in any case 316 grade stainless steel was used to avoid any corrosive effects. The hydrophobic membrane cassette were placed in between the two system cooling plates. The membrane was in direct contact with the heated feedwater side whilst there was an air-gap of approximately 3mm between the membrane and cooling plates on each side.

To enhance the AGMD system performance and maintain cleanliness of the membrane during operation, two ultrasound transducers (model CU18A, Etrema Products, Inc.) were mounted externally on the AGMD module (i.e. one per module). Ultrasonic power was controlled by changing the supplied current and voltage as in the system described elsewhere (Naji et al., 2019). The applied ultrasonic power was in the range of 3.5 - 30 W (40-120W/m^2) (maximum recommended power of transducers for vibrating the plates in a non-cavitational power region). The ultrasonic waves could not efficiently be transmitted through the original soft plastic spacers without significant attenuation, so the plastic spacers were replaced with laser cut 316 stainless steel metallic spacers directly connected to the ultrasonic transducers. The dimensions of the metallic spacers were 43 cm (length) × 26 cm (width) × 1 mm (thickness). The ultrasonic transducers were connected to the spacers through two 6mm threaded metallic rods. The (ATRFT-IR) (model IRAffinity-1S, supplied by SHIMADZU) was used to measure the fouled level on both membrane surfaces.

5.3 AGMD process

The feedwater and permeate compartments of the AGMD module were connected to the heating and cooling systems, respectively. The membrane was placed between the two compartments with the selective layer facing the feedwater side of module while the air-gap between the other side of membrane and coolant side was assured using a 1 mm stainless steel condensation plate. The feedwater solution flowed between the two membranes placed at two sides of the module's cassette and

permeate was collected from the other two sides of cassette which were connected to the permeate tank.

Fig. 5.34(a) shows two ultrasound transducers (model CU18A, Etrema Products, Inc.) were mounted outside the AGMD module. Because the ultrasonic waves could not effectively pass through the soft plastic spacers and caused significant attenuation, the plastic spacers were replaced with the metallic spacers which were in direct contact with the ultrasound transducers Fig.5.34(c). The dimensions of metallic spacers were 43 cm (length) x 1 cm (width) x 26 cm (height). The ultrasonic transducers were connected to the AGMD cell through two metallic threaded rods which allowed the ultrasound waves to freely pass through the horns into the metallic spacers. Ultrasonic power was controlled using a system shown in Fig.5.34(b). A detailed description of the system can be found elsewhere (Al-Juboori et al., 2016), to which ultrasonic power levels in the range of 40 - 120W/m^2 were applied.

The effect of AGMD run-time on process efficiency was tested over 70 hrs and the permeate flux was measured every 10 hrs. The experiments with no ultrasound treatment, continuous ultrasound and post ultrasound treatments were conducted by varying feedwater temperature and flow rates as was done previously. The effect of ultrasound power on permeate flux was then able to be evaluated in a separate set of experiments.

The effect of the feedwater temperature on the process efficiency was tested at three different temperatures (50°C, 60°C and 70°C) and the coolant temperature was kept at a constant at 20°C. The inlet and outlet temperatures difference at feedwater side was maintained at 2°C. Feedwater and coolant systems were continuously heated and cooled, respectively to maintain required temperatures. To test the effect of the feedwater flow rate, feedwater flow rates of 50 L/hr, 100 L/hr and 150 L/hr were applied, whilst the coolant flow rate was set at 200 L/hr.

The water vapour flux (J) and rejection of conductivity-causing compounds (R) were calculated according to Equations 1 and 2, respectively:

$$J = \frac{m_W}{At} \tag{5.1}$$

$$R = \left(1 - \frac{C_p}{C_f}\right) 100 \tag{5.2}$$

where m_W is the permeate weight (kg), A is the membrane area (m^2), t is the time (h), C_p is conductivity of permeate (µS/cm), and C_f is conductivity of feedwater (µS/cm).

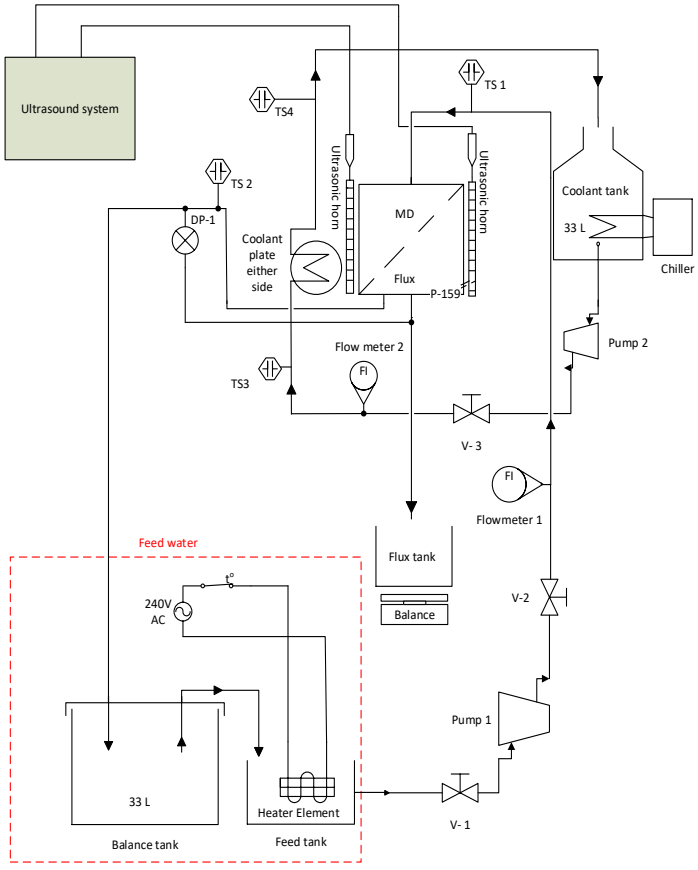

Item	Description
Pump 1	submersible Model: LVMI3I 24 Volt DC-2.5 Amp flow rate 4 L/min
Pump 2	submersible Model: LVMI3I 24 Volt DC-2.5 Amp flow rate 4 L/min
V1	manual valve, control on the flow rate on/off heat side
V2	Manual valve, control on the flow rate, heat side
V3	Manual valve, control on the flow rate, coolant side
Flow meter 1,2	Variable area flow meter type 335 range 50-500 L/hr
TS	RTD Sensor -Pt100 with Pot Seal, Operating range: -75ºC to +350ºC, 3mm dia x 100mm long
DP-1	Wika, Differential pressure transmitter, Model: DP-10 Range: 0-250 mbar
Chiller	Model: RC1, Volt: 240 V/50Hz,Range: 0-30°C
Heater	Range 0-90°C
Ec-1	0 to 1 V DC or 0 to 5 V DC Outputs, k=1.0 Sensor....0 to 19.99 uS/cm
Ec-2	0 to 1 V DC or 0 to 5 V DC Outputs, k=0.1 Sensor....0 to 19.99 uS/cm
Ion Fl	0.02 to 19 000 mg/L F-, 0 to 60 °C (32 to 140 °F

Figure 5.32: Schematic representation of the ultrasonicated AGMD setup

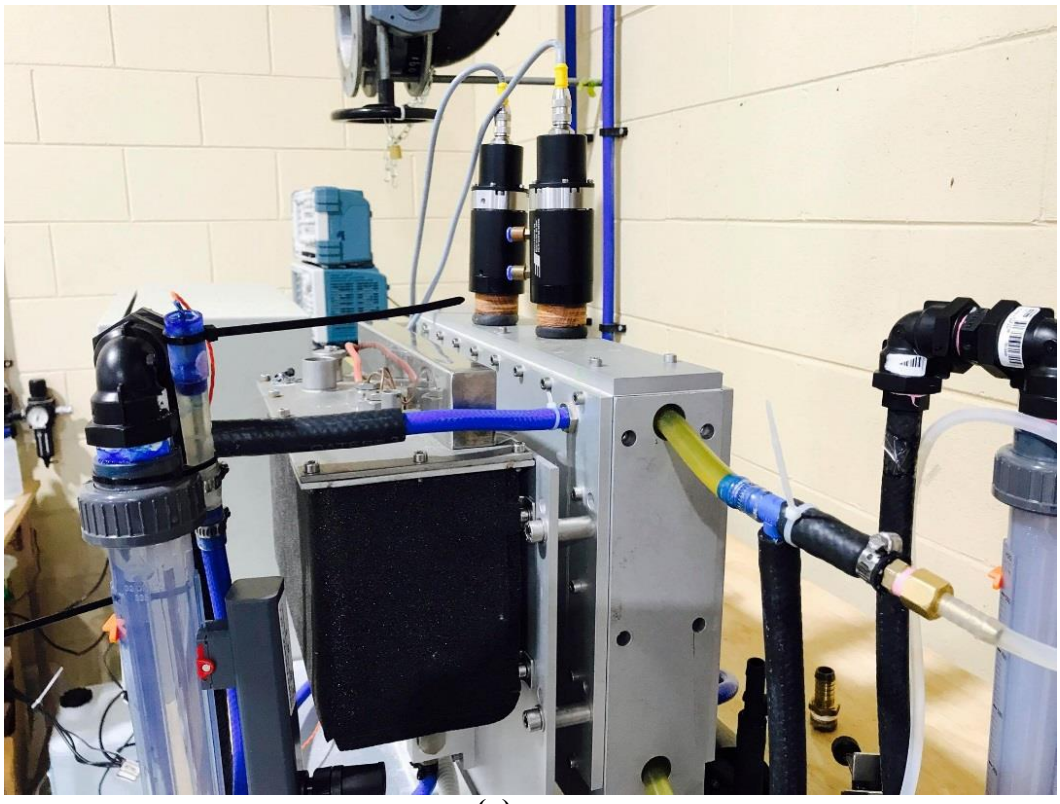

(a)


Tektronix
TPS 2014
Tektronix
AFG 3022B
PEMEX
550 WATTS x 2
IP-8.5C

(b)

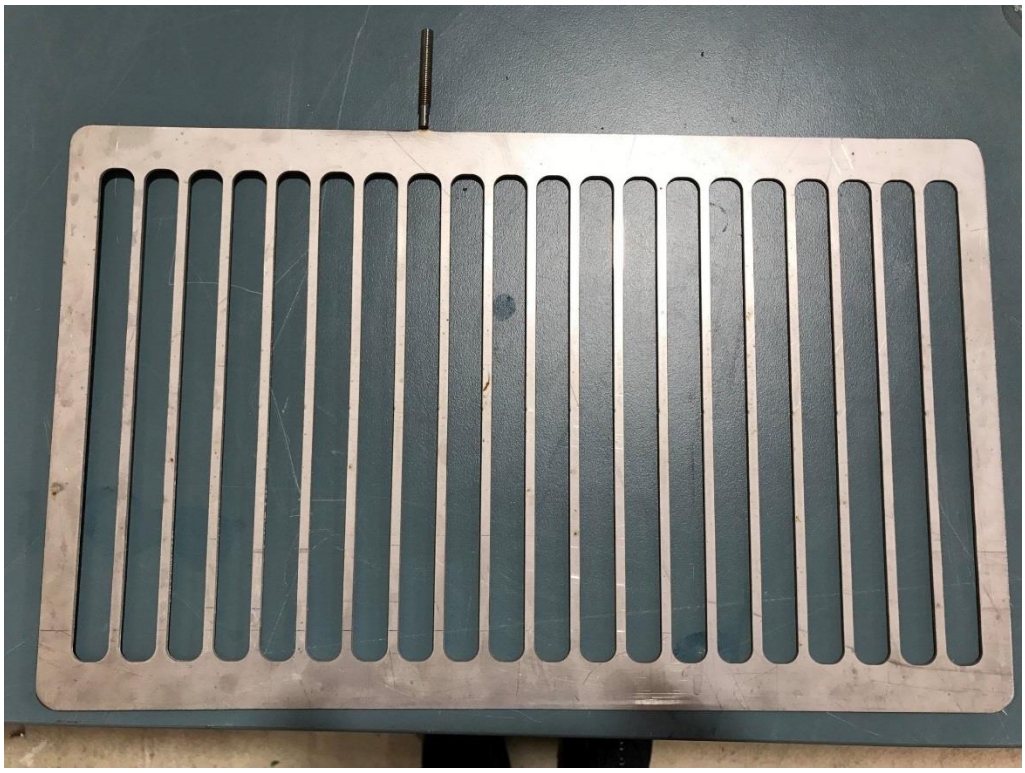

(c)

Figure 5.33: Images of (a) AGMD module connected to ultrasonic transducer and (b) ultrasound control system (c) metallic spacers.

5.4 Analytical methods

Conductivity of the feedwater and permeate samples was measured by Microchem Conductivity Transmitters (supplied by TPS). Scanning electron microscopy (Model JCM-6000 BENCHTOP, supplied by JEOL) was used to investigate the changes in membrane morphology as a result of membrane fouling and ultrasonication treatment. A Fourier transform infrared (FT-IR) spectrometer (Model IRAffinity-1S, supplied by SHIMADZU) with an attenuated total reflectance (ATR) accessory was used to study the surface functional groups of unused, fouled and cleaned membranes.

5.5 Specification of membranes

The commercially available PTFE laminated on typar 3161L spunbond polypropylene and PVDF membranes were supplied by Donaldson Filtration Solutions and the main characteristics of membranes are shown in Table 3.2. The dimensions of the membrane cassette were as follows: 42 cm (length) × 1 cm (thickness) × 24 cm (width). Membranes were installed on either side of the membrane cassette, with the total effective surface area of 0.2016 m^2 in total.

5.6 Results and discussion

5.6.1 Effects of feedwater temperature on permeate flux

Figures 5.35, 5.36 shows permeate flux as a function of the feedwater temperature in the AGMD process with, without and after ultrasound using PTFE and PVDF membranes. As shown in Figs.5.35 and 5.36 permeate flux increased with increasing feedwater temperature from 50°C to 70°C for both membrane types. The driving force of the MD process is defined as the temperature gradient across the membrane which is generated by the vapour pressure difference between the sides of the membrane (Xu et al., 2016). As such, an increase in feedwater temperature enhanced the driving force of the AGMD process and as a consequence, improved permeate flux. However, as shown in Fig. 5.35, the extent of the flux increase was determined by the feedwater temperature. Thus, the increase in permeate flux when the feedwater temperature was increased from 50°C to 60°C was smaller compared to that when the feedwater temperature was increased from 60°C to 70°C. As known, water vapour pressure increases exponentially with the temperature increase (Xu et al., 2016). Accordingly, the increment of the vapour pressure increase was higher when the temperature was raised from 60°C to 70°C compared to that of 50°C to 60°C. As such, significantly more vapour was produced and passed through the membrane pores at a feedwater temperature of 70°C as compared to that at 50°C and 60°C. On the other side, the increase in the feedwater temperature reduced temperature polarization (Phattaranawik and Jiraratananon, 2001). Therefore, increasing feedwater temperature to 70°C not only reduced the heat losses associated with temperature polarization as compared to those observed at lower feedwater temperatures, it also improved corresponding permeate fluxes and process efficiency.

The application of ultrasound treatment to enhance the AGMD process resulted in a significant increase of permeate flux on both PTFE and PVDF membranes. When ultrasound treatment was applied after 70 hrs of AGMD operation, permeate fluxes were higher than those obtained without ultrasound treatment with unused membranes. Thus, permeate fluxes achieved at 70°C on PTFE membrane increased by 20% and 24% for natural groundwater and RO reject water respectively; and permeate fluxes achieved with D_{20} membrane increased by 21% and 37% for natural groundwater and RO reject, respectively.

The permeate flux of NW appeared to be higher than that of RW because NW is prone to relatively less fouling effects compared with RW. Moreover, a far superior performance of the AGMD process was achieved when ultrasound treatment was applied continuously. In this case, the permeate flux doubled on both types of membranes regardless of the feedwater type, as compared to the AGMD process with no ultrasound treatment. (Zhu and Liu, 2000) theoretically proved that permeate flux in the MD process could be increased by 200% when an ultrasonic intensity of 5 W/cm^2 or 50 000 W/m^2, was applied to the whole system. The results of our experimental study where significant permeate flux increase was observed at a sonication power of 40 W/m^2 are in good correlation with Zhu and Lin's study, confirming the hypothesis that ultrasound can enhance permeate flux of the MD process. The fact that we applied our ultrasound only where it was required, meant that we needed only a small fraction of the power Zhu and Lin used to achieve the same benefit.

The fact that permeate flux increased after ultrasonication treatment of a membrane subjected to 70 hrs of AGMD process suggests that ultrasound technique is capable of not only removing the cake layer formed on the membrane surface, but also prevents deposition of foulants during operational periods. The reason behind no fouling is that the spacer kept vibrating, so that the fouling layer built on the membrane surface could be disturbed and the feedwater flow could carry it out to the feedwater tank and the membrane surface subsequently remained clean. Moreover, the ultrasound had no effect on the boundary layer of the membrane as it was generated from the from air-gap side, e.g. on the other side of the membrane. A clean membrane surface was also observed after prolonged ultrasonic treatment of ceramic membranes (Lamminen et al., 2004b).

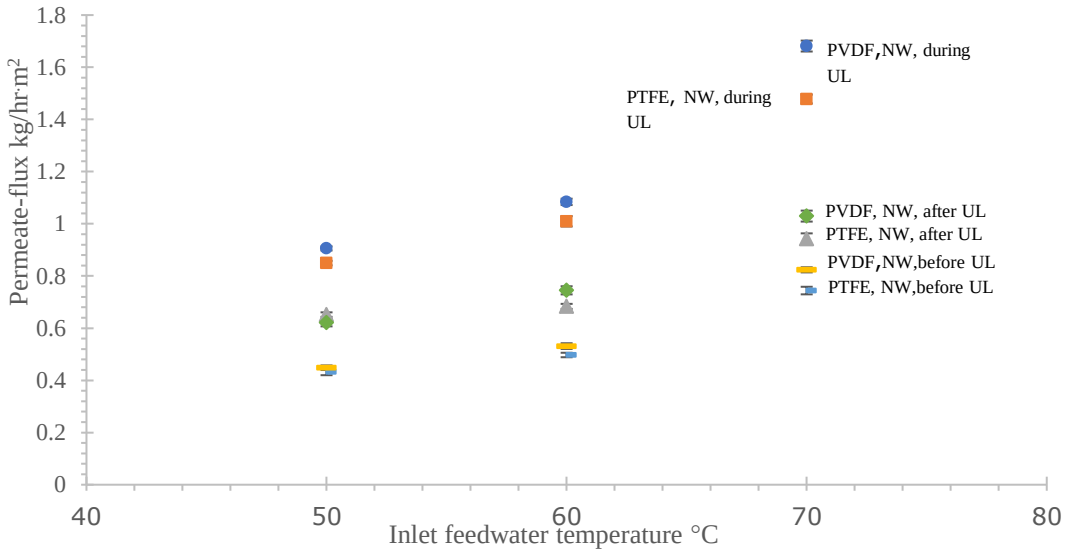

Figure 5.34: Effect of feedwater temperature before, during and after ultrasound on permeate-flux for PTFE and PVDF membranes with natural groundwater (NW). Feedwater:150 L/hr at 3970µS/cm, Coolant = 200L/hr at 20°C, Ultrasound Power = 40 W/m².

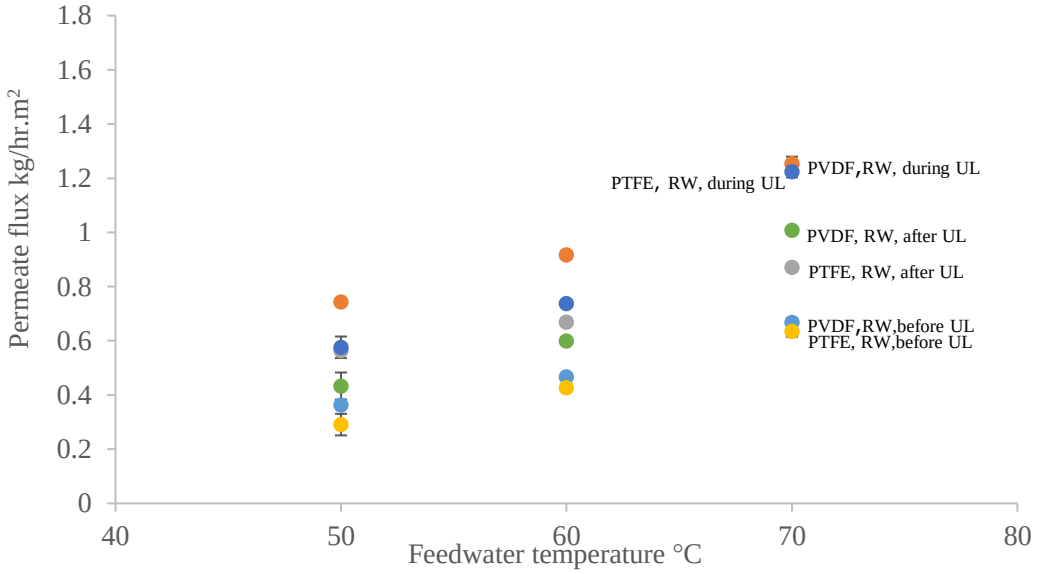

Figure 5.35: Effect of inlet feedwater temperature before, during and after ultrasound on permeate-flux using PTFE and PVDF membranes for RO reject water (RW). Feedwater: 150 L/hr at 12 760 µS/cm, Coolant: 200 L/hr at 20 °C, Ultrasound Power = 40W/m².

5.7 Effects of feedwater flow rate on permeate-flux

The feedwater flow rate is an important parameter which significantly influences the efficiency of the MD process (Alsaadi et al., 2013). The effect of the feedwater flow rate in a range of 50 L/hr -150 L/hr) with, without and after ultrasound treatment on the permeate flux was investigated for PTFE and PVDF membranes and the results are shown in Figs. 5.37 and 5.38. As seen in Fig.5.37, the permeate flux of the AGMD process increased with increasing feedwater flow rate for all tested conditions.

However, the rate of this increase was higher when the feedwater flow rate was increased from 100 L/hr to 150 L/hr compared to that of 50 L/hr to 100 L/hr. The observed effect can be explained as follows. The residence time of the feedwater in the AGMD module at low feedwater flow rates was longer compared to that at high feedwater flow rates leading to a decrease in the temperature gradient across the module. The thickness of the boundary layers corresponding to temperature and concentration polarizations was also less influenced by the low feedwater flow rate (Alklaibi and Lior, 2005b).

At high feedwater flow rates, the reduction in temperature polarization as a result of increasing feedwater flow rate as well as lower feedwater residence time, reduced the conductive heat transfer across the membrane and increased the mass transfer resulting in larger permeate fluxes. There is also a good chance that the flow is transitioning from laminar at low flows to transient to turbulent flow as the rates increase. When comparing permeate fluxes achieved with and without ultrasonication, it can be observed that the efficiency of the AGMD processes increased for both types of ultrasound treatment compared to experiments without ultrasonication.

The AGMD process combined with continuous ultrasonication resulted in a higher increase in permeate flux for all tested feedwater flow rates as compared to that when ultrasonication was applied only after membrane fouling. Moreover, as seen in Fig. 5.38, resultant permeate flux for continuous ultrasonication was double that compared to experiments without ultrasonication for any tested feedwater flow rate. Such a significant increase in the permeate flux during the ultrasonication process was likely a combined result of mass transfer efficiency improvement and cake layer removal, by the shearing action of the ultrasonic waves which were continually applied to the membrane surface.

It can be noticed that ultrasound cleaning resulted in almost 50% increase the flux for all treatments. The increment rate of NW flux due to ultrasound cleaning was almost the same for all tested flow rates. However, the improvement of RW flux was more pronounced in high flowrate as opposed to low flowrate. This can be attributed to the high salinity of RW where high flowrate combined with acoustic streaming effect generate high turbulences that reduce concentration polarisation at the membrane surface and resulted in less foulants adherence (Sajjadi et al., 2017). Mass transfer improvement resulted in about 100% increase in the flux. The flux rate increased became sharper when the flowrate increased from 100 to 150 L/h, and this again confirms the impact of the synergistic effect of flow generated and ultrasound induced turbulences that helps in improving vapour transfer across the membrane. The rejection of conductivity-caused compounds were higher than 98 % for all treatments.

The ultrasonication process had no effect on the boundary layer and temperature polarization in this study because they were mounted outside the feedwater module, attached to the spacer placed in the air gap. The ultrasound in this study was not directly applied to the feedwater side as in other studies, instead the ultrasound was connected to the spacer (part of AGMD system). The waves of the ultrasound were able to pass through the hard metal spacers and vibrate the membrane surface, which broke the caked layer which was built up on the feedwater side of the membrane surface, preventing further build-up while the ultrasonic waves were applied.

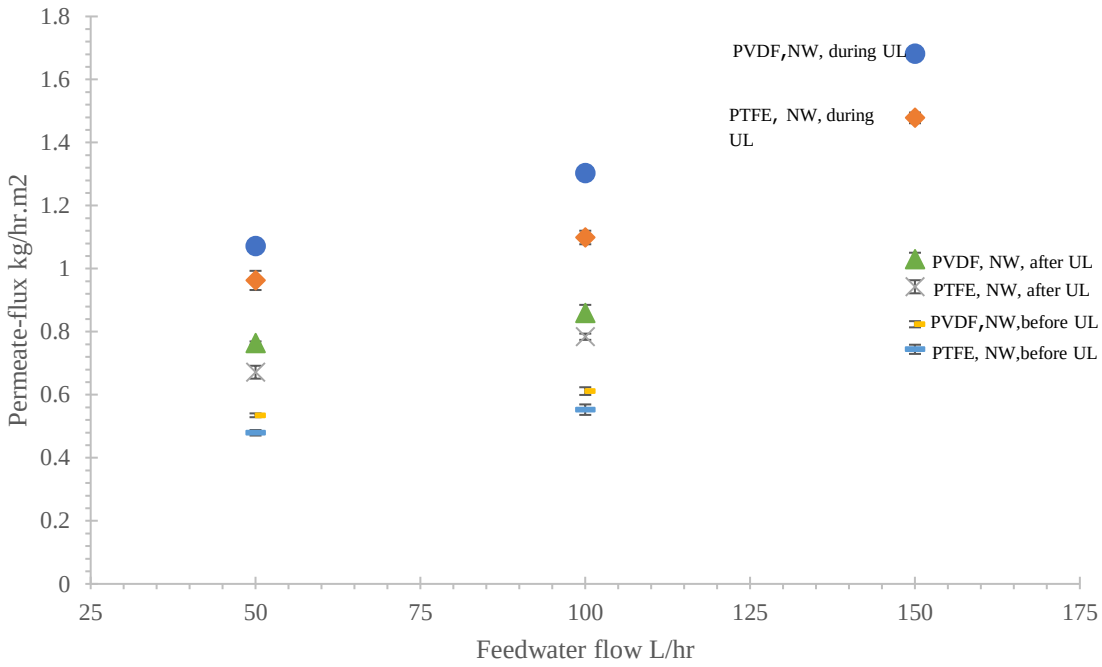

Figure 5.36: Effect of inlet feedwater flow rate before, during and after ultrasound on permeate-flux using PTFE and PVDF membranes for natural groundwater (NW). Feedwater = 70°C, Feedwater conductivity = 3970 µS/cm, Coolant = 20°C, Coolant flow rate= 200L/hr, Power 40W/m^2.

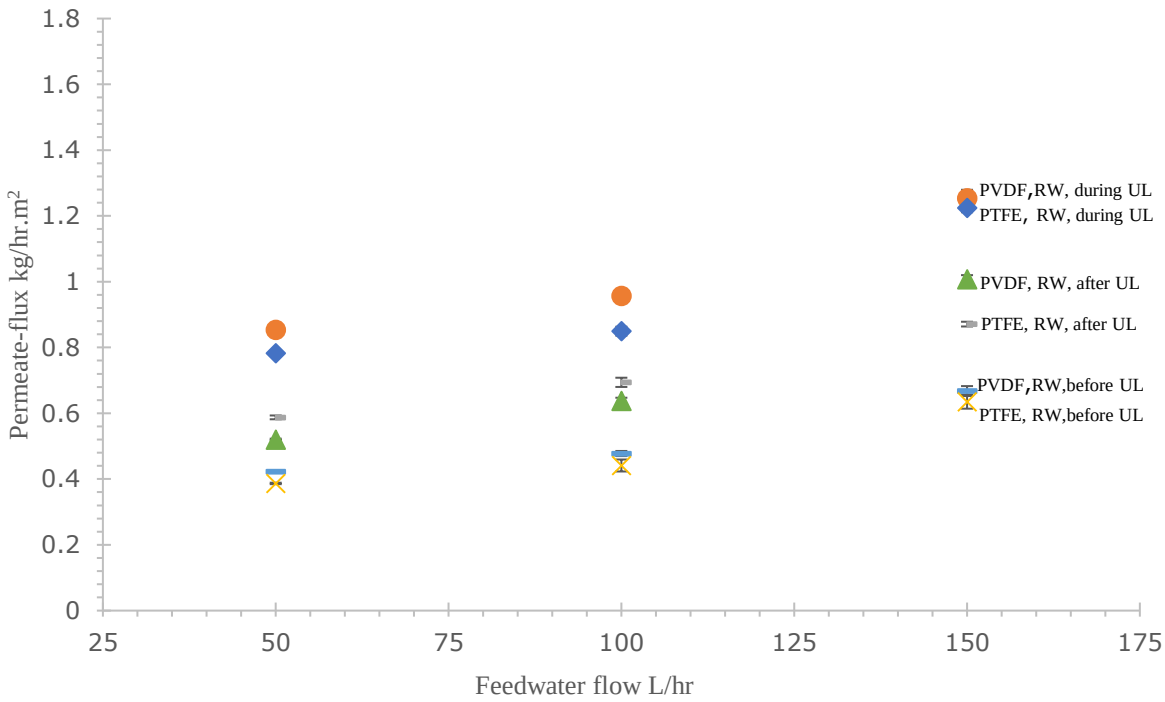

Figure 5.37: Effect of inlet feedwater flow before, during and after ultrasound on permeate-flux using PTFE for RO reject water (RW). Feedwater = 70°C, Feedwater conductivity = 12 760 µS/cm, Coolant = 20°C, Coolant flow rate = 200 L/hr, 40 W/m.

5.8 Effects of ultrasound power on permeate flux

The effect of ultrasound power ranging from 40-120W/m^2 on permeate flux achieved on PTFE membrane was also investigated. As shown in Fig. 5.39, permeate flux was doubled by increasing the ultrasound power from 40 -120 W/m^2 (from 0.65 L/m^{2}·h to 1.19 L/m^{2}·h). The ultrasound did not damage the membrane surface as observed through the membrane surface characterization (see Fig. 5.41) and permeate water analysis (based on 100% rejection of conductivity-causing compounds). However, higher power or the longer treatment time of ultrasound needs to be further investigated as this may result in damage to the membrane surface [22].

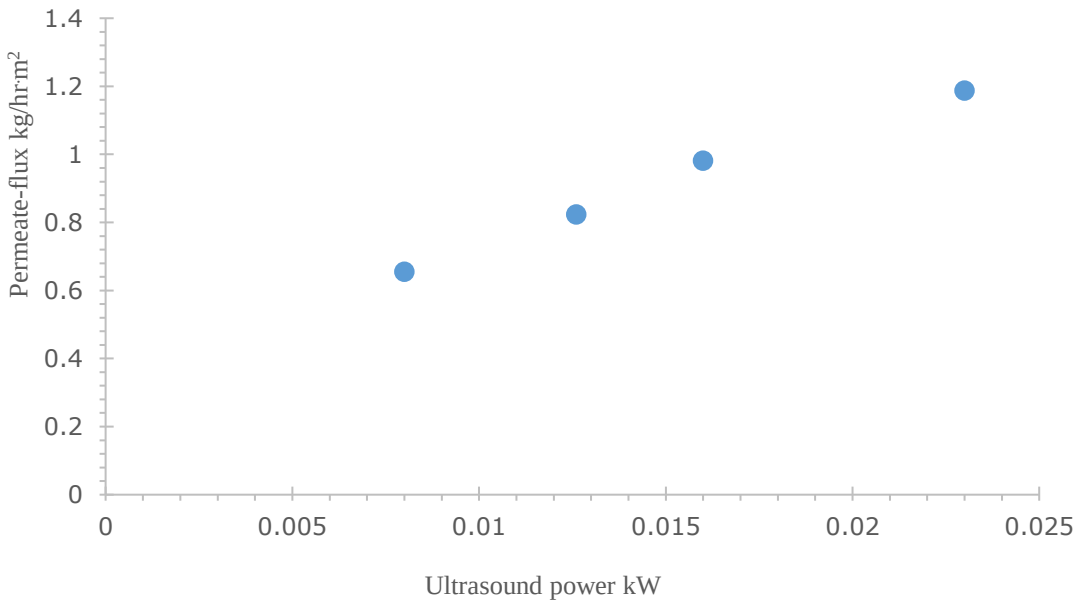

Figure 5.38: Ultrasound power effect on the permeate-flux. Feedwater = 70°C, Feedwater conductivity = 12 760 µS/cm, Coolant = 20°C, Coolant flow rate = 200 L/hr.

The vibration mechanism does not require high power compared with the cavitation mechanism (Al-Juboori et al., 2015b). This could allow ultrasound to work in a low power range (40 -120 W/m^2). With this low level of ultrasonic power, the occurrence of cavitation effect is unlikely. and this was proven by calculating of the cavitation threshold for bubbles with an initial diameter of 10 µm (commonly assumed value for cavitation calculation (Al-Juboori and Yusaf, 2012)) and conditions similar to those inside the membrane module (Temperature = 50˚C and Pressure = 3400 Pa) by applying Equation 3 (Qasim et al., 2018).

The threshold pressure was then compared to the acoustic pressure generated from a power level of 40 W/m^2. The acoustic pressure was calculated using Equation 4 (Al-Juboori and Yusaf, 2012). The permeate flux improvement was most likely attributed to the cleaning effects and the mass and conductive heat transfer enhancements. Cleaning effects of the ultrasound were detected through the microscopy examination of the membrane surface which showed no sign of damage (see Section 5.3.2).

$$P_b = P_o + \frac{2}{3}\sqrt{\frac{\left(2\sigma/R_o\right)^3}{3\left(P_o + 2\sigma/R_o\right)}} \tag{5.3}$$

$$P_A = \sqrt{2I\rho C} \tag{5.4}$$

where, P_b is the threshold pressure (Blake threshold) (Pa), P_o is the pressure of the water without ultrasound effect (Pa), σ is the water surface tension (N/m), R_o is the initial bubble radius (m), P_A is the acoustic pressure (Pa), I is the ultrasonic intensity (W/m^2), ρ is the water density (kg/m^3) and C is the sound velocity in water (≈ 1500 m/s).

Several factors can influence the efficiency of ultrasound treatment. These are orientation and position of the ultrasonic field, ultrasonic power intensity and frequency, membrane material, membrane housing, operating pressure, and fouling material (Lamminen et al., 2004b). In our study, the ultrasound was applied to vibrate the stainless-steel condensation plate of 1 mm thickness, which was placed between the membrane surface and coolant side (in the air-gap). The waves of the ultrasound transferred to the metallic spacers once the ultrasound started working. At the time when ultrasound was applied, the spacers started shaking immediately on both sides of the membrane as a result of the ultrasound waves. The fouling layer which tends to deposit on the membrane surface started losing interaction with the membrane surface due to the shaking effect (vibration), and then the feedwater flow carried the foulants away from the membrane surface and into the suspension to the brine outlet assisted by the effect of shear forces and crossflow velocity. This resulted in keeping the membrane surface clean and stabilized the permeate flux.

Our results are in agreement with other studies which reported that using ultrasound for cleaning the membrane fouling could result in the effective removal of particles from the membrane surface (Kobayashi et al., 2003). This approach has several advantages, such as cleaning the membrane during operation time, no need for chemical cleaning, no damage occurring to the membrane surface as the treatment is non-invasive, possibility of control of the ultrasound application, decreased conductive heat transfer, increased permeate-flux and reduced fouling layer. Additionally, the energy of the ultrasound is transformed to heat which can reduce the conductive heat transfer from the membrane to the coolant side (Berlan and Mason, 1992), contributing to direct membrane surface heating. Once the conductive heat transfer is reduced as a result of ultrasound energy, the feedwater temperature will remain constant which will further reduce temperature drop/loss inside the module, hence reducing the temperature polarization effect which is one of the main limiting factors of the MD process (Alsaadi et al., 2014). This condition led to increasing mass transfer through the membrane.

The extent of ultrasonic effect on AGMD process in the present configuration (Fig.5.32) depends on the applied ultrasonic parameters and the medium being irradiated. In the case of AGMD, there are three media; water, membrane and air and vapour mixture. The effect of ultrasound in the latter two is in the form of acoustic streaming. However, chemical, extreme localised physical effects (i.e. high temperature and pressure) and mechanical effects such as micro jets and shock waves may occur in water due to the generation and subsequent collapse of cavitating bubbles (Al-Juboori Raed and Yusaf, 2012). Cavitational bubbles can only occur when the applied ultrasonic pressure for given conditions of irradiated water exceeds the cohesive forces for water. This can be determined through calculating cavitation threshold using equations 1 and 2 (Qasim et al., 2018, Al-Juboori and Yusaf, 2012).

5.9 ATR FT-IR analysis of membrane surface.

ATR FT-IR was employed in this study to evaluate the surface functionality of PTFE membrane before and after ultrasound treatments, and corresponding ATR FT-IR spectra of unused, fouled and cleaned PTFE membrane surfaces are shown on Fig. 5.40. The spectrum of unused membrane revealed the presence of a set of peaks which are characteristic of PTFE material (Fig. 5.40a). The bands at 1199 and 1146 cm^{-1} were assigned to CF_2 symmetric stretching vibrations (Alpatova et al., 2015) while the band at 640 cm^{-1} was attributed to the rolling vibrations of CF_2 group (Fazullin et al., 2015). The band at 553 cm^{-1} corresponded to CF_2 deformation (Fazullin et al., 2015). The wide band appeared in the spectrum of the fouled membrane at 1001 cm^{-1} (Fig. 5. 40b) which could be attributed to silica precipitation (Miller and Wilkins, 1952) and/or gypsum scaling ($CaSO_4 \cdot 2H_2O$) (Coates, 2006). Comparing spectra of the fouled and ultrasonic-cleaned membranes (Figs. 5.40 b and c), it can be clearly observed that ultrasonication was very effective in removing foulants from the membrane surface. The characteristic PTFE peaks which were supressed in the spectrum of the fouled membrane (Fig. 5.40b), fully reappeared in the spectrum of the cleaned membrane (Fig. 5.40c). Moreover, the ultrasonication exhibited superior performance in removing silica/gypsum fouling. As seen in Fig. 5.40c, the intensity of the band at 1001 cm^{-1} was significantly reduced after ultrasonication compared to that of the fouled membrane (Fig. 5.40b). This is an important finding as it suggests that the ultrasound-assisted membrane cleaning method could be a feasible tool in eliminating persistent membrane foulants which are difficult to remove with existing cleaning techniques.

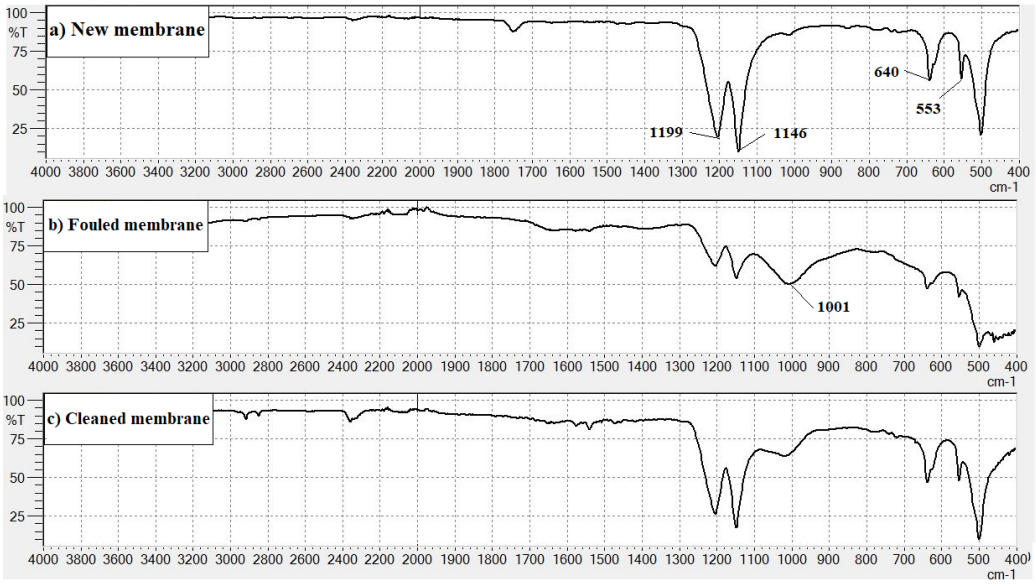

Figure 5.39: ATR FTIR spectra of (a) Unused PTFE membrane, (b) Fouled PTFE membrane, and (c) Ultrasonically-cleaned PTFE membrane.

5.10 Membrane surface characterization

SEM imaging was employed in this study to investigate the morphology of membranes before and after ultrasound treatments. Figure 5.38(a, b, c) shows the surfaces of unused, fouled for 70 hrs and ultrasound-treated PTFE membrane. As seen in Fig. 5.38, significant fouling was observed on the surface of the membrane after 70 hrs of operation Fig. 5.38(b) as compared to surface of the unused membrane Fig. 5.38(a). The subsequent ultrasound treatment removed the layer of fouling from the membrane surface and, as seen in Fig. 5.38(c), its surface became clean and smooth with no obvious sings of fouling. Also, no signs to damage of the membrane surface were observed implying that the applied ultrasound did not affect membrane integrity.

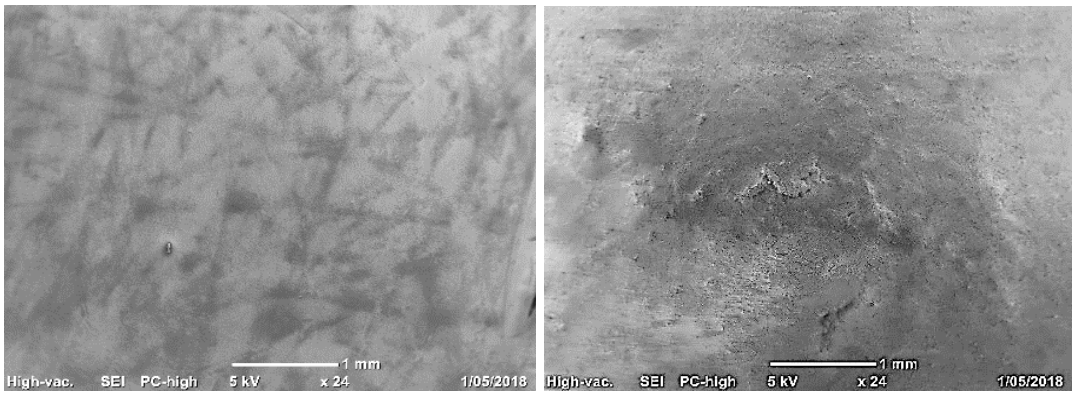

(a) **(b)**

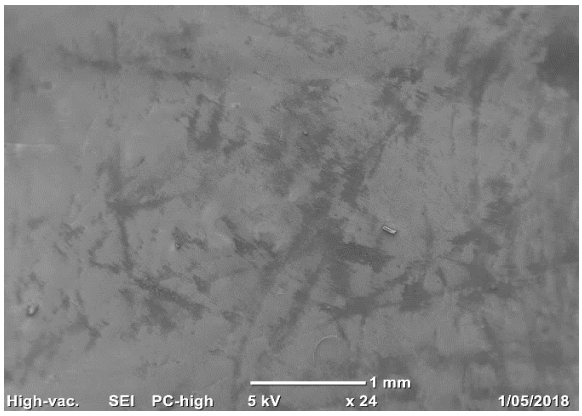

(c)

Figure 5.40: SEM images of unused (a), fouled (b) cleaned by ultrasound (c) PTFE membrane.

5.11 Chapter summary

The effect of ultrasound with an applied power range of 40 - 120 W/m^2 on membrane fouling and permeate flux enhancement using a pilot-scale AGMD module was investigated. The results showed that ultrasound can reduce membrane fouling by inducing mechanical vibrations in the membrane spacers on either side of the module's cassette. The permeate fluxes achieved on both tested membranes (PTFE and PVDF) were doubled when the lowest level ultrasonic treatment of 40 W/m^2 was applied. Our study also revealed that ultrasound treatment did not exert any negative effects on membrane integrity and was able to return a significantly fouled membrane back into service. This study also showed that the ultrasound-assisted AGMD process was effective in treating water with very different physicochemical properties, namely high salinity groundwater and RO reject water. The rejection of the salts with and without ultrasound was >98%, which proves that the AGMD system is suitable for treatment of highly saline water sources such as RO reject water.

6

CHAPTER 6: CONCLUSIONS

Membrane distillation (MD) is a promising alternative technological application for pilot-scale drinking water production in remote and regional areas. Existing technologies, such as reverse osmosis (RO), face implementation challenges in these areas primarily due to the high salinity of treated waters which require additional brine treatment, extensive pre-treatment and suffer severe membrane fouling and premature failure. The feasibility of MD depends on whether it can demonstrate its advantages over already established technologies. In this study, the feasibility of pilot-scale AGMD was evaluated with respect to different membrane types, different feedwater types and operating conditions. The operating conditions of the AGMD system were selected as follows: feedwater temperature ranging from 50 - 70°C, coolant temperature kept constant at 20°C, feedwater flow rate varying in the range of 50 - 50 L/hr and coolant flow kept constant at 200 L/hr. Two membrane types (PTFE and PVDF) were tested. These two membranes were characterised by slightly different thicknesses (PTFE 254 µm, PVDF 154 µm) and porosity (PTFE 75%, PVDF 80%).

The efficiency of the pilot-scale AGMD system in fluoride removal from synthetic water was studied under different operating parameters. In addition, the effect of feedwater with two types, natural groundwater (3,790 µS/cm) and RO reject water (12 760 µS/cm), was also tested. Fluoride rejection was >98% overall operating ranges. The increase in feedwater conductivity, from 3790 µS/cm to 12 760 µS/cm, resulted in a slight decrease in permeate-flux production.

In addition, this study has determined and statistically validated the key factors influencing flux production in this pilot-scale AGMD process. Thus, providing greater insight and certainty into the mechanics of the AGMD process.

The effect of the effective membrane area on process performance has been studied in detail. The membrane effective area in this study was 0.2016 m^2 which is approximately 14 - 18 times larger than those in studies previously reported in recent literature using flat membrane sheets. The increase in the effective area of AGMD showed a significant decrease in permeate-flux production. Where other larger scale systems have used higher pressures, we were limited to a much lesser operational pressure range, as we had a large flat membrane surface, attached only at the cassette edges. This issue can be resolved by using longitudinal straws or spiral topologies, which have been applied to other membrane technologies. Unfortunately, this would mean a complete system redesign, especially with respect to the application of the ultrasound.

Ultrasonic treatment has been tested and optimised for the AGMD system, targeting the removal of fouling from the membrane surface. This fouling removal and other associated benefits resulting in the permeate-flux rate increasing by 200 - 300% was compared to the same system parameters without the application of ultrasound. The assistance to the passage of water vapour through the membrane from the mechanical vibration created by the ultrasonic waves accounted for the bulk of this efficiency improvement. The SEM imaging and ATR FTIR results revealed that ultrasound had no negative effect on either of the membranes tested, safely returning the fouled membranes to near unused condition and with improved performance after only 30 mins.

This study has conclusively proven that an AGMD system combined with the application of non-cavitational ultrasonic energy is effective for use with natural groundwater, high salinity groundwater and RO reject feedwaters in Australia. Taking AGMD to a global industrial level still requires a good deal of further investigation and optimisation to meet the inherent low energy requirements. But it is clear, that the use of ultrasound at sonication power levels (non-cavitational) to enhance the performance of AGMD, is certainly a promising approach.

The level of power needed for industrial applications of AGMD technology with sonication also requires further work, as our results show significant benefit from application of a very low level of ultrasonic power. Further work in the scaling and fouling area is required to see if this lower level application is effective on a broader range of membrane types, and with the full range of water foulants encountered in the various surface and groundwater, types found around the globe. This work would also require the sonication aspects of frequency, amplitude and mode (pulsed or continuous) to be evaluated and correlated to permeate flux production performance and include deterioration studies to investigate longer term mechanical degradation effects.

Whilst in a laboratory environment, the current approach of inserting an active transducer into the AGMD system is effective, it is not considered a practical solution in the harsh environments typically encountered by industrial water treatment systems. The use of a non-invasive and inherently sealed sonication unit is the subject of further work being undertaken by this research team.

REFERENCES

ABEJÓN, A., GAREA, A. & IRABIEN, A. 2015. Arsenic removal from drinking water by reverse osmosis: Minimization of costs and energy consumption. *Separation and Purification Technology,* 144**,** 46-53.

AL-AMOUDI, A. S. 2010. Factors affecting natural organic matter (NOM) and scaling fouling in NF membranes: a review. *Desalination,* 259**,** 1-10.

AL-JUBOORI, R. A., ARAVINTHAN, V. & YUSAF, T. 2015a. Impact of pulsed ultrasound on bacteria reduction of natural waters. *Ultrasonics sonochemistry,* 27**,** 137-147.

AL-JUBOORI, R. A., BOWTELL, L. A., YUSAF, T. & ARAVINTHAN, V. 2016. Insights into the scalability of magnetostrictive ultrasound technology for water treatment applications. *Ultrasonics sonochemistry,* 28**,** 357-366.

AL-JUBOORI, R. A. & YUSAF, T. 2012. Identifying the optimum process parameters for ultrasonic cellular disruption of E. coli. *International Journal of Chemical Reactor Engineering,* 10.

AL-JUBOORI, R. A., YUSAF, T. & ARAVINTHAN, V. 2012. Investigating the efficiency of thermosonication for controlling biofouling in batch membrane systems. *Desalination,* 286**,** 349-357.

AL-JUBOORI, R. A., YUSAF, T., BOWTELL, L. & ARAVINTHAN, V. 2015b. Energy characterisation of ultrasonic systems for industrial processes. *Ultrasonics,* 57**,** 18-30.

AL-OBAIDANI, S., CURCIO, E., MACEDONIO, F., DI PROFIO, G., AL-HINAI, H. & DRIOLI, E. 2008. Potential of membrane distillation in seawater desalination: thermal efficiency, sensitivity study and cost estimation. *Journal of Membrane Science,* 323**,** 85-98.

ALKHUDHIRI, A., DARWISH, N. & HILAL, N. 2012a. Membrane distillation: a comprehensive review. *Desalination,* 287**,** 2-18.

ALKHUDHIRI, A., DARWISH, N. & HILAL, N. 2012b. Treatment of high salinity solutions: application of air gap membrane distillation. *Desalination,* 287**,** 55-60.

ALKLAIBI, A. & LIOR, N. 2005a. Membrane-distillation desalination: status and potential. *Desalination,* 171**,** 111-131.

ALKLAIBI, A. & LIOR, N. 2005b. Transport analysis of air-gap membrane distillation. *Journal of membrane science,* 255**,** 239-253.

ALKLAIBI, A. & LIOR, N. 2006. Heat and mass transfer resistance analysis of membrane distillation. *Journal of membrane science,* 282**,** 362-369.

ALKLAIBI, A. M. & LIOR, N. 2005c. Membrane-distillation desalination: status and potential. *Desalination,* 171**,** 111-131.

ALKLAIBI, A. M. & LIOR, N. 2007. Comparative study of direct-contact and air-gap membrane distillation processes. *Industrial & engineering chemistry research,* 46**,** 584-590.

ALPATOVA, A., MESHREF, M., MCPHEDRAN, K. N. & GAMAL EL-DIN, M. 2015. Composite polyvinylidene fluoride (PVDF) membrane impregnated with Fe2O3 nanoparticles and multiwalled carbon nanotubes for catalytic degradation of organic contaminants. *Journal of Membrane Science,* 490**,** 227-235.

ALSAADI, A. S., FRANCIS, L., AMY, G. L. & GHAFFOUR, N. 2014. Experimental and theoretical analyses of temperature polarization effect in vacuum membrane distillation. *Journal of Membrane Science,* 471**,** 138-148.

ALSAADI, A. S., FRANCIS, L., MAAB, H., AMY, G. L. & GHAFFOUR, N. 2015. Evaluation of air gap membrane distillation process running under sub-atmospheric conditions: Experimental and simulation studies. *Journal of Membrane Science,* 489**,** 73-80.

ALSAADI, A. S., GHAFFOUR, N., LI, J.-D., GRAY, S., FRANCIS, L., MAAB, H. & AMY, G. L. 2013. Modeling of air-gap membrane distillation process: a theoretical and experimental study. *Journal of membrane science,* 445**,** 53-65.

AMY, G., GHAFFOUR, N., LI, Z., FRANCIS, L., LINARES, R. V., MISSIMER, T. & LATTEMANN, S. 2017. Membrane-based seawater desalination: Present and future prospects. *Desalination,* 401**,** 16-21.

ANDERSSON, S.-I., KJELLANDER, N. & RODESJÖ, B. 1985. Design and field tests of a new membrane distillation desalination process. *Desalination,* 56**,** 345-354.

BANAT, F. A. & SIMANDL, J. 1994. Theoretical and experimental study in membrane distillation. *Desalination,* 95**,** 39-52.

BERLAN, J. & MASON, T. J. 1992. Sonochemistry: from research laboratories to industrial plants. *Ultrasonics,* 30**,** 203-212.

BONYADI, S. & CHUNG, T.-S. 2009. Highly porous and macrovoid-free PVDF hollow fiber membranes for membrane distillation by a solvent-dope solution co-extrusion approach. *Journal of membrane science,* 331**,** 66-74.

BONYADI, S. & CHUNG, T. S. 2007. Flux enhancement in membrane distillation by fabrication of dual layer hydrophilic–hydrophobic hollow fiber membranes. *Journal of membrane science,* 306**,** 134-146.

BONYADI, S., CHUNG, T. S. & RAJAGOPALAN, R. 2009. A novel approach to fabricate macrovoid-free and highly permeable PVDF hollow fiber membranes for membrane distillation. *AIChE journal,* 55**,** 828-833.

BOUBAKRI, A., BOUCHRIT, R., HAFIANE, A. & BOUGUECHA, S. A.-T. 2014. Fluoride removal from aqueous solution by direct contact membrane distillation: theoretical and experimental studies. *Environmental Science and Pollution Research,* 21**,** 10493-10501.

BOUGUECHA, S., CHOUIKH, R. & DHAHBI, M. 2003. Numerical study of the coupled heat and mass transfer in membrane distillation. *Desalination,* 152**,** 245-252.

BROWN, E., COLLING, A., PARK, D., PHILLIPS, J., ROTHERY, D. & WRIGHT, J. 1995. *Seawater: its composition, properties and behaviour*, Butterworth-Heinemann.

CAMACHO, L. M., DUMÉE, L., ZHANG, J., LI, J.-D., DUKE, M., GOMEZ, J. & GRAY, S. 2013. Advances in membrane distillation for water desalination and purification applications. *Water,* 5**,** 94-196.

CHAI, X., KOBAYASHI, T. & FUJII, N. 1999. Ultrasound-associated cleaning of polymeric membranes for water treatment. *Separation and Purification Technology,* 15**,** 139-146.

CHEN, D., HE, Z., WEAVERS, L. K., CHIN, Y.-P., WALKER, H. W. & HATCHER, P. G. 2004. Sonochemical reactions of dissolved organic matter. *Research on chemical intermediates,* 30**,** 735-753.

CHEN, D., WEAVERS, L. K. & WALKER, H. W. 2006. Ultrasonic control of ceramic membrane fouling: effect of particle characteristics. *Water research,* 40**,** 840-850.

CHEN, T.-C., HO, C.-D. & YEH, H.-M. 2009. Theoretical modeling and experimental analysis of direct contact membrane distillation. *Journal of Membrane Science,* 330**,** 279-287.

CHERNYSHOV, M., MEINDERSMA, G. & DE HAAN, A. 2005. Comparison of spacers for temperature polarization reduction in air gap membrane distillation. *Desalination,* 183**,** 363-374.

CHERNYSHOV, M. N., MEINDERSMA, G. W. & DE HAAN, A. B. 2003. Modelling temperature and salt concentration distribution in membrane distillation feedwater channel. *Desalination,* 157**,** 315-324.

COATES, J. 2006. *Interpretation of Infrared Spectra, A Practical Approach,* U.S.A., John Wiley & Sons, Ltd.

CURCIO, E., JI, X., DI PROFIO, G., FONTANANOVA, E. & DRIOLI, E. 2010a. Membrane distillation operated at high seawater concentration factors: Role of the membrane on CaCO3 scaling in presence of humic acid. *Journal of Membrane Science,* 346**,** 263-269.

CURCIO, E., JI, X., DI PROFIO, G., FONTANANOVA, E. & DRIOLI, E. 2010b. Membrane distillation operated at high seawater concentration factors: role of the membrane on CaCO 3 scaling in presence of humic acid. *Journal of Membrane Science,* 346**,** 263-269.

DOS SANTOS BAZANELLA, G. C., DA SILVA, G. F., VIEIRA, A. M. S. & BERGAMASCO, R. 2012. Fluoride removal from water using combined Moringa oleifera/ultrafiltration process. *Water, Air, & Soil Pollution,* 223**,** 6083-6093.

DROUICHE, N., GHAFFOUR, N., LOUNICI, H., MAMERI, N., MAALLEMI, A. & MAHMOUDI, H. 2008. Electrochemical treatment of chemical mechanical polishing wastewater: removal of fluoride—sludge characteristics—operating cost. *Desalination,* 223**,** 134-142.

DROUICHE, N., LOUNICI, H., DROUICHE, M., MAMERI, N. & GHAFFOUR, N. 2009. Removal of fluoride from photovoltaic wastewater by electrocoagulation and products characteristics. *Desalination and Water Treatment,* 7**,** 236-241.

DUONG, H.C., CHIVAS, A.R., NELEMANS, B., DUKE, M., GRAY, S., CATH, T.Y., & NGHIEM, L.D. (2015). Treatment of RO brine from CSG produced water by spiral-wound air gap membrane distillation - a pilot study. *Desalination,* 336, 121-129.

EL-BOURAWI, M., DING, Z., MA, R. & KHAYET, M. 2006. A framework for better understanding membrane distillation separation process. *Journal of membrane science,* 285**,** 4-29.

ELEIWI, F., GHAFFOUR, N., ALSAADI, A. S., FRANCIS, L. & LALEG-KIRATI, T. M. 2016. Dynamic modeling and experimental validation for direct contact membrane distillation (DCMD) process. *Desalination,* 384**,** 1-11.

Eykens, L., et al., *Direct contact and air gap membrane distillation: differences and similarities between lab and pilot-scale.* Desalination, 2017. **422**: p. 91-100.

FAZULLIN, D. D., MAVRIN, G. V., SOKOLOV, M. P. & SHAIKHIEV, I. G. 2015. Infrared spectroscopic studies of the PTFE and nylon membranes modified polyaniline *Modern Applied Science,* 9**,** 242-249.

FIGOLI, A., CASSANO, A., CRISCUOLI, A., MOZUMDER, M. S. I., UDDIN, M. T., ISLAM, M. A. & DRIOLI, E. 2010. Influence of operating parameters on the arsenic removal by nanofiltration. *Water research,* 44**,** 97-104.

FINDLEY, M. 1967. Vaporization through porous membranes. *Industrial & Engineering Chemistry Process Design and Development,* 6**,** 226-230.

FLEMMING, H.-C., SCHAULE, G., MCDONOGH, R. & RIDGWAY, H. F. 1994. Effects and extent of biofilm accumulation in membrane systems. *Biofouling and biocorrosion in industrial water systems***,** 63-89.

FORTUNATO, L., JANG, Y., LEE, J.-G., JEONG, S., LEE, S., LEIKNES, T. & GHAFFOUR, N. 2017. Fouling development in direct contact membrane distillation: Non-invasive monitoring and destructive analysis. *Water research*.

FRANCIS, L., GHAFFOUR, N., ALSAADI, A. A. & AMY, G. L. 2013. Material gap membrane distillation: a new design for water vapor flux enhancement. *Journal of membrane science,* 448**,** 240-247.

FRANCIS, L., GHAFFOUR, N., ALSAADI, A. S., NUNES, S. P. & AMY, G. L. 2014. Performance evaluation of the DCMD desalination process under bench scale and large scale module operating conditions. *Journal of Membrane Science,* 455**,** 103-112.

FRANKEN, A., NOLTEN, J., MULDER, M., BARGEMAN, D. & SMOLDERS, C. 1987. Wetting criteria for the applicability of membrane distillation. *Journal of Membrane Science,* 33**,** 315-328.

GÁLVEZ, J. B., GARCÍA-RODRÍGUEZ, L. & MARTÍN-MATEOS, I. 2009. Seawater desalination by an innovative solar-powered membrane distillation system: the MEDESOL project. *Desalination,* 246**,** 567-576.

GHAFFOUR, N., MISSIMER, T. M. & AMY, G. L. 2013. Technical review and evaluation of the economics of water desalination: current and future challenges for better water supply sustainability. *Desalination,* 309**,** 197-207.

GONG, Y., WANG, X.-L. & LI-XIN, Y. 2005. Process simulation of desalination by electrodialysis of an aqueous solution containing a neutral solute. *Desalination,* 172**,** 157-172.

GRAY, G. T., MCCUTCHEON, J. R. & ELIMELECH, M. 2006. Internal concentration polarization in forward osmosis: role of membrane orientation. *Desalination,* 197**,** 1-8.

GRYTA, M. 2002. The assessment of microorganism growth in the membrane distillation system. *Desalination,* 142**,** 79-88.

GRYTA, M. 2008. Fouling in direct contact membrane distillation process. *Journal of membrane science,* 325**,** 383-394.

GRYTA, M. & BARANCEWICZ, M. 2010. Influence of morphology of PVDF capillary membranes on the performance of direct contact membrane distillation. *Journal of Membrane Science,* 358**,** 158-167.

GRYTA, M. & KARAKULSKI, K. 1999. The application of membrane distillation for the concentration of oil-water emulsions. *Desalination,* 121**,** 23-29.

GRYTA, M., TOMASZEWSKA, M. & MORAWSKI, A. 2001. A capillary module for membrane distillation process. *CHEMICAL PAPERS-SLOVAK ACADEMY OF SCIENCES,* 54**,** 370-374.

GUILLÉN-BURRIEZA, E., BLANCO, J., ZARAGOZA, G., ALARCÓN, D.-C., PALENZUELA, P., IBARRA, M. & GERNJAK, W. 2011. Experimental analysis of an air gap membrane distillation solar desalination pilot system. *Journal of Membrane Science,* 379**,** 386-396.

GUILLEN-BURRIEZA, E., THOMAS, R., MANSOOR, B., JOHNSON, D., HILAL, N. & ARAFAT, H. 2013. Effect of dry-out on the fouling of PVDF and PTFE membranes under conditions simulating intermittent seawater membrane distillation (SWMD). *Journal of membrane science,* 438**,** 126-139.

GUNKO, S., VERBYCH, S., BRYK, M. & HILAL, N. 2006. Concentration of apple juice using direct contact membrane distillation. *Desalination,* 190**,** 117-124.

GUTMAN, R. 1987. *Membrane filtration: the technology of pressure-driven crossflow processes*, Adam Hilger.

HERCZEG, A., DOGRAMACI, S. & LEANEY, F. 2001. Origin of dissolved salts in a large, semi-arid groundwater system: Murray Basin, Australia. *Marine and Freshwater Research,* 52**,** 41-52.

HO, W. & SIRKAR, K. 1992. Membrane Handbook Van Nostrand Reinhold New York Google Scholar.

HOU, D., WANG, J., WANG, B., LUAN, Z., SUN, X. & REN, X. 2010. Fluoride removal from brackish groundwater by direct contact membrane distillation. *Water Science and Technology,* 61**,** 3178-3187.

IZQUIERDO-GIL, M., GARCıA-PAYO, M. & FERNÁNDEZ-PINEDA, C. 1999. Air gap membrane distillation of sucrose aqueous solutions. *Journal of membrane science,* 155**,** 291-307.

JIAO, B., CASSANO, A. & DRIOLI, E. 2004. Recent advances on membrane processes for the concentration of fruit juices: a review. *Journal of food engineering,* 63**,** 303-324.

KARAKULSKI, K., GRYTA, M. & SASIM, M. 2006. Production of process water using integrated membrane processes. *Chemical Papers,* 60**,** 416-421.

KEMER, B., OZDES, D., GUNDOGDU, A., BULUT, V. N., DURAN, C. & SOYLAK, M. 2009. Removal of fluoride ions from aqueous solution by waste mud. *Journal of hazardous materials,* 168**,** 888-894.

KHALIFA, A. E. 2015. Water and air gap membrane distillation for water desalination–An experimental comparative study. *Separation and Purification Technology,* 141**,** 276-284.

KHAYET, M., MENGUAL, J. & MATSUURA, T. 2005. Porous hydrophobic/hydrophilic composite membranes: application in desalination using direct contact membrane distillation. *Journal of Membrane Science,* 252**,** 101-113.

KOBAYASHI, T., KOBAYASHI, T., HOSAKA, Y. & FUJII, N. 2003. Ultrasound-enhanced membrane-cleaning processes applied water treatments: influence of sonic frequency on filtration treatments. *Ultrasonics,* 41**,** 185-190.

KUBOTA, S., OHTA, K., HAYANO, I., HIRAI, M., KIKUCHI, K. & MURAYAMA, Y. 1988. Experiments on seawater desalination by membrane distillation. *Desalination,* 69**,** 19-26.

KUEHN, T., KITTELSON, D., WU, Y. & GOUK, R. 1996. Particle removal from semiconductor wafers by megasonic cleaning. *Journal of Aerosol Science,* 27**,** S427-S428.

KULLAB, A. 2011. *Desalination using membrane distillation: experimental and numerical study.* KTH Royal Institute of Technology.

LAMMINEN, M. O., WALKER, H. W. & WEAVERS, L. K. 2004a. Mechanisms and factors influencing the ultrasonic cleaning of particle-fouled ceramic membranes. *Journal of membrane science,* 237**,** 213-223.

LAMMINEN, M. O., WALKER, H. W. & WEAVERS, L. K. 2004b. Mechanisms and factors influencing the ultrasonic cleaning of particle-fouled ceramic membranes. *Journal of Membrane Science,* 237**,** 213-223.

LAWSON, K. W. & LLOYD, D. R. 1997. Membrane distillation. *Journal of membrane Science,* 124**,** 1-25.

LE MY, D. 2015. *Membrane Distillation Application in Purification and Process Intensification.* Asian Institute of Technology.

LEE, J.-G., ALSAADI, A. S., KARAM, A. M., FRANCIS, L., SOUKANE, S. & GHAFFOUR, N. 2017. Total water production capacity inversion phenomenon in multi-stage direct contact membrane distillation: A theoretical study. *Journal of Membrane Science,* 544**,** 126-134.

LI, J., SANDERSON, R. & JACOBS, E. 2002a. Ultrasonic cleaning of nylon microfiltration membranes fouled by Kraft paper mill effluent. *Journal of Membrane Science,* 205**,** 247-257.

LI, J., SANDERSON, R. & JACOBS, E. 2002b. Ultrasonic cleaning of nylon microfiltration membranes fouled by Kraft paper mill effluent. *Journal of Membrane Science,* 205**,** 247-257.

LI, S., WANG, Y., WANG, T., TIAN, D., ZHENG, L. & LUO, Q. 2010. Removal of fluorions from trifluoroacetic acid by reverse osmosis. *Desalination and Water Treatment,* 20**,** 66-71.

LIU, H. & WANG, J. 2013. Treatment of radioactive wastewater using direct contact membrane distillation. *Journal of hazardous materials,* 261**,** 307-315.

MAHESHWARI, R. 2006. Fluoride in drinking water and its removal. *Journal of Hazardous materials,* 137**,** 456-463.

MASON, T. J. & PETERS, D. 2002. *Practical sonochemistry: Power ultrasound uses and applications*, Woodhead Publishing.

MEHTA, G. D. 1982. Comparison of membrane processes with distillation for alcohol/water separation. *Journal of membrane science,* 12**,** 1-26.

MEINDERSMA, G., GUIJT, C. & DE HAAN, A. 2006. Desalination and water recycling by air gap membrane distillation. *Desalination,* 187**,** 291-301.

MENGUAL, J., KHAYET, M. & GODINO, M. 2004. Heat and mass transfer in vacuum membrane distillation. *International Journal of Heat and Mass Transfer,* 47**,** 865-875.

MILLER, F. A. & WILKINS, C. H. 1952. Infrared Spectra and Characteristic Frequencies of Inorganic Ions. *Analytical Chemistry,* 24**,** 1253-1294.

MINIS, I. 2010. *Supply Chain Optimization, Design, and Management: Advances and Intelligent Methods: Advances and Intelligent Methods*, IGI Global.

MOHAPATRA, M., ANAND, S., MISHRA, B. K., GILES, D. E. & SINGH, P. 2009. Review of fluoride removal from drinking water. *Journal of environmental management,* 91**,** 67-77.

MONTGOMERY, D. C. 2017. *Design and analysis of experiments*, John wiley & sons.

NOBLE, R. D. & STERN, S. A. 1995. *Membrane separations technology: principles and applications*, Elsevier.

ORGANIZATION, W. H. 2004. *Guidelines for drinking-water quality: recommendations*, World Health Organization.

ORGANIZATION, W. H. 2006. *Guidelines for the safe use of wastewater, excreta and greywater*, World Health Organization.

PAL, P. & MANNA, A. K. 2010. Removal of arsenic from contaminated groundwater by solar-driven membrane distillation using three different commercial membranes. *water research,* 44**,** 5750-5760.

PENG, P., FANE, A. & LI, X. 2005. Desalination by membrane distillation adopting a hydrophilic membrane. *Desalination,* 173**,** 45-54.

PÉREZ-SICAIROS, S., LIN, S. W., FÉLIX-NAVARRO, R. M. & ESPINOZA-GÓMEZ, H. 2009. Rejection of As (III) and As (V) from arsenic contaminated water via electro-cross-flow negatively charged nanofiltration membrane system. *Desalination,* 249**,** 458-465.

PHATTARANAWIK, J. & JIRARATANANON, R. 2001. Direct contact membrane distillation: effect of mass transfer on heat transfer. *Journal of Membrane Science,* 188**,** 137-143.

PIÑÓN-MIRAMONTES, M., BAUTISTA-MARGULIS, R. G. & PÉREZ-HERNÁNDEZ, A. 2003. Removal of arsenic and fluoride from drinking water with cake alum and a polymeric anionic flocculent. *Fluoride,* 36**,** 122-128.

PIRNIE, M. 1999. Technologies and costs for removal of arsenic from drinking water. *Technologies and costs for removal of arsenic from drinking water.* EPA.

PLATTNER, J., NAIDU, G., WINTGENS, T., VIGNESWARAN, S. & KAZNER, C. 2017. Fluoride removal from groundwater using direct contact membrane distillation (DCMD) and vacuum enhanced DCMD (VEDCMD). *Separation and Purification Technology,* 180**,** 125-132.

PONTIÉ, M., DACH, H., LEPARC, J., HAFSI, M. & LHASSANI, A. 2008. Novel approach combining physico-chemical characterizations and mass transfer modelling of nanofiltration and low pressure reverse osmosis membranes for brackish water desalination intensification. *Desalination,* 221**,** 174-191.

POVEY, M. J. & MASON, T. J. 1998. *Ultrasound in food processing*, Springer Science & Business Media.

QASIM, M., DARWISH, N., MHIYO, S., DARWISH, N. & HILAL, N. 2018. The use of ultrasound to mitigate membrane fouling in desalination and water treatment. *Desalination,* 443**,** 143-164.

RAMDANI, A., TALEB, S., BENGHALEM, A. & GHAFFOUR, N. 2010. Removal of excess fluoride ions from Saharan brackish water by adsorption on natural materials. *Desalination,* 250**,** 408-413.

RANJAN, D., SRIVASTAVA, P., TALAT, M. & HASAN, S. 2009. Biosorption of Cr (VI) from water using biomass of Aeromonas hydrophila: central composite design for optimization of process variables. *Applied biochemistry and biotechnology,* 158**,** 524-539.

RICHARDS, B. S. & SCHÄFER, A. I. 2003. Photovoltaic-powered desalination system for remote Australian communities. *Renewable Energy,* 28**,** 2013-2022.

RICHARDS, L. A., RICHARDS, B. S. & SCHÄFER, A. I. 2011. Renewable energy powered membrane technology: salt and inorganic contaminant removal by nanofiltration/reverse osmosis. *Journal of Membrane Science,* 369**,** 188-195.

RUIZ ESPEJO, M. 2006. Design of experiments for engineers and scientists. Taylor & Francis.

SATO, Y., KANG, M., KAMEI, T. & MAGARA, Y. 2002. Performance of nanofiltration for arsenic removal. *Water Research,* 36**,** 3371-3377.

SCHNEIDER, K., HÖLZ, W., WOLLBECK, R. & RIPPERGER, S. 1988. Membranes and modules for transmembrane distillation. *Journal of membrane science,* 39**,** 25-42.

SHIH, M.-C. 2005. An overview of arsenic removal by pressure-drivenmembrane processes. *Desalination,* 172**,** 85-97.

SONG, L., LI, B., SIRKAR, K. K. & GILRON, J. L. 2007. Direct contact membrane distillation-based desalination: novel membranes, devices, larger-scale studies, and a model. *Industrial & engineering chemistry research,* 46**,** 2307-2323.

SUSANTO, H. 2011. Towards practical implementations of membrane distillation. *Chemical Engineering and Processing: Process Intensification,* 50**,** 139-150.

TARLETON, E. & WAKEMAN, R. J. 1990. Microfiltration enhancement by electrical and ultrasonic force fields. *Filtration & Separation,* 27**,** 192-194.

TEOH, M. M. & CHUNG, T.-S. 2009. Membrane distillation with hydrophobic macrovoid-free PVDF–PTFE hollow fiber membranes. *Separation and Purification Technology,* 66**,** 229-236.

THOMPSON, L. & DORAISWAMY, L. 1999. Sonochemistry: science and engineering. *Industrial & Engineering Chemistry Research,* 38**,** 1215-1249.

TIJING, L. D., WOO, Y. C., CHOI, J.-S., LEE, S., KIM, S.-H. & SHON, H. K. 2015. Fouling and its control in membrane distillation—a review. *Journal of Membrane Science,* 475**,** 215-244.

TOMASZEWSKA, M. 2000. Membrane distillation-examples of applications in technology and environmental protection. *Polish Journal of Environmental Studies,* 9**,** 27-36.

TRINH, T. K. & KANG, L.-S. 2010. Application of response surface method as an experimental design to optimize coagulation tests. *Environmental Engineering Research,* 15**,** 63-70.

VELEY, R. J. 1992. Advantages and limitations of water-supply alternatives. US Geological Survey, Dept. of the Interior.

VELIZAROV, S., CRESPO, J. G. & REIS, M. A. 2004. Removal of inorganic anions from drinking water supplies by membrane bio/processes. *Reviews in Environmental Science and Bio/Technology,* 3**,** 361-380.

VENKATESAN, G., KULASEKHARAN, N., MUTHUKUMAR, V. & INIYAN, S. 2015. Regression analysis of a curved vane demister with Taguchi based optimization. *Desalination,* 370**,** 33-43.

WALTON, J., LU, H., TURNER, C., SOLIS, S. & HEIN, H. 2004. Solar and waste heat desalination by membrane distillation. *Desalination and water purification research and development program report***,** 20.

WARSINGER, D. M., SWAMINATHAN, J., GUILLEN-BURRIEZA, E. & ARAFAT, H. A. 2015. Scaling and fouling in membrane distillation for desalination applications: A review. *Desalination,* 356**,** 294-313.

WATER, U. 2012. Managing water under uncertainty and risk, The United Nations world water development report 4, UN Water Reports, World Water Assessment Programme. UNESCO, Paris, France.

WEYL, P. K. 1967. Recovery of demineralized water from saline waters. Google Patents.

WU, Y., KONG, Y., LIN, X., LIU, W. & XU, J. 1992. Surface-modified hydrophilic membranes in membrane distillation. *Journal of membrane science,* 72**,** 189-196.

XU, J., BETTAHALLI, N. S., CHISCA, S., KHALID, M. K., GHAFFOUR, N., VILAGINES, R. & NUNES, S. P. 2018. Polyoxadiazole hollow fibers for produced water treatment by direct contact membrane distillation. *Desalination,* 432**,** 32-39.

XU, J., SINGH, Y. B., AMY, G. L. & GHAFFOUR, N. 2016. Effect of operating parameters and membrane characteristics on air gap membrane distillation performance for the treatment of highly saline water. *Journal of Membrane Science,* 512**,** 73-82.

XU, L., GAO, X., LI, Z. & GAO, C. 2015. Removal of fluoride by nature diatomite from high-fluorine water: an appropriate pretreatment for nanofiltration process. *Desalination,* 369**,** 97-104.

YANG, X., WANG, R., SHI, L., FANE, A. G. & DEBOWSKI, M. 2011. Performance improvement of PVDF hollow fiber-based membrane distillation process. *Journal of Membrane Science,* 369**,** 437-447.

ZHANG, J. 2011. *Theoretical and experimental investigation of membrane distillation.* Victoria University.

ZHANG, J., DUKE, M., XIE, Z. & GRAY, S. 2010. Performance of asymmetric hollow fibre membranes in membrane distillation under various configurations and vacuum enhancement. *Journal of Membrane Science,* 362**,** 517-528.

ZHU, C. & LIU, G. 2000. Modeling of ultrasonic enhancement on membrane distillation. *Journal of Membrane Science,* 176**,** 31-41.

APPENDIX A: Conductivity Probes and Transmitters

micro*CHEM*-Cond Transmitter Module

Handbook Version : 1.02 Date : 23-Nov-2006

TPS Pty Ltd

4 Jamberoo Street Springwood, Brisbane, Australia, 4127

Phone: (07) 32 900 400

International : 61 7 32 900 400

Fax: (07) 3808 4871

International : 61 7 3808 4871 Email: tps@tps.com.au

Web Site : www.tps.com.au

Conductivity Sensors…

1. k=0.1 GK Series Conductivity Sensor, 5m.112205
2. k=1.0 GK Series Conductivity Sensor, 5m..... 112206
3. k=10 GK Series Conductivity Sensor, 5m..... 112207

Specifications

Ranges

k=0.1 Sensor: 0 to 20.00 µS/cm, 0 to 200.0 µS/cm, 0 to 2000 µS/cm

k=1.0 Sensor: 0 to 200.0 µS/cm, 0 to 2000 µS/cm, 0 to 20.00 mS/cm

k=10 Sensor: 0 to 2000 µS/cm, 0 to 20.00 mS/cm, 0 to 200.0 mS/cm

Resolution: ±1mV (0 – 1 V DC Output) or ±5mV (0 – 5 V DC Output)

Accuracy: ±1mV (0 – 1 V DC Output) or ±5mV (0 – 5 V DC Output)

Linearity: ±1mV (0 – 1 V DC Output) or ±5mV (0 – 5 V DC Output)

Repeatability: ±1mV (0 – 1 V DC Output) or ±5mV (0 – 5 V DC Output)

Ambient Drift .....<0.02% / °C

Long term drift .....<0.1% per year

Zero Range ..... ±5 %

Span Range..... 70 to 130%

Temperature Compensation ..... Automatic, 0 to 100.0 °C

Enclosure.....Polycarbonate, waterproof to IP65

Analogue Outputs: 0 to 1 V DC or 0 to 5 V DC Isolation .....

Galvanic isolation of sensor input

Power .....12V DC, approx 10mA

Dimensions: Enclosure: 125 x 85 x 56 mm

PCB only:115 x 77 mm (82 x 58 mm mounting hole centres)

Mass .....Instrument only: Approx 250 g

Full Kit : Approx 1.0 kg

Operating Environment: Temperature 0 to 45 °C, Humidity: 0 to 95 % R.H.

1. Installation and Set-up

2.1. Connection and Configuration Diagram

The diagram below is provided as a reference for the terminal connections, configuration jumpers and user-adjustable trimmers that are discussed throughout this section.

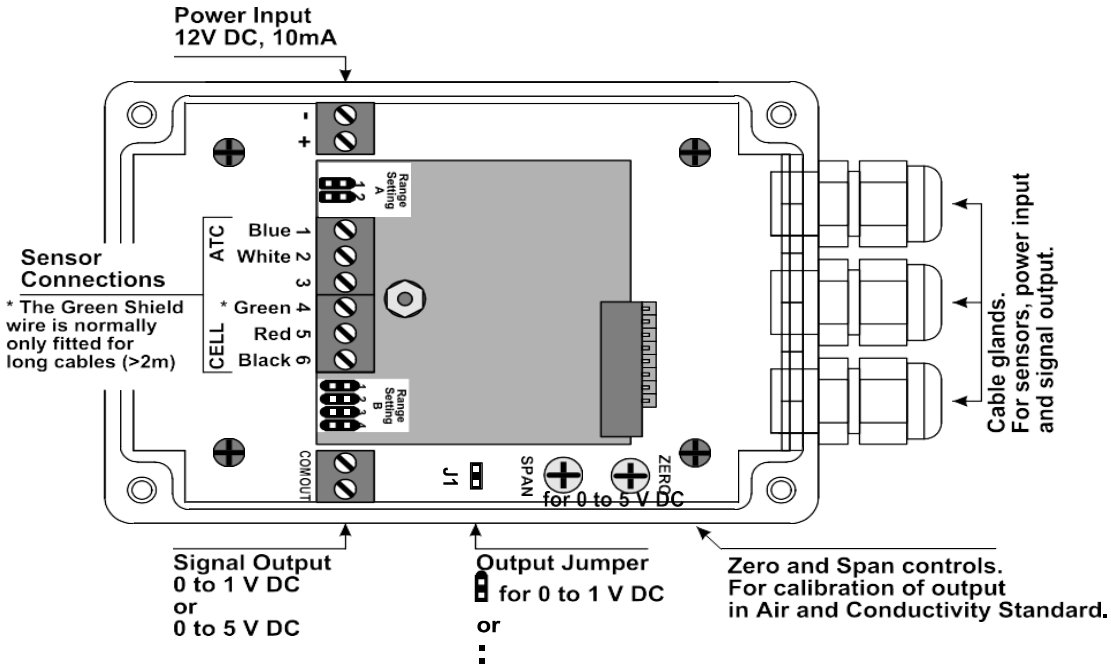

2.2. Mounting the Enclosure

The micro*CHEM*-Cond can be mounted directly onto a wall or into a separate enclosure using the mounting kit supplied. Please use the screws supplied to ensure that the waterproof integrity of the enclosure is not compromised.

2.3. Mounting the Sensors

Mounting the sensor is a very important aspect of the installation, and is often done incorrectly. In automatic control situations, the sensor should always be mounted as close as possible to the injection point. This will cause the sensor to detect the added chemicals or water immediately, and shut the addition off until mixing has taken place. For in-line mounting, it is important that injection is upstream. Additionally, the line must be run through a mixing chamber, such as a large drum, to ensure that the injected chemical or water has mixed in properly by the time the solution flows past the sensor. There must always be adequate flow of fresh sample past the sensor for accurate monitoring. The diagrams below show typical mounting arrangements for “dip” mounting and in-line mounting.

Dip Mounting

1. Injection point close to sensor.
2. Continuous stirring.

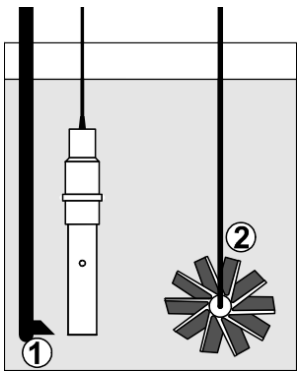

In-line Mounting

1. Injection point upstream from and close to sensor.
2. Mixing container after injection and before sensor.
3. A flow-through assembly for in-line mounting is available from TPS.

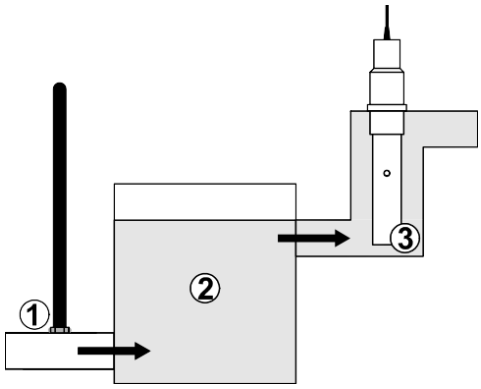

2.4. Terminal Connections

Terminal No.	Connection	Colour
Sensor Connections		
1	Conductivity Sensor ATC	Blue
2	Conductivity Sensor ATC	White
3	No Connection	
4	Shield (if fitted to cable)	Green or Braid
5	Conductivity Sensor Cell	Red
6	Conductivity Sensor Cell	Black
Power Input Connections		
–	Negative of 12V DC Input	Customer-defined
+	Positive of 12V DC Input	Customer-defined
Signal Output Connections		
COM	Common of voltage output	Customer-defined
OUT	Positive of voltage output	Customer-defined

Selecting 0 to 1 V DC or 0 to 5 V DC Output

1. Locate the jumper labelled J1 on the main circuit board.
2. Set J1 to closed to select 0 to 1 V DC output.
3. Set J1 to open to select 0 to 5 V DC output.

0 to 1 V DC 0 to 5 V DC

Note

When setting J1 to open, we recommend that it is fitted to one of the pins.

This is a safe place to keep it, in case the micro*CHEM*-Cond needs to be reset for 0 to 1 V DC output in the future.

3. Calibration

3.1. Calibration Procedure

1. Switch the micro*CHEM*-Cond on.
2. Ensure that the Conductivity sensor is correctly connected (see section 2.4).
3. For the GK-1 sensor (part no 112206), ensure that the white protective cover is fitted with the vent hole towards the cable end of the sensor.
4. Rinse the Conductivity sensor in distilled water and blot dry.

Zero Calibration

5. Shake the Conductivity sensor dry and hang it in air. DO NOT wipe the platinised platinum electrode surface, as this will remove the platinum-black layer.
6. When the reading has stabilised, adjust the ZERO control until the output is exactly 0 mV.

Span Calibration

7. Place the Conductivity sensor into a small sample of Conductivity standard. A suitable standard should be chosen for the display range of the unit.
9. For GK-1 (part no 112206) and GK-10 (part no 112207) sensors, ensure that they are immersed at least to the vent hole in the white plastic cover. The GK-0.1 (part no 112205) sensor does not have a cover, so it should be immersed to the large thread (see diagrams below).

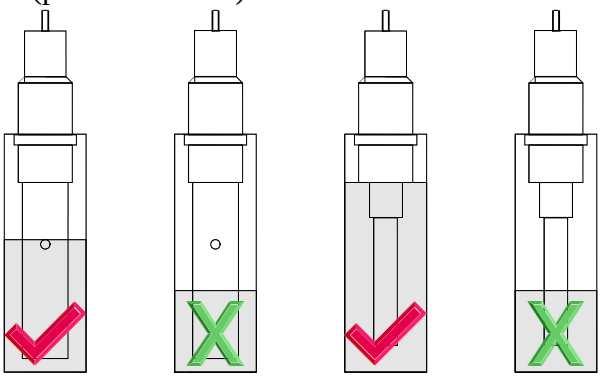

10. When the reading has stabilised, adjust the SPAN control until the output corresponds to the value shown in the Calibration Data table in section 3.3.
11. Rinse the Conductivity sensor in distilled water and blot dry.
12. The micro*CHEM*-Cond is now calibrated and ready for Conductivity measurements.

3.2. Calibration Notes

1. The Zero calibration is quite stable long term, and only needs to be performed monthly as a routine check. In applications where the sensor can become dirty or coated with oils etc., a Zero calibration may need to be done weekly.
2. A Span calibration should be performed at least weekly. Of course, more frequent calibration will result in greater confidence in results.

3.3. Calibration Data

The following table details the output for Conductivity standards available from TPS to suit the ranges of the micro*CHEM*-Cond. Other Conductivity standards may be used, in which case you will need to calculate the output of your micro*CHEM*-Cond for the standard being used.

Range	Standard	
	Output 0 to 1 V	Output 0 to 5 V
0 to 20 µS/cm	No standard available for this range.	
0 to 200 µS/cm	150 µS/cm	
	750 mV	3750 mV
0 to 2000 µS/cm	1413 µS/cm	
	706.5 mV	3533 mV
0 to 20 mS/cm	2.76 mS/cm	
	138 mV	690 mV
0 to 200 mS/cm	58.0 mS/cm	
	290 mV	1450 mV

4. Troubleshooting

4.1. Instrument Function Troubleshooting

Symptom	Possible Causes	Remedy
Incorrect analogue output signal.	1. J1 Output Jumper incorrectly set for required output. 2. Instrument is faulty.	Check that the J1 Output Jumper is correctly set for 0 to 1 V DC or 0 to 5 V DC output, as per requirements. Adjust if necessary (see section 2.5). Return to TPS for repair.

4.2. Conductivity Troubleshooting

Symptom	Possible Causes	Remedy
Zero calibration fails (insufficient range with ZERO control).	1. Electrode has Zero error. 2. Sensor is faulty.	Thoroughly rinse electrode in distilled water and allow to completely dry in air before attempting zero calibration. If instrument does not calibrate at Zero with electrode disconnected, then the instrument is faulty. Replace sensor.

Standard calibration fails, reading is too low and cannot be adjusted high enough.	1. Electrode is not immersed deeply enough. 2. Electrode may have a build-up of dirt or oily material on electrode wires. 3. Platinum-black coating has worn off. 4. Standard solution is inaccurate. 5. Electrode is faulty.	Immerse electrode at least to the vent hole in the white plastic cover. Clean electrode, as per the instructions detailed in section 6.2.2. Electrode requires replatinisation. Return to the factory, or see details in section 6.2.3. Replace standard solution. Return electrode to factory for repair or replacement.

Conductivity Troubleshooting, continued…

Standard calibration fails, reading is too high and cannot be adjusted low enough.	1. White protective cover is not fitted (GK-1 sensor). 2. Standard solution is inaccurate. 3. Electrode may have a build-up of conductive material, such as salt. 4. Electrode is faulty.	The white protective cover MUST be fitted for correct readings for GK-1 sensor. Replace standard solution. Clean electrode, as per the instructions detailed in section 6.2.2. Return electrode to factory for repair or replacement.
Inaccurate readings, even when calibration is successful.	1. Electrode may have a build-up of dirt or oily material on electrode wires. 2. Platinum-black coating has worn off.	Clean electrode, as per the instructions detailed in section 6.2.2. Electrode requires replatinisation. Return to the factory, or see details in section 6.2.3.
Readings drift.	1. Electrode may have a build-up of dirt or oily material on electrode wires.	Clean electrode, as per the instructions detailed in section 6.2.2.
Readings are low or near zero.	1. Electrode may have a build-up of dirt or oily material on electrode wires. 2. Electrode is not immersed deeply enough. 3. Electrode is faulty.	Clean electrode, as per the instructions detailed in section 6.2.2. Immerse electrode at least to the vent hole in the white plastic cover. Return electrode to factory for repair or replacement.

5. Warranty

TPS Pty. Ltd. guarantees all instruments and electrodes to be free from defects in material and workmanship when subjected to normal use and service. This guarantee is expressly limited to the servicing and/or adjustment of an instrument returned to the Factory, or Authorised Service Station, freight prepaid, within twelve (12) months from the date of delivery, and to the repairing, replacing, or adjusting of parts which upon inspection are found to be defective. Warranty period on electrodes is three (3) months.

There are no express or implied warranties which extend beyond the face hereof, and TPS Pty. Ltd. is not liable for any incidental or consequential damages arising from the use or misuse of this equipment, or from interpretation of information derived from the equipment.

Shipping damage is not covered by this warranty.

PLEASE NOTE:

A guarantee card is packed with the instrument or electrode. This card must be completed at the time of purchase and the registration section returned to TPS Pty. Ltd. within 7 days. No claims will be recognised without the original guarantee card or other proof of purchase. This warranty becomes invalid if modifications or repairs are attempted by unauthorised persons, or the serial number is missing.

PROCEDURE FOR SERVICE

If you feel that this equipment is in need of repair, please re-read the manual. Sometimes, instruments are received for "repair" in perfect working order. This can occur where batteries simply require replacement or re-charging, or where the electrode simply requires cleaning or replacement.

TPS Pty. Ltd. has a fine reputation for prompt and efficient service. In just a few days, our factory service engineers and technicians will examine and repair your equipment to your full satisfaction.

TO OBTAIN THIS SERVICE, PLEASE FOLLOW THIS PROCEDURE:

Return the instrument AND ALL SENSORS to TPS freight pre-paid and insured in its original packing or suitable equivalent. INSIST on a proof of delivery receipt from the carrier for your protection in the case of shipping claims for transit loss or damage. It is your responsibility as the sender to ensure that TPS receives the unit

Please check that the following is enclosed with your equipment:

- Your Name and daytime phone number.
- Your company name, ORDER number, and return street address.
- A description of the fault. (Please be SPECIFIC.)
  (Note: "Please Repair" does NOT describe a fault.)

Your equipment will be repaired and returned to you by air express where possible.

For out-of-warranty units, a repair cost will be calculated from parts and labor costs. If payment is not received for the additional charges within 30 days, or if you decline to have the equipment repaired, the complete unit will be returned to you freight paid, not repaired. For full-account customers, the repair charges will be debited to your account.

Always describe the fault in writing.

Always return the sensors with the meter

Re-setting the Measurement Range

The range of the micro*CHEM*-Cond may be re-set using the table of jumper settings shown below. Refer to the diagram in section 2.1 for the location of the A and B range jumper blocks. Attach spare jumpers off single unused pins for safe storage.

	Sensor k Factor		
Range	**k=0.1**	**k=1.0**	**k=10**
0 to 20 uS/cm	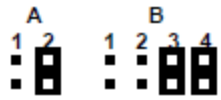	This range not available for k=1.0 sensor.	This range not available for k=10 sensor.
0 to 200 uS/cm	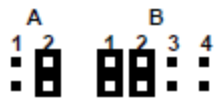	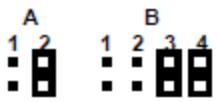	This range not available for k=10 sensor.
0 to 2000 uS/cm		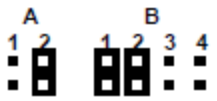	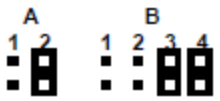
0 to 20 mS/cm	This range not available for k=0.1 sensor.	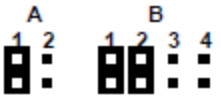	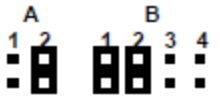
0 to 200 mS/cm	This range not available for k=0.1 sensor.	This range not available for k=1.0 sensor.	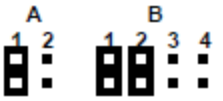

6. Care, Cleaning and Maintenance of Conductivity Electrodes

1.1. Care of Conductivity electrodes

The conductivity section of the electrode supplied with your micro*CHEM*-Cond consists of two platinum wires that are plated with a layer of "platinum-black". This is quite a soft layer and is required for stable, accurate measurements. In time, the platinum-black layer may wear off in some applications, at which time the electrode will require replatinising (see section 6.2.3). You can help to maintain the platinum-black layer by following these simple rules:

1. NEVER touch or rub the electrode wires with your fingers, cloth etc.
2. Avoid using the electrode in solutions that contain a high concentration of suspended solids, such as sand or soil, which can abrade the electrode wires. Filter these types of solutions first, if possible.
3. Avoid concentrated acids. If you must measure acids, remove the electrode immediately after taking the measurement and rinse well with distilled water.

Conductivity electrodes can be stored dry. Ensure that the electrode is stored in a covered container, to avoid dust and dirt build-up.

1.2. Cleaning Conductivity of Electrodes

Platinised platinum Conductivity electrodes can only be cleaned by rinsing in a suitable solvent. DO NOT wipe the electrode wires, as this will remove the platinum-black layer.

1. Rinsing in distilled water will remove most build-ups of material on the electrode wires.
2. Films of oils or fats on the electrode wires can usually be removed by rinsing the electrode in methylated spirits.

3. Stubborn contamination can be removed by soaking the electrode in a solution of 1 part Concentrated HCl and 10 parts distilled water. The electrode should not be soaked for more than approximately 5 minutes, otherwise the platinum- black layer may start to dissolve.
4. If all of these methods fail, then the last resort is to physically scrub the electrode wires, which will remove the contaminant and the layer of platinum- black. Use only a cloth or nylon scouring pad. DO NOT USE STEEL WOOL. The electrode will then need to be cleaned in HCl, as per step 3 and replatinised, as per section 6.2.3.

APPENDIX B Fluoride Probe

Version 2.2
03-Mar-2011

TPS uniPROBE Fluoride (F^-) ISE

Introduction
The TPS Fluoride ISE belongs to a bold new line of ion sensors that offer superb versatility, performance, and savings. It is based on standard lanthanum fluoride crystal technology, where the crystal is bonded to a replaceable rubber tip that fits onto a combination electrode barrel.

- **Silicone rubber seal**

Fluid leakage around the lanthanum fluoride crystal is the most common mode of failure in a fluoride ISE. This is due to the fact that there are no long lasting adhesive that will stick to the crystal, especially in an underwater environment. The silicone rubber tip forms a robust mechanical seal to the inert lanthanum fluoride crystal. Water will not affect the seal and temperature expansion and contraction is compensated for by the elasticity of the silicone rubber.

- **Replaceable tip**

The lanthanum fluoride sensor tip is easily removed from the electrode body. This allows the internal filling solution to be replenished in the event that it dries out, or the entire tip can be replaced at considerable savings if it becomes inoperable.

- **Replaceable Double Junction Reference Gel**

The double junction reference design allows the reference junction to be easily renewed by replacing the outer reference gel.

- **Interchangeable sensor tips**

In many instances the same electrode barrel can be used with other sensing tips, such as chloride, nitrate, ammonium, calcium, potassium, sodium, and others. These tips can be ordered separately. In some instances a different reference gel will be required. Consult your TPS representative.

TPS uniPROBE ISE Probe Parts

Electrode Barrel | Plastic Stem | Reference Sleeve | Sensing Tip

TPS Pty Ltd
A.B.N. No 30 009 773 371
4 Jamberoo Street
Springwood, Brisbane,
AUSTRALIA, 4127
Phone Australia (07) 32 900 400
International 61 7 32 900 400
Email tps@tps.com.au
Fax Australia (07) 3808 4871
International 61 7 3808 4871
Web www.tps.com.au

Preparing the Electrode

1. Remove the reference sleeve and rinse the plastic stem with deionised water.

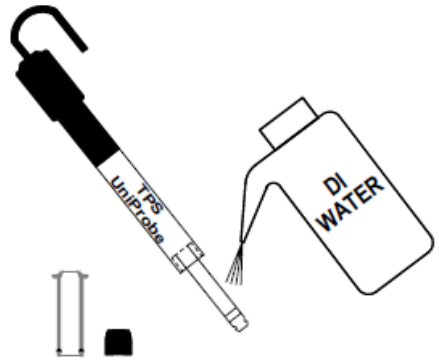

2. Fill the well around the stem with Potassium Chloride Reference Electrolyte Gel.

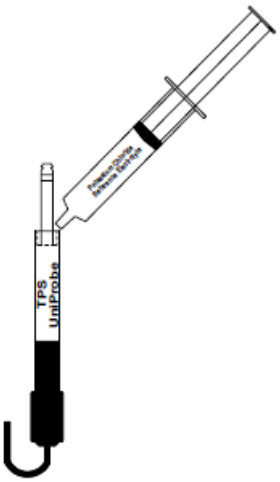

3. Slide the reference sleeve over the plastic stem until the black O ring is 4mm inside the body. Some force may be required. Reference Electrolyte Gel will be expelled from the end of the stem. Rinse with deionised water. Dry the end of the plastic stem with a tissue.

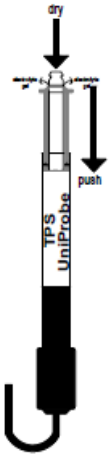

4. Fill a green fluoride silicone rubber tip with Internal Filling Solution. Before filling, fit the black tube supplied into the nozzle of the bottle. Carefully insert the tube into the sensing tip and fill it from the bottom up. This procedure prevents air traps.

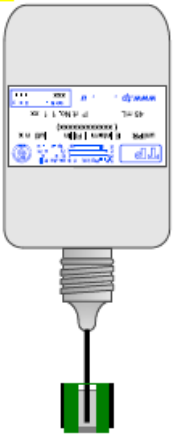

5. **Gently** push the tip onto the plastic stem until it stops.
DO NOT FORCE IT BEYOND THE STOP POSITION.
DO NOT TOUCH THE SENSING SURFACE.
Rinse with deionised water. Condition the ISE overnight, if possible, or until the reading no longer drifts.

TPS Pty Ltd
A.B.N. No 30 009 773 371
4 Jamberoo Street
Springwood, Brisbane,
AUSTRALIA, 4127
Phone Australia (07) 32 900 400
International 61 7 32 900 400
Email tps@tps.com.au
Fax Australia (07) 3808 4871
International 61 7 3808 4871
Web www.tps.com.au

Ordering Information

	Part No
Complete TPS Fluoride ISE Analysis Kit	121560
Includes 1 x Combination ISE Body	121500
1 x Fluoride ISE Membrane / IFS / Electrolyte Kit	121562
1 x 1000ppm F^- Standard (200mL)	121564
1 x TISAB Solution (200mL)	121820
1 x Fluoride ISE Instruction Manual	130050

Spare parts and accessories…

Combination Intermediate Junction ISE Barrel	121500
Fluoride ISE Membrane Kit	121562
Includes 1 x Green Membrane tip	
1 x Internal Filling Solution (IFS), 45mL	121806
1 x External Reference Electrolyte Gel, 10mL	121811
Internal Filling Solution (IFS), 45mL	121806
External Reference Electrolyte Gel, 10mL	121811
1000ppm F^- Standard (200mL)	121564
1000ppm F^- Standard (1 Litre)	121566
TISAB Solution (200mL)	121820
TISAB Solution (1 Litre)	121822
Fluoride ISE Instruction Manual	130050

uniPROBE Membrane Kits are available for the following Ions. All Membrane Kits are supplied with 1 or more colour-coded sensing tips, 45mL internal filling solution and 10mL external electrolyte gel.

Species	Tip Colour Code
• Fluoride	Green
• Chloride	Yellow
• Iodide	Purple
• Cyanide	Purple
• Bromide	Natural
• Sulphide	Black

Ammonia is also available, but is not interchangeable with the other uniPROBE sensor tips and does not include the external electrolyte gel.

TPS Pty Ltd
A.B.N. No 30 009 773 371
4 Jamberoo Street
Springwood, Brisbane,
AUSTRALIA, 4127
Phone Australia (07) 32 900 400
International 61 7 32 900 400
Email tps@tps.com.au
Fax Australia (07) 3808 4871
International 61 7 3808 4871
Web www.tps.com.au

The TPS Fluoride ISE is a potentiometric sensor, meaning that is develops a potential (or voltage) proportional to the concentration of the ion to which it responds. The mathematical equation that describes this relationship is called the Nernst Equation:

$$E = E^{\circ} + S \log_{10} [Ion]$$

where E is the measured voltage, E° is a constant, S is the slope factor, and [Ion] is the concentration of the ion to which it responds. The relationship between the measured potential and the concentration is logarithmic, which explains why potentiometric sensors are described as having exceptional working ranges, but limited accuracy. The slope factor, S, is dependent on the temperature of the solution, which is why it is best to measure both standards and samples at the same temperature. It has a theoretical value of about 59/n mV at 25°C, where n is the charge of the ion being measured. Ions such as F^- and NO_3^- have a theoretical slope of -59 (n=-1), while ions like Ca^{+2} have a theoretical slope of +29 (n=+2). By plotting the measured potential (E) of several standards versus the $\log_{10}$ of their concentration, it is possible to generate a linear calibration curve. In reality, the slope of the calibration curve has an acceptable range, which for the fluoride ISE is –57 +/-3 mV. The calibration curve becomes non-linear below 1.9ppm F, where the electrode starts to reach the limits of its capabilities. At this point the slope begins to fall until it reaches the detection limit of 0.02ppm F.

Interferences

The fluoride ISE is highly selective for fluoride and suffers from only a few interferences. Hydroxide ions will affect the reading, which is why TISAB is added to buffer the standards and samples to a constant pH. Metal ions such as Al^{+3}, $Fe^{+2/3}$, and complex fluoride and prevent it from being sensed by the electrode. TISAB contains a strong complexing agent that displaces the F ion from the metal ion and allows it to be sensed by the electrode.

Reference:

TISAB Solution = 0.06M CDTA / 1M sodium citrate / 1M NaCl / adjusted to pH 6.0 – 6.5 with 40% NaOH

Specifications:	
Concentration Range	0.02ppm F to 19000ppm F ($1x10^{-6}$M to 1M)
Linear Range	1.9ppm F to 19000ppm F ($1x10^{-4}$M to 1M)
Slope	-57mV/decade +/-3mV
Response Time	<1 minute for 90% of final value

Ordering Information

	Part No
Complete TPS Fluoride ISE Analysis Kit	121560
Includes 1 x Combination ISE Body	121500
1 x Fluoride ISE Membrane / IFS / Electrolyte Kit	121562
1 x 1000ppm F^- Standard (200mL)	121564
1 x TISAB Solution (200mL)	121820
1 x Fluoride ISE Instruction Manual	130050

Spare parts and accessories…

Combination Intermediate Junction ISE Barrel	121500
Fluoride ISE Membrane Kit	121562
Includes 1 x Green Membrane tip	
1 x Internal Filling Solution (IFS), 45mL	121806
1 x External Reference Electrolyte Gel, 10mL	121811
Internal Filling Solution (IFS), 45mL	121806
External Reference Electrolyte Gel, 10mL	121811
1000ppm F^- Standard (200mL)	121564
1000ppm F^- Standard (1 Litre)	121566
TISAB Solution (200mL)	121820
TISAB Solution (1 Litre)	121822
Fluoride ISE Instruction Manual	130050

uniPROBE Membrane Kits are available for the following Ions. All Membrane Kits are supplied with 1 or more colour-coded sensing tips, 45mL internal filling solution and 10mL external electrolyte gel.

Species	Tip Colour Code
• Fluoride	Green
• Chloride	Yellow
• Iodide	Purple
• Cyanide	Purple
• Bromide	Natural
• Sulphide	Black

Ammonia is also available, but is not interchangeable with the other uniPROBE sensor tips and does not include the external electrolyte gel.

TPS Pty Ltd
A.B.N. No 30 009 773 371
4 Jamberoo Street
Springwood, Brisbane,
AUSTRALIA, 4127
Phone Australia (07) 32 900 400
International 61 7 32 900 400
Email tps@tps.com.au
Fax Australia (07) 3808 4871
International 61 7 3808 4871
Web www.tps.com.au

END OF THESIS